

University of Strathclyde

Department of Electronic & Electrical Engineering

Self Optimising Algorithms for C-T Load
Tolerant Antennae

Andrew G Borthwick

MPhil Thesis, 2009

Declaration of Authenticity

This thesis is the result of the author's original research. It has been composed by the author and has not been previously submitted for examination which has led to the award of a degree.

The copyright of this thesis belongs to the author under the terms of the United Kingdom Copyright Acts as qualified by University of Strathclyde Regulation 3.50. Due acknowledgement must always be made of the use of any material contained in, or derived from, this thesis.

Signed:

Date:

Acknowledgements

This work was funded jointly by the United Kingdom Engineering and Physical Sciences Research Council and by the European Communities under the contract of Association between EURATOM and UKAEA. The views and opinions expressed herein do not necessarily reflect those of the European Commission. This work was carried out within the framework of the European Fusion Development Agreement.

Abstract

The performance of RF antennae for ion cyclotron heating applications of fusion plasmas have hitherto been greatly degraded by the presence of instabilities in the plasma edge. These appear electrically as fast transient reflections on the RF circuit. The conjugate-T (CT) architecture achieves resilience by arranging two straps in parallel with a tuning component on each arm. If properly configured, a symmetrical disturbance to both straps will result in the reflected power destructively interfering at the T point.

The objective of the research reported here is to lay the foundations of a control methodology to enable an in-vessel matched CT antenna to self configure in order to achieve optimal resilience and perfect matching for any given plasma state. Highly non linear steady state models of the electrical behavior are derived, and parameter scans of the non ideal variables such as mutual impedance, asymmetry and reactive disturbances are investigated. Finally, the basis of a self optimising control algorithm is presented and performance validated for resistive disturbances. Options for fully reactive and resistive disturbance resilience are proposed.

Contents

Declaration of Authenticity.....	ii
Acknowledgements.....	iii
Abstract.....	iv
1. Introduction.....	1
1.1. Synopsis.....	2
1.2. Original contributions.....	6
2. General background.....	9
2.1. Overview of Nuclear Fusion.....	9
2.2. Magnetically Confined Fusion.....	11
2.3. Ion Cyclotron Resonant Heating (ICRH) Systems.....	14
2.3.1. Physics of Ion cyclotron Heating & Current Drive.....	14
2.3.2. Overview of ICRH Systems.....	16
2.4. Plasma coupling.....	23
2.5. Strategies to enhance load variation tolerance.....	27
2.6. Conjugate T (CT) resilient architectures.....	31
2.6.1. CT architecture overview.....	31
2.6.2. JET ITER Like Antenna (ILA).....	32
3. Conjugate T (CT) circuit model.....	38
3.1. Lumped element CT circuit.....	38
3.1.1. Circuit description.....	38
3.1.2. Definition of resistive asymmetry.....	39
3.1.3. Equivalent circuit model including mutual coupling.....	40
3.2. 2nd Stage Matching Circuits.....	42
3.3. Models of plasma disturbance.....	44
4. Resilience performance indicator.....	46
4.1. Definition of resilience.....	46
4.2. Derivation of optimal set-points for ideal circuits.....	46
4.3. Derivation of numerical solution algorithms.....	50
4.3.1. Resilience solver.....	50
4.3.2. Optimal set point derivation.....	52
5. Feedback control of optimal resilience.....	56
5.1. ILA Control System – Fixed T resilience control.....	56
5.1.1. Shortcomings.....	56
5.1.2. Fixed – T performance model.....	57
5.2. Arm phase control.....	59
5.3. Sensitivity studies.....	62
5.3.1. Rationale.....	62
5.3.2. Mutual Reactance.....	65
5.3.3. Mutual Resistance.....	66
5.3.4. Asymmetry.....	67
5.3.5. Summary of effects & proposals.....	68
5.4. Non Ideal parameter compensation.....	70
5.5. Algorithm assessment.....	74
5.5.1. Base load variation.....	75
5.5.2. Mutual reactance variation.....	76
5.5.3. Mutual resistance variation.....	78

5.5.4.	Asymmetry variation.....	79
5.6.	Discussion	81
6.	Average coupled power performance indicator	83
6.1.	Reactive disturbances.....	83
6.2.	Average coupled power model.....	83
6.3.	Coupled power modelling.....	86
6.3.1.	Derivation of coupled power performance measure	86
6.3.2.	Numerical average X-R performance model	90
6.3.3.	Numerical Set point solver.....	92
7.	Implications of reactive ELMs.....	94
7.1.	Sensitivity studies	94
7.1.1.	Phase load invariance.....	94
7.1.2.	Mutual reactance sensitivity.....	98
7.1.3.	Mutual resistance sensitivity.....	100
7.1.4.	Resistive asymmetry sensitivity.....	101
7.1.5.	Summary of sensitivity study findings.....	103
7.2.	Proposals	104
7.2.1.	Gross angle compensation.....	104
7.2.2.	Net angle compensation	107
8.	Future work	108
9.	Conclusions	111
10.	References	113
11.	Appendix A: Derivation of 2 nd Stage Match Parameters.....	116
12.	Appendix B	119
13.	Appendix C	120
14.	Appendix D	124
15.	Appendix E	128
16.	Appendix F.....	130
17.	Appendix G.....	133
18.	Appendix H.....	138

1. Introduction

Environmental concerns, and limited reserves of fossil fuels, necessitate the development of alternative sources of energy in the medium to long term. Of the candidate solutions envisaged, controlled nuclear fusion is one of the most promising, yet highly technically challenging.

One such challenge requiring a solution is the need of a reactor to heat its plasma to the required energies necessary for sustained fusion reactions, and to provide steady state non inductive current drive to sustain the magnetic confinement fields holding the plasma away from the reactor walls.

One candidate heating and current drive system is Ion Cyclotron Resonant Heating (ICRH), which heats plasma by a high power electromagnetic wave. However, the performance of such systems is greatly degraded in the presence of plasma edge instabilities. These appear electrically as fast transient loads on the RF circuit, of frequency beyond that which may be compensated for in real time. As such circuits are highly tuned, the load variations result in large transient reflections of RF power. In response protection interlocks will shut down the generator momentarily. However the cumulative effect of these outages is a large decrease in duty cycle, reducing the average delivered power.

This study concerns the investigation of the conjugate T load resilient architecture, and develops control algorithms that enable the maximum power transfer to the plasma, as well as maximising the passive disturbance rejection of the electrical system.

1.1. Synopsis

The objective of this study is to understand the behavior of optimally resilient circuits, and so develop control algorithms that drive the antenna toward a perfectly matched, resilient state. The manner in which this is achieved is summarised below:

ICRH systems and fusion power in general is described by way of introduction in chapter 2. In this regard, basic principles of fusion and its magnetic confinement are described in section 2.1 & 2.2. This is necessary to understand the toroidal geometry frame used throughout the text.

An introduction to ICRH is provided in section 2.3. This section explains the physical processes of coupling power to the plasma, and the systems required to achieve this. A brief introduction to the RF actuators and design techniques is provided, as these will be used throughout.

As this study is primarily focused on load disturbance rejection, the mechanism of loading the antenna, and the known type of disturbances encountered are described in section 2.4. Unfortunately, most physical data is available from studies by Monakhov (2003) on antennae geometries not consistent with the modern short strap designs assumed in this study.

A review of candidate fast matching and resilient methodologies is included in section 2.5. Various methods from active compensation (Fast Ferrite Tuners, Lin et al, 2008) to passive are summarised. Most antennae use a combination of active and passive means, and the conjugate T circuit is introduced as an architecture capable of coupling power through plasma edge disturbances.

The CT circuit is discussed at depth in section 2.6. In this regard, the JET ILA is introduced as a modern short strap conjugate T antenna, which serves as the design basis for this study.

With suitable introductions in place, in Chapter 3 the study reviews the mathematical model of one CT circuit. In this regard, a simplified model that includes asymmetries and mutual impedance effects is developed in section 3.1.

The second stage matching circuits are mathematically described in section 3.2. Two basic models are proposed; one a simplified circuit suitable for resistive variations, and the second a more accurate realisation required for multidimensional disturbance modelling.

The phenomenological model of loading disturbance is set out in section 3.3. This model is based on that described by Lamalle (2005). Only two models were considered in this study; a purely resistive disturbance, and a combined resistive-reactive disturbance.

With the mathematical models now established, in chapter 4 the study can proceed to defining the conditions of a CT circuit for optimal resilience. Firstly, resilience is mathematically defined in section 4.1, using a purely resistive variation following on from work by Durodie (M65).

The optimal configuration of an ideal CT circuit is derived algebraically in section 4.2. However, the complexity of incorporating non ideal parameters requires a numerical solver. As the resilience solution space contains mathematical discontinuities, custom solvers were written, and these are summarised in section 4.3.

Having developed the mathematical tools necessary to calculate the optimal set point of any given circuit, in chapter 5 the study proceeds to develop control heuristics for optimal resilience.

To serve as reference, the fixed T point control methodology of the ILA, as developed by Durodie (M68) is described, and the model thereof summarised in section 5.1.

In section 5.2 an alternative methodology is proposed that controls the arm current phase rather than antenna impedance. This was demonstrated to be load invariant, yet would require feedback control of the second stage circuit for automatic matching.

The influence of non ideal parameters was investigated using numerical tools. The sensitivity and set point loci are published in section 5.3. Consequently, general control heuristics were developed for the phase control methodology, and the non ideal parameters shown to have a strong influence on performance.

A novel methodology using a diagnostic sideband, amplitude modulated on the main heating frequency is proposed in section 5.4 for non ideal parameter compensation. The resulting control algorithm was tested against the fixed T method in section 5.5 and shown to have significantly superior performance.

It is known that plasma disturbances are multidimensional events, and therefore, the one dimensional methods investigated thus far were insufficient. Therefore, in chapter 6 an alternative average coupled power performance measure is proposed that is more scalable in dimensions and better captures system behavior. The performance measure is mathematically described in section 6.3.1. Numerical tools

for calculating performance and the consequential optimal configuration are described in sections 6.3.2 & 6.3.3 respectively.

The sensitivity studies were repeated for multidimensional disturbances in chapter 7. It was found that reactive disturbances had prominent detrimental effects on the system performance. Additionally, the amplitude modulation diagnostic required modification. Proposals to address some of the reactive ELM implications are set out in section 7.2

The study leaves many issues outstanding, and the proposed further work is discussed in chapter 8. Of particular note is the overarching requirement to gain a better understanding of plasma disturbance by direct measurement on the ILA.

The study concludes in chapter 9 by summarising the useful contributions by developing a better understanding of the non ideal parameters on CT performance, and has proposed the framework for a control methodology whereby both matching and resilience are controlled under feedback, and the use of diagnostic sidebands to indicate the state of the antenna.

References used in this study are reported in chapter 10.

Appendix A contains the derivation and code realisation of the required input parameters of a phase shifter – stub 2nd stage match, as used in the modelling of section 6.3.2

Appendix B contains a measured impedance matrix provided by the ILA commissioning team. This was used to set bounds on non ideal parameters

Appendix C contains the MATLAB code for the resilience performance assessment for an arbitrary CT circuit, as used for studies in chapters 4 & 5.

Appendix D contains the MATLAB code for the adaptive mesh optimization solver that was written to extract optimal CT configuration when the solution lies on a mathematical discontinuity. This was used for sensitivity studies of section 5.3

Appendix E contains the code that derives the CT circuit configuration required for a fixed T point algorithm. This was used as reference for the algorithm assessments of section 5.5.

Appendix F contains the code for the amplitude modulation algorithm, which was assessed in section 5.5.

Appendix G records the code for the averaged coupled power in disturbance X-R space as used to assess the impact of multidimensional ELMs.

Appendix H contains the code for the modified adaptive mesh optimization algorithm that extracts the maximum performance from the average coupled power model of Appendix G. This was used for the sensitivity studies of section 7.1.

1.2. Original contributions

The original work presented in this study to which the author made significant contributions is the following:

Chapter 4: The derivation, in section 4.3.1, of a systematic approach to modelling resilience by defining a performance measure rather than VSWR contours.

The development and validation, in section 4.3.2, of numerical method to extract the optimal configuration of an arbitrary CT circuit, including mutual impedance and resistive asymmetry

Chapter 5: The derivation, in section 5.2, of the definition of a resilient circuit as defined by arm phase.

The proposal, in section 5.2, of a control methodology whereby resilience is optimised by feedback control to deliver the optimal arm phases, and resulting floating T point impedance matched by feedback control of the 2nd stage circuit.

The parametric investigation, in section 5.3, of non ideal parameters of mutual impedance and resistive asymmetry on optimal configuration set points for resistive disturbances.

The proposal, in section 5.4, of adding diagnostic sidebands to the heating frequency, and so enable automatic compensation of varying non ideal parameters.

The validation, in section 5.5, of the amplitude modulated arm phase control algorithm, demonstrating superior and broadband resilience performance for resistive disturbances.

Chapter 6: The proposal & development, in section 6.2, of a revised average coupled power model of resilience performance, enabling multi dimensional scaling, non path dependant disturbances, and capturing interlock functionality.

The development, in section 6.3.3, of numerical method to extract the optimal configuration of an arbitrary CT circuit, including mutual impedance and resistive asymmetry using the average coupled power performance measure.

Chapter 7: The parametric investigation, in section 7.1, of non ideal parameters of mutual impedance and resistive asymmetry on optimal configuration set points for combined resistive - reactive disturbances.

The proposal, in section 7.2, of adding a diagnostic sideband to the heating frequency, of frequency chosen so that when the sideband is controlled to the nominally optimal locus, the resulting offset from optimal on the drive frequency provides a cushion to absorb the reactive component of the ELM, yet uses the sideband as a “handrail” to provide automatic compensation for mutual reactance and asymmetry variations.

2. General background

2.1. Overview of Nuclear Fusion

Nuclear fusion is the process whereby elements of low atomic number are combined into heavier elements, and is the mechanism that powers the stars. The process releases very large amounts of energy, with significant power amplification. However, the initiating energy trigger is substantial. Notwithstanding the consequential difficulties, the large resulting power, amplification and readily available fuel sources make the prospect of a controlled fusion power plant attractive.

The most efficient reaction to utilise fusion on earth is the DT reaction in which nuclei of the two Hydrogen isotopes Deuterium (D) and Tritium (T) are forced together to overcome the rejection due to their electric charge and so allow them to fuse due to the strong nuclear force between them. The product of this reaction is a Helium nucleus and a neutron, both with very high kinetic energy.

Due to losses in any confinement system, three parameters, temperature, density and confinement time, need to be simultaneously achieved for sustained fusion to occur in a given volume. The product of these parameters is called the fusion (or triple) product, and provides a figure of merit for a candidate fusion device. Breakeven (energy input equal to energy output) is represented by a fixed value of $5 \times 10^{21} \text{m}^{-3} \text{keVs}$, however no experimental device has yet attained this figure (Wesson 1999).

Fusion reactions occur at a sufficient rate only at very high temperatures and consequently in the fourth state of matter known as plasma - when electrons

disassociate from their nuclei and co exist in an electrically neutral, yet conductive medium of free moving electrons and ion species.

The high temperatures confer a large kinetic energy to the ions, so enabling them to overcome the electrostatic repulsive force and approach each other sufficiently to be captured by the strong nuclear force and so fuse. For the DT reaction an optimal temperature near 300M K exists (Wesson, 2004), although lower temperatures of ~200M K are typically used on contemporary experiments (Wesson 1999)

The number of fusion reactions per unit volume is roughly proportional to the square of the density. Therefore the density of fuel ions must be sufficiently large for fusion reactions to take place at the required rate. Contemporary devices can attain $1-2 \times 10^{20}$ particles m^{-3} , however greater densities are limited by the onset of plasma instability with currently available magnetic confinement field strengths (Wesson 1999).

The Energy Confinement Time is a measure of how long the energy in the plasma is retained before being lost. It is defined as the ratio of the thermal energy contained in the plasma to the power input required to maintain these conditions. This figure is limited by convective losses from the plasma edge and radiation. The confinement time increases dramatically with plasma size (large volumes retain heat much better than small volumes) - the ultimate example being the Sun whose energy confinement time is massive. Confinement times of 4-6 seconds are necessary for attainable temperatures and density; however present records are just greater than 1s.

2.2. Magnetically Confined Fusion

To achieve the necessary triple product for sustained fusion, various confinement devices have been designed and researched. Among these the tokamak is the most highly developed.

Since plasma comprises charged particles, magnetic fields can be used to isolate the plasma from the walls of the containment vessel. This isolation reduces the conductive heat loss to the vessel, enabling the high temperatures discussed in section 2.1 to be achieved. It also minimises the release of impurities from the vessel walls into the plasma that would contaminate and further cool the plasma by radiation.

In a tokamak, plasma is confined in a toroidal chamber. This toroidal geometry is illustrated in Figure 1, which defines the coordinate frame that shall be used throughout.

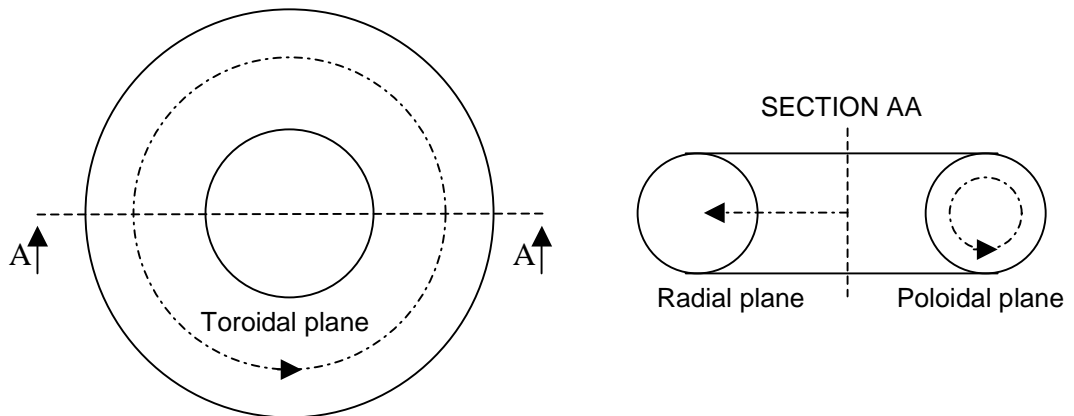


Figure 1: Toroidal Geometry (simplified)

The confinement is achieved by arranging magnetic coils toroidally to form a circular magnetic field when viewed in plan. This enables the plasma to loop back on itself and so avoid the “end” problem with a cylindrical geometry.

The internal plasma pressure is reacted by exciting a toroidal current in the plasma itself. The resulting magnetic field “pinches” the plasma away from the vacuum vessel wall. This current is achieved by induction, where the plasma serves as the secondary winding of a transformer.

The plasma vertical position is stabilised by arranging large coils in the toroidal plane to form a poloidal field that can manipulate the plasma’s vertical location and cross sectional shape.

The resulting interaction yields magnetic field lines that orbit both poloidally and toroidally to “corkscrew” around the vessel and so form closed magnetic surfaces. Plasma species move along the field lines and are therefore confined. This principle is illustrated in Figure 2. A more comprehensive review of Tokomaks is reported by Wesson (2004).

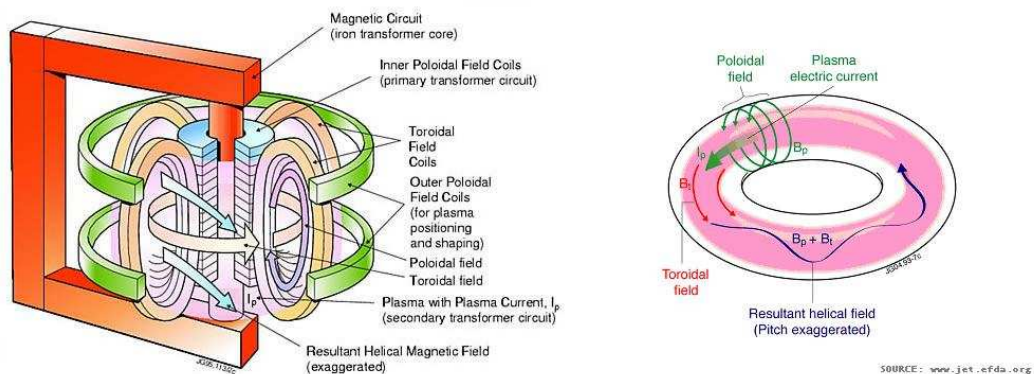


Figure 2: Principle of magnetic confinement in a Tokamak

Plasma heating is achieved by three principle means; ohmic heating, neutral beam injection and RF systems.

As discussed above, large currents are required to flow in the plasma to complete the magnetic confinement. These currents are of order 5MA on contemporary devices such as JET. Although plasma has a low electrical resistance significant heating is achieved through classical resistive losses. However, plasma

resistance decreases with temperature and so complimentary additional heating systems are required.

Neutral Beam injection is the primary heating system on contemporary tokomaks, and consists of an ion source and accelerator to produce focused ionised beams. These are neutralized in order to penetrate the plasma's magnetic confinement and heat the plasma by kinetic energy conversion.

Radio Frequency (RF) systems heat the plasma by exploiting a resonance of the plasma species. Plasma particles orbit magnetic field lines with a characteristic cyclotron frequency. An electromagnetic wave of the same frequency is preferentially absorbed by such particles, and the wave energy converted to kinetic energy, or "heat". Different RF systems target the various plasma species. GHz band ECRH (Electron Cyclotron Resonant Heating) systems heat the plasma electrons, whereas shortwave ICRH (Ion cyclotron Resonant Heating) systems target the ions.

The three heating systems are illustrated in Figure 3

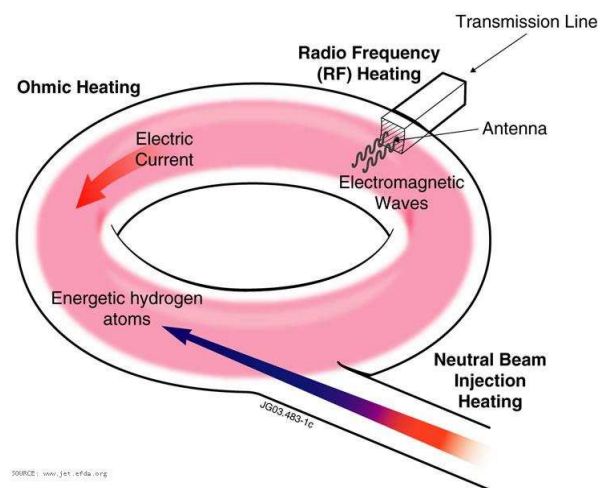


Figure 3: Illustration of Tokomak additional heating systems

2.3. Ion Cyclotron Resonant Heating (ICRH) Systems

2.3.1. Physics of Ion cyclotron Heating & Current Drive

In plasma, ions orbit magnetic field lines with a characteristic cyclotron frequency, ω_c , which depends only on three quantities: charge and mass of the particle, and magnetic field strength, as defined below:

$$\omega_{cs} = \frac{Z_s e B}{m_s} \quad [1]$$

Where subscript 's' denotes the plasma species, Z_e the species' charge, 'B' the magnetic flux density and 'm' the mass.

Due to the circular geometry of the Tokamak, the toroidal magnetic field drops off as a consequence of Amperes law in proportion to R^{-1} , where R is the radius from the major axis of the torus (see Figure 1).

Therefore, if an electromagnetic wave is launched into the plasma, specific plasma species can be targeted by gross selection of frequency band dependant on the species charge & mass. Because field changes by a factor of 2 over the plasma cross section, the geometrical absorption location can be accurately controlled to a narrow vertical layer by fine variation of frequency.

This control of power deposition is a unique feature of ICRH RF systems, and enables an enhanced confinement time as power is delivered straight to the plasma core, not losing power to the edge.

Ion cyclotron heating and current drive exploits the interaction mechanisms of the fast magnetosonic wave in plasma, as discussed in section 2.4. The resonance condition for a species 's' is mathematically described as:

$$\omega + p\omega_{CS} + k_{\parallel}v_{\parallel s} = 0 \quad [2]$$

Where ‘ p ’ is the cyclotron harmonic number (0,1,2..), ‘ ω ’ is the wave angular frequency, ‘ k_{\parallel} ’ the parallel component of the velocity ‘ v_s ’ along the field line, and ‘ k_{\parallel} ’ the component of the wave vector parallel to the magnetic field.

The velocity component in the relation results in more significant heating for fast particles than for slow particles, especially for higher order harmonics. This introduces temperature dependencies as well as distortion in thermal distribution due to the heating.

The main interaction processes are cyclotron heating of the ions ($p>0$, $s = \text{ions}$), and transit time magnetic pumping (e-TTMP) or Landau damping of electrons (ELD) ($p=0$, $s=\text{electrons}$). Additionally, the fast magnetosonic wave can be converted into short wavelength electrostatic waves (e.g. Ion Bernstein waves) which can damp their energy into ions and electrons. A comprehensive review of the plasma physics involved with IC heating and current drive is reported by Becoulet (1996).

In the ion heating regime the direct coupling to the ions is a distinct feature of ICRH systems and can be exploited to enhance plasma reactivity, and so burn control on future reactors (Koch 1993). Three distinct ion species are typically targetted:

- The second harmonic of tritium (Rogers 1996)
- The fundamental of ^3He as minority species in Helium doped plasmas
- The fundamental of deuterium (although this is in competition with plasma impurities such as Beryllium)

The presence of k_{\parallel} in the resonance condition allows the wave to generate current in the plasma (Fisch 1987). This is obtained by combining multiple toroidal antennae in a progressively phased array. The resulting constructive and destructive

interference can be used to steer the wave propagation front and obtain a toroidally asymmetric wave spectrum. A resonant condition takes place when particles parallel velocity matches the fast wave parallel phase velocity. The opposite sign of the two processes involved (e-TTMO & ELD) lowers the overall absorption, and so coupling is reduced. However, this resonant condition occurs at different frequencies, and so heating and current drive functions can be decoupled. The ability to drive steady state DC current is important for commercial reactors, as contemporary induction driven machines are inherently pulsed.

2.3.2. Overview of ICRH Systems

An ICRH system can be decomposed into four distinct parts, the generators, matching network, antenna and protection systems.

Generators:

ICRH systems use sufficiently low frequencies to enable the use of conventional and commercially available amplification devices. The generators consist of an amplitude or phase modulated milli-Watt frequency sources that drives a train of cascaded amplifiers.

A typical RF generator layout consists of a four stage amplifier, including a wideband solid state amp (~0.5kW) followed by three tube powered tuned stages; a pre driver (20kW), a driver-stage (200kW) and an end stage (~2MW). This typical configuration is shown in Figure 4 (as per ITER WBS 5.1).

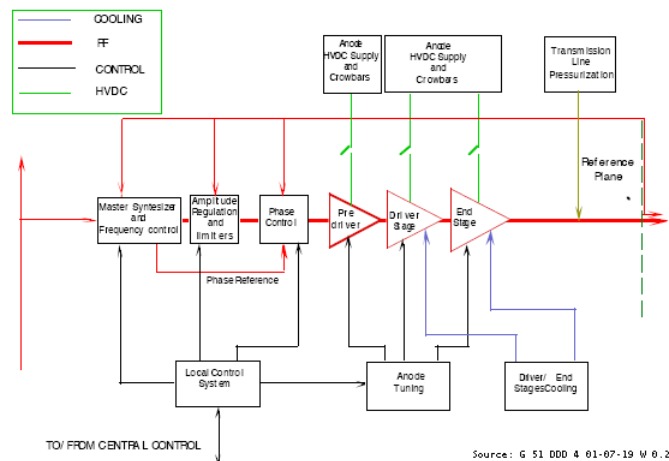


Figure 4: RF Power source block diagram

All power stages have input and output cavities that are mechanically adjusted to cover the frequency range. The use of coaxial cavities leads to a relatively simple mechanical layout. With amplitude feedback the generator bandwidth about the matched frequency can be as high as 4MHz although only 400kHz is actively used (Sibley 1999).

Tubes are typically operated in class B. However, Generator efficiencies of 65% conversion of DC to RF input have been achieved, making ICRH one of the most efficient additional heating systems available (Sibley 1999).

Generators are capable of controlling under feedback the relative phase (between generators), modulation, output power and frequency.

Matching Networks:

In order to satisfy ohms law for propagating electrical waves in a conductor, a proportion of any incident wave is reflected at an impedance discontinuity (Da Silva 2002). This reflected wave will alter the effective output impedance of the tube. As this impedance moves out of the correct range the screen grid and anode currents will exceed limits as the tube responds to maintain power. Consequently, the output impedance of the generators is matched to the characteristic impedance of the

transmission lines by the amplifiers output cavity, and in turn the transmission line is matched to the antenna.

The coupling load of the antenna is very low for reasons to be discussed in Section 2.4. Consequently it must be transformed to a suitable impedance (preferably real) using matching stubs and trombones. The choice of transmission line characteristic impedance is chosen to be sufficiently low to ease the matching requirement, but sufficiently high so that the innate voltage carrying capacity of the line is maintained. A value of 30Ω is typically used (Wade 1994). Coaxial transmission lines are employed due to the compact mechanical realisation and natural isolation conferred.

Antenna matching employs classic microwave techniques. The combination of a forward and reflected wave leads to the creation of a standing wave pattern along the transmission line with a maximum every half wavelength. Therefore, at any given location on the line the input impedance, defined as voltage/current, varies.

Various methods of matching exist, but most exploit the ability of a termination load to be changed when seen through varying lengths of transmission line. The generic matching components are summarised below:

Trombone, line stretcher phase shifter or transformer: This component is an adjustable length of transmission line, much like a trombone's slider. The variable length can be used to change the phase of a perfectly matched RF wave due to the increased propagation delay associated with a longer line. This is mathematically expressed as follows:

$$\Delta\phi = \frac{\omega}{u_p} \Delta x \quad [3]$$

Where ' $\Delta\phi$ ' is the change in phase, ' ω ' the angular frequency of the wave, ' u_p ' the wave velocity and ' Δx ' the change in transmission line length. Alternately, the same component can be used as a transformer to convert an unmatched load from one impedance to another by the relation:

$$Z_{in} = Z_0 \left[\frac{Z_0 \sinh(\gamma l) + Z_L \cosh(\gamma l)}{Z_0 \cosh(\gamma l) + Z_L \sinh(\gamma l)} \right] \quad [4]$$

Where ' Z_{in} ' is the input impedance, ' Z_L ' the load impedance ' Z_0 ' the line characteristic impedance, ' γ ' the propagation constant, and ' l ' the length of the transmission line.

Variable stub: A stub is a section of coaxial line terminated with a short circuit, therefore $Z_L = 0$, and for a lossless line $\gamma = j\beta$, where ' β ' is the phase shift index defined as $2\pi/\lambda$, where ' λ ' is the wavelength. By equation 4, the resulting input impedance is given by the equation:

$$Z_{in} = Z_0 (j \tan(\beta l)) \quad [5]$$

Therefore the inclusion of a stub in series with a circuit appears as a pure shunt reactance. By varying the length ' l ' of the input to the location of the short, the reactance may be varied. A capacitive effect can be achieved for lengths of $l > \lambda/4$, whereas an inductive effect can be achieved for lengths of $l < \lambda/4$.

For lengths equal to a quarter wavelength, the input impedance appears infinite and the stub plays no part in the electrical behavior of the system. Such fixed stubs are employed to introduce services such as coolant or instrumentation to the electrically isolated core conductor.

Variable capacitor: These elements are conventional capacitors, and are realised as a set of two isolated coaxial interlocking cylinder arrays. These are installed in

line with the coaxial transmission line. The capacitance is varied by simply altering the overlapping areas of the two cylinder arrays. However, the capacitor will have its own parasitic inductance, and so appears as a series combination of variable capacitor and fixed inductance. Therefore the capacitor may behave as an inductor for low capacitor stroke values:

$$X = \omega L_f - \frac{1}{\omega C(x)} = \frac{\omega^2 L_f C(x) - 1}{\omega C(x)} \text{ for } e^{+j\omega t} \quad [6]$$

Where ‘X’ is the series reactance, ‘L_f’ the fixed inductance and ‘C(x)’ the capacitance as a function of displacement ‘x’.

Fixed stubs & transformers are also used to perform the bulk of a matching solution. This enables the variable elements to have a lower dynamic range to account for coupling and frequency variations.

Antennae:

The low frequencies of the ion cyclotron range means that the vacuum wavelength lies in the range of approximately 5-10m. As this dimension significantly exceeds physical the dimensions of even the largest tokomaks, conventional resonant antennae are not possible.

However, the equivalent dielectric constant of plasma is sufficiently high to enable a reduction in wavelength to approximately 10-20cm, which can propagate. Therefore, coupling will occur if the plasma is located within the evanescent field of the antenna, enabling the RF to “tunnel” the vacuum gap.

This has two consequences; firstly that coupling is strongly dependant on the characteristics of the plasma edge (Lamalle, 2004), and secondly that the radiation resistance of the antenna is very low (Kaye, 1994).

The radiating section of an antenna consists of strip-line “current straps” shorting the core conductor to the outer. The outer flairs into a cavity or “strap housing”, the design of which maximises the magnetic flux linkage to the plasma whilst minimising impedance transitions (Kaye 1994). The straps run poloidally so as best to excite a wave polarised perpendicular to the magnetic field. Typically a faraday screen shields the straps from the plasma and completes the polarisation closer to the true field incidence angle; although this component is omitted in some modern designs.

Modern strap design makes no attempt to tune the length of the strap to the midband frequency, rather single or parallel combinations of short straps are preferred, as short strap’s lower inductance requires less driving voltage to achieve the same current. Such a configuration is illustrated in the concept model of the ITER antenna (Borthwick, 2008).

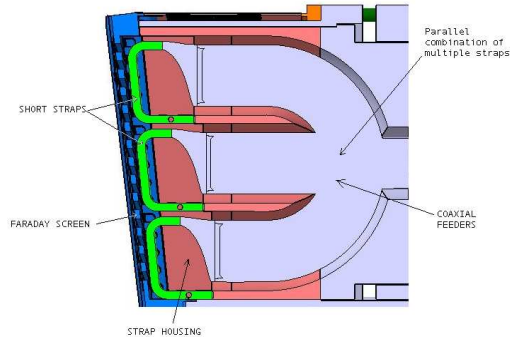


Figure 5: Example of Strap Design for ITER concept

Finally, the antenna is always located on the equatorial plane of the low field side of the torus, as illustrated in Figure 6. This is for, amongst other reasons, ease of access, and to enable refraction on the plasma edge to focus the power near the centre of the plasma, as illustrated in Figure 6.

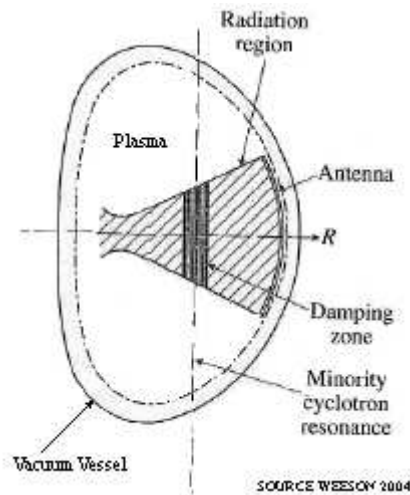


Figure 6: Location of Antennae in Vessel Wall.

Protection Systems

ICRH systems are equipped with a variety of protection systems. These systems interact with any controller and so this section shall summarise the generic requirements. These are broadly to i) Protect the generators from excess power dissipation (e.g. excessive reflected power), ii) Prevent the onset of arcs (by limiting voltage in various components), and iii) Protect the system in the event of arcs (by tripping the power). Protection systems can take several levels of intervention. These are:

- **Terminating the pulse** in response to a system threatening event, such as an arc or excessive power dissipation in the Tetrode.
- **Power trip & restore** in response to fault events that may be transient or cleared by removing the RF temporarily. The trip window is typically of order 5-20ms.
- **Power limitation** in response to off normal conditions that may be tolerated, such as high reflected power, voltage limits and generator dissipation.

Protection systems are highly complex, with a more comprehensive summary of their operation is given by Wade (1994).

2.4. Plasma coupling

In the ion cyclotron range of frequency, the amount of RF power that can be transferred to the plasma depends, in a complex way, on the plasma geometry, location and density profile, the scrape off layer density profile and array parameters.

In the cold plasma limit, two generally uncoupled waves co-exist in the plasma: the fast and slow magnetosonic waves with dispersion relations:

$$n_{\perp F} = S - n_{\parallel}^2 - \frac{D^2}{S - n_{\parallel}^2} \quad (\text{fast wave}) \quad [7]$$

$$n_{\perp S} = P \left[1 - \frac{n_{\parallel}^2}{S} \right] \quad (\text{slow wave}) \quad [8]$$

Where ' n_{\perp} ' & ' n_{\parallel} ' are the perpendicular and parallel components of the wave vector $n = k/k_0$, $k_0 = \omega/c$. S, D & P are the dielectric tensor elements as defined by Stix (1992).

In plasma, the slow wave is strongly evanescent ($n_{\perp S}^2 < 0$), with a typical evanescence length of approximately 0.6mm. The polarisation vector has the main component of the electric field in the toroidal direction, reflecting the fact that the plasma is a very good conductor in the parallel direction. This screens out the parallel electric field by allowing image currents to flow over one skin depth. The fast wave propagates instead with typical wavelength $\lambda_{\perp F} = 2\pi/k_{\perp} \cong 0.12m$ inside the plasma. This scales with density, so wavelength increases toward the plasma edge.

At the very edge, density falls to near zero, and so $S \cong 0$ & $D \cong 0$, and the fast wave connects to the vacuum wave polarised with electric field perpendicular to the static magnetic field. As described in section 2.3.2, the vacuum wave is strongly

evanescent. Defining ' $k_{||c}$ ' the characteristic parallel wave number ($n_{||}=ck_{||}/\omega$) of the driving frequency, the electromagnetic field decays as $e^{-k_{||c}r}$ where ' r ' is the distance from the strap in vacuum.

It is therefore very difficult to couple power over large vacuum gaps, so by design these are made small. However, the sensitivity of coupling to distance is consequently very high. Therefore variations in plasma position or geometry are seen by the antenna as pronounced changes in coupling resistance. Secondary effects such as the density profile of the scrape off layer also result in changes for the same reason.

The parameters of plasma position, shape & density profile all vary from pulse to pulse. In addition, the large number of parameters makes predicting the coupling for a given scenario problematic, and this can be performed using 3D electromagnetic simulations of plasma simulated by dielectric layer stack (Lamalle 2004).

Importantly, the plasma geometry also changes during the pulse. This can be due to actions of the plasma position feedback control system, changes to the confinement mode, and edge instabilities known as sawtooth or Edge Localised Modes (ELMs). Of these ELMs and mode transitions are most reported on.

Mode changes: In modern tokomaks plasma confinement is achieved in two modes; L mode and H mode. L mode is the conventional confinement mode characterised by a Gaussian cross sectional density distribution. Consequently, the plasma edge is closer and more diffuse and relatively high coupling is achieved.

With sufficient additional heating, a higher H mode confinement is obtained. Consequently, the plasma edge density profile is steeper and further away, increasing the reflection (Wesson 1999).

As all plasmas begin in L mode, the transition of L to H mode is seen by the antenna as a sharp decrease in coupling. Experimental studies (Monahkov 2003) on the JET A2 antennae using fast data acquisition suggests an approximate 50% base load reduction in coupling and an associated approximate 2cm increase in strap equivalent length. This can occur in a time frame as short as approximately 10ms. A typical trace showing an H-L-H mode transition is shown in Figure 7, where the strap is modelled as a resistive load seen through an equivalent length of a 30Ω transmission line. It should be noted that the millisecond response rate of the disturbances is insignificant in response to the MHz RF. Therefore, no circuit transient dynamics are included in the analysis.

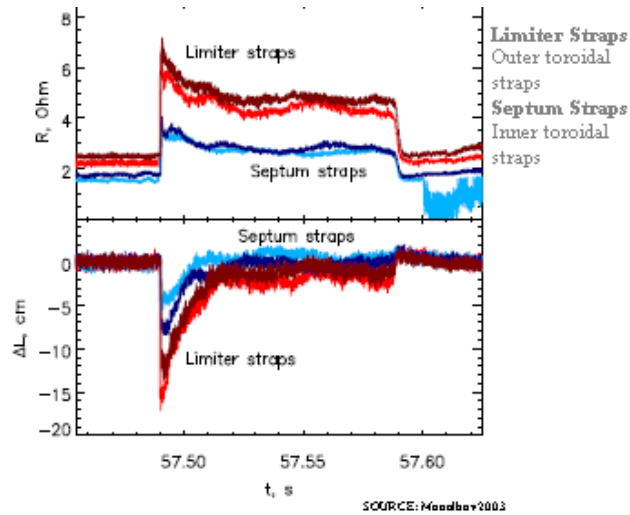


Figure 7: H-L-H mode transition electrical response (42.1 MHz, JET A2 antenna)

As the L-H transition requires additional heating to be sustained, the antennae must continue to couple power throughout this disturbance.

ELMs: The ELM is an instability of the plasma edge associated with H-mode plasmas only. It is characterised by a poloidally localised cyclical collapse in the density gradient of the plasma edge, at a frequency of between 1-40Hz. This appears as plasma filaments expelled from the main plasma and following the magnetic field.

The scale of the release of plasma is inversely proportional to the frequency, with small “grassy” ELMs occurring at high frequency, and “giant” Type 1 ELMs at low frequency. The duration of an ELM is of order 2-5ms. Electrical models of the impact of the ELM are not well developed, but the collapse of the edge brings plasma well within the evanescent field of the antenna, and so coupling increases. Experimental measurements (Monakhov 2003) observed that:

- There is a significant effect on coupling, of up to 7Ω difference.
- There is a significant decrease in equivalent length of the A2 antenna transmission line model of around 40cm.
- The change of coupling impedance with time throughout an ELM varies from ELM type to type
- The electrical disturbance on the A2 antenna is of similar scale for all ELMs, regardless of type (type of ELM denoted by the $D\alpha$ radiation diagnostic – see Figure 8)
- No change to mutual coupling was detected between toroidally adjacent antennae.
- Change in coupling was frequency independent.
- The asymmetric loading of the A2 antenna can change during ELM in a variable fashion.

Typical traces of ELMs illustrated below demonstrate the high variation of traces between ELMs, and the pronounced variation in resistive loading and appreciable change in electrical length (reactive part).

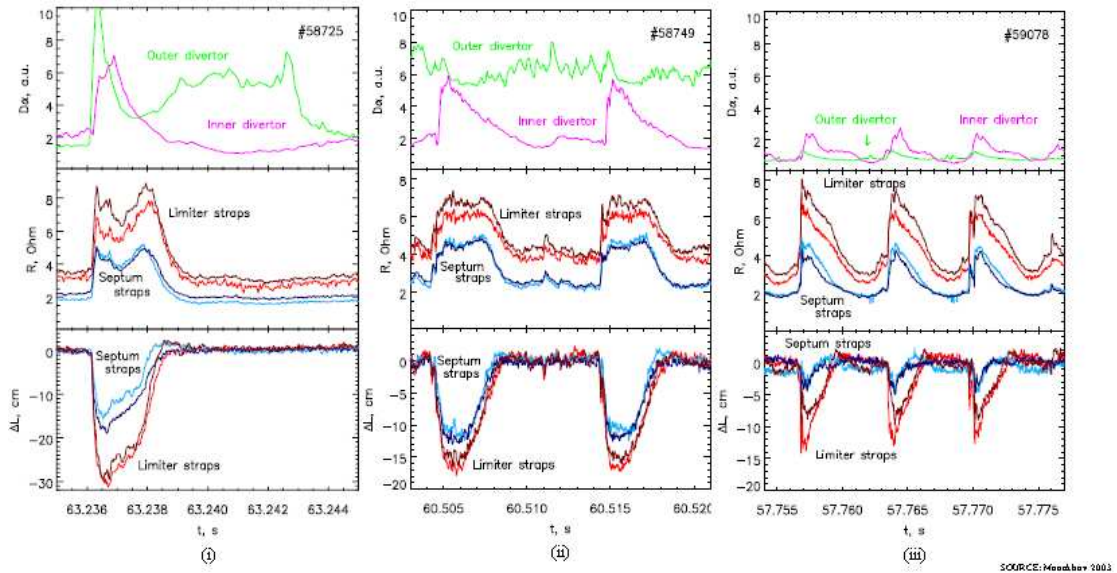


Figure 8: Examples of ELM behaviour for the JET A2 Antenna (i) Type 1 (ii) "Type III" (iii) "Grassy"

It should be stressed, however, that the above data was collected from the JET A2 antenna, and extrapolation from one antenna geometry to another is dangerous. The above data can only be used as a guide.

2.5. Strategies to enhance load variation tolerance

The objective of any Antenna control system is to:

- Control the generator frequency for the required plasma resonance chord
- Control the output power to an operator command level by varying the driving voltage (within limits of anode current and max line voltage)
- Match the circuit to the antenna load, with high disturbance rejection so that the L-H mode transition is matched within 100ms ($1/5^{\text{th}}$ of a typical confinement time, Durodie (3))
- Control the relative phasing of toroidal antennae arrays (complicated by mutual coupling and interaction with power control)

This report concerns only the matching control of ICRH systems. As summarised in 2.3.2, ICRH antennae do not resonate in vacuum, and consequently are matched to the generator by a highly tuned matching circuit. General matching solutions are pre-calculated and configured offline. Such matching networks are typically variations on classic stub – transformer phase shifter matching circuits, as reported by Lamalle (2003) JET ILA 2nd stage match or Hofmeister (1994) on the ASDEX upgrade. In such configurations the real part of the load is transformed to the line characteristic impedance using fixed $1/4\lambda$ transformers and trombones. The residual reactive element is eliminated by variable stubs.

However, as discussed in 2.4, the load seen by the antenna varies throughout the pulse, and is subject to fast transient variations. The combination of a highly tuned circuit and significant load variations results in a large reflected power.

Such transient reflections are detected by the antenna protection interlocks, as summarised in section 2.3.2. The excessive transient reflections induced by ELMs prompt the interlocks to shut down the generator momentarily. However the cumulative effect of these outages is a large decrease in duty cycle, reducing the average delivered power.

Therefore, automatic matching is required to i) compensate for inaccuracies in the pre calculation ii) follow base load variations, & iii) disturbance rejection from plasma instabilities.

The classic matching components discussed above require large stroke lengths and are generally insufficiently fast to achieve the required settling time specification. A number of solutions have been developed to address this issue. These are summarised below:

Coupling Resistance Feedback & frequency control: This method pioneered on JET (Wade 1994) changes the frequency of the RF to alter the location of the standing waves in the matching circuit. This is used to eliminate the reactive part of the matched load. The plasma radial location is then varied to provide independent control over coupling resistance and so match the real part of the load. The response of both actuators involved (oscillator & field coils) are very fast, and hence this method has successfully achieved matching across the L-H transition. However, plasma position and the resonant chord of the plasma both become coupled to the antenna operation and this may be undesirable for certain experiments. Additionally, the very fast transients involved with ELMs are beyond the response rate of the actuators.

Fast Ferrite Tuners: The electrical length, and hence phase delay, of a transmission line is dependent on the wave velocity. Velocity in turn is dependent on the magnetic permeability and dielectric constant of the conductor inter-space. Compact phase shifters have been developed that utilise ferrite in the inter-space, whose magnetic permeability can be varied by an applied magnetic field. Therefore the wave speed is varied electrically, and thus the FFT behaves like a compact phase shifter with no moving parts. Successful test have been reported by Lin (2008) showing the successful tracking of the L-H mode transition. However, ELMs again, have a dynamic range beyond that which may be compensated for in real time, and the devices present many practical challenges that have limited their use.

Liquid filled Tuners: As above, the electrical length of a transmission line is dependent on the properties of the dielectric. Vertical stubs or transmission lines of fixed length can have a controllable phase delay by pumping in variable level of a

fluid dielectric such as silicon based oil. This solution is still under development, with high power static tests reported by Yoon (2007), and low power dynamic tests by Saito (2006)

3dB splitters: This strategy adopts a passive disturbance rejection methodology. In this approach, one generator feeds two straps (or antennae) via a 3dB splitter. This is realised as a section of edge coupled transmission line, so that forward power is distributed 50:50 on the two output ports with a 180° phase shift (Pozar 2005). Likewise, reflected power is coupled to a sister “dump” port terminated in a matched load. Therefore transient reflections are not conducted back to the generator, yielding a more robust system. This approach is adopted on, amongst others, ASDEX upgrade (Wesner 1998). However, this dumping of reflections reduces the average power transferred to plasma, unless an automatic matching system is included downstream of the splitter as in the JET ILA (Durodie 2005). Additionally, it requires a balanced junction, so differential load control may be necessary.

Conjugate T matching: This method again achieves a passive disturbance rejection. The approach seeks to connect two straps in parallel with a tuning component on each arm. If properly configured, a symmetrical disturbance to both straps will result in the reflected power destructively interfering at the T point. The advantage of this methodology is that power is coupled to the plasma even through a disturbance, and not dumped on a dummy load as with the 3dB splitter. This report primarily focuses on the control of the CT circuit.

2.6. Conjugate T (CT) resilient architectures

2.6.1. CT architecture overview

The CT control methodology is based on the Resonant Double Loop (RDL) architecture. This comprises two straps connected in parallel with an active tuning component on each arm. This was initially developed to increase the power density of antennae (Hoffman, 98), although it was later found that if properly configured the load variation tolerance, or resilience, of the matching circuit was significantly improved (Bosia, 2003).

Rather than follow transients by active compensation of the matching elements, the CT design minimises reflections by resonating this power between the two parallel straps. This condition is met when one arm of the RDL is inductive, and the other capacitive. Thus, a symmetrical disturbance to both straps will result in the reflected power destructively interfering at the T point. Therefore, the CT design is inherently load resilient. Two CT architectures exist, those being in-vessel matching, and ex-vessel matching as discussed below. This configuration is shown electrically in Figure 9.

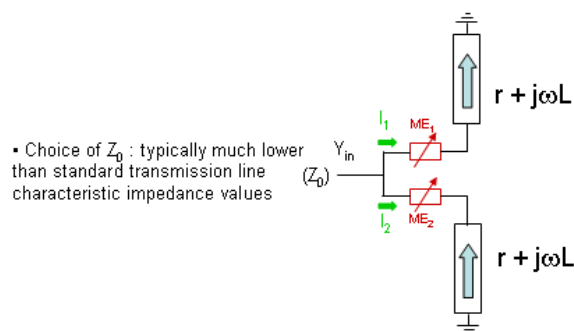


Figure 9: Simplified electrical circuit for the CT architecture

Ex-vessel matching, as reported by Monahkov (2005), places tuning elements, typically trombones, outside of the antenna structure. This enables modular stock tuning items to be used, and as each arm is typically connected to arrays of straps the circuit has greater loading. However, the remote location of the CT junction results in the requirement for large stroke, bulky devices. This limits their dynamic response (unless an FFT were used) and increases the amount of RF infrastructure.

In-vessel matching strives to achieve a compact matching configuration located immediately to the rear of the straps. The compact geometry enables a low stroke actuator to be used, typically a capacitor, as dimensions are small with respect to the wavelength. Therefore, the transmission line electric fields are minimised (with consequently high fields in the capacitor where superior vacuum insulation and build quality confer a superior break down limit). Additionally, the low stroke enables fast matching to track plasma base load variations. Finally, the compact realisation results in less RF infrastructure and a lower standing wave ratio on the transmission line (Bremond, 2001). However, the complexity of the antenna itself is significantly increased, and the CT circuit is less loaded (each strap is connected in a CT circuit)

This study adopts as reference an in-vessel matched antenna. The antenna model used is loosely based on the JET ITER Like Antenna (ILA), as reported by Durodie (2005). However, not all aspects are captured in their entirety, rather the ILA was taken to provide candidate realistic values for parameters.

2.6.2. JET ITER Like Antenna (ILA)

The ILA consists of a tightly packed 4x2 array of straps, needed to deliver a high power density of $\sim 8\text{MW/m}^2$. Poloidally adjacent straps are connected in a conjugate-

T (CT) configuration by feeding them through variable capacitors from a common vacuum transmission line (VTL). This forms a resonant double loop (RDL). The antenna array therefore comprises eight straps (1 – 8) and four RDLs (P-S) as shown in Figure 10.

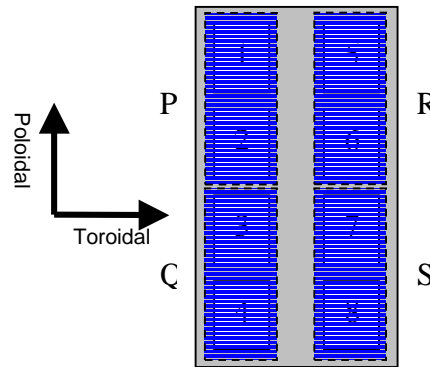
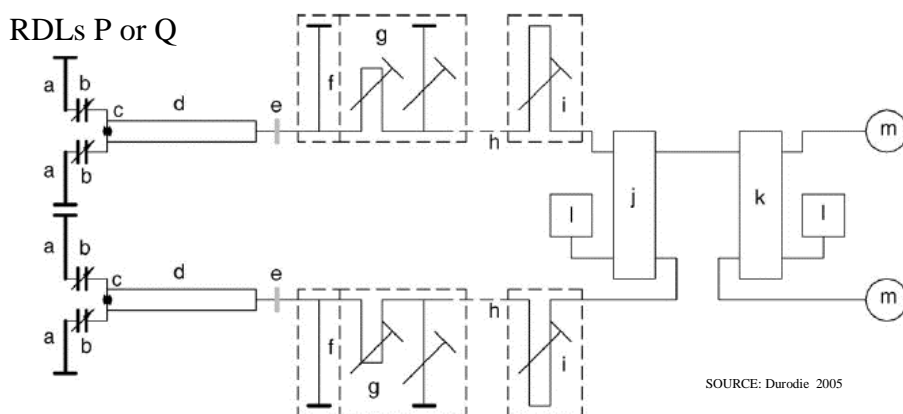


Figure 10: ILA Antenna array showing strap & RDL I.D. (as viewed looking toward plasma)

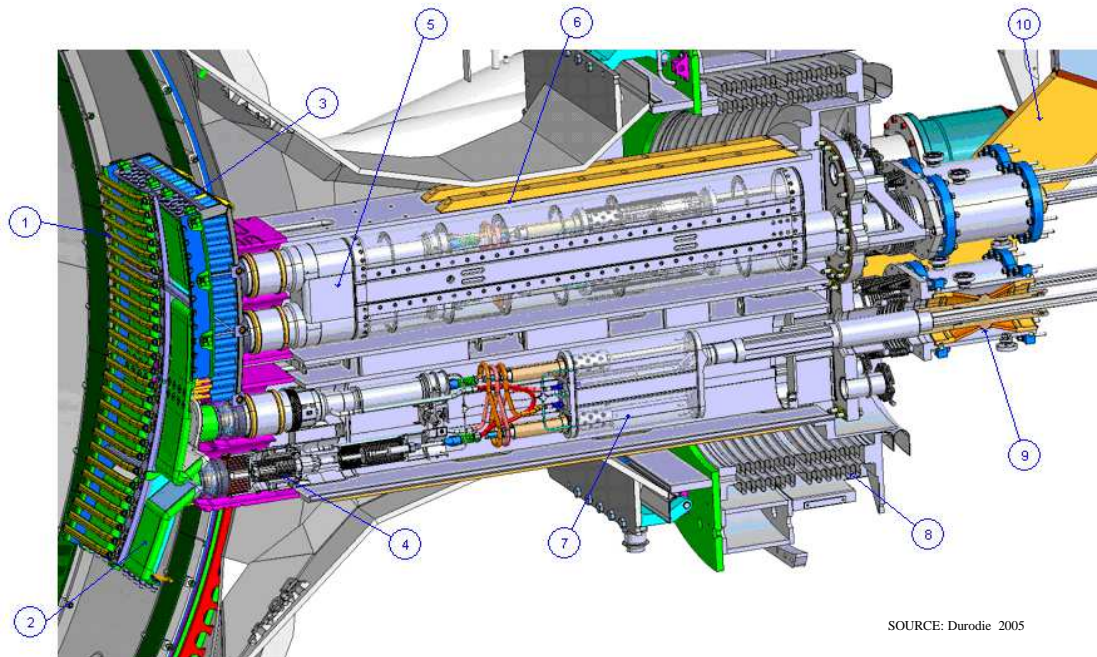
Matching is physically achieved by driving the RDL variable capacitors by hydraulic actuators. Due to physical design limitations, the drive system and feedback sensors were located remotely from the capacitors. The RF circuit of the antenna is poloidally symmetric. The circuit diagram for one poloidal half is shown in Figure 11. The parameters of each sub component is summarised in Table 1.



SOURCE: Durodie 2005

RDLs R or S

Figure 11: RF circuit diagram of one poloidal half of the ILA.



SOURCE: Durodie 2005

Figure 12: Poloidal cut illustrating mechanical realisation of one toroidal half of the ILA:

The mechanical implementation of the in-vessel matched RDL is illustrated in Figure 12. The key features of the antenna are: (1) faraday screen protective shield, (2) straps, (3) antenna housing, (4) matching capacitors, (5) inner VTL, (6) outer VTL & support, (7) hydraulic actuator system, (8) main vacuum sealing bellows, (9) high power RF vacuum feedthroughs, (10) support structure.

It should be noted that the 2nd stage match is not entirely displayed in the above section, as it is located ex vessel. This consists of the low impedance $1/4\lambda$ fixed transformer ('d' as per Figure 11, (5) in figure 3), a fixed stub ('f'), and a variable stub & trombone ('g').

The present control methodology of the ILA is described by Durodie (M65). The control methodology has two components, an open loop resilience control system, and a closed loop matching control system.

For resilience control, an optimal T point impedance is calculated pre-pulse, using target plasma parameters, calculated antenna loading, and a detailed calibration of the antenna. The two elements of the second stage match are then configured to transform this target impedance to 30Ω .

For matching control the T point impedance is measured, and the two capacitors of the RDL are controlled to deliver the pre-calculated T point impedance, and so complete the matching arrangement.

However, this inherently limits the circuit to be optimally resilient at one plasma load only, whereas the base load is known to vary throughout the pulse as described in section 2.4. The ILA algorithm addresses this by setting the H-mode ELM affected plasma as the reference matching impedance for two reasons.

Firstly, the L mode does not give rise to ELMs and so presents a quiescent load sympathetic to the generators and so a less resilient system response is required.

Secondly, the response of the CT circuit to varying load is asymmetric about the matched location, as shall be discussed in section 3. The sensitivity of the circuit to increasing loads is significantly lower than that for decreasing loads. Therefore matching to the lowest base load anticipated (H mode) means that the resulting steady state reflection encountered in off design plasma loads (L mode) is minimised. Additionally, this adds “padding” to the system so that the L-H mode transition does not introduce large reflections.

Table 1: RF Circuit Parameters for the ILA

Item	Description	Purpose	Parameters
a	Strap	Couples RF to plasma	30cm, 2-3Ω/m, 50cm of 200nH/m
b	Variable Capacitor	Active tuning element for RDL	C: 80 – 300pF, parasitic L: 20nH
c	CT Junction	Connects two strap & tuning element combinations in parallel	Modelled as transmission line, 0.14m, 20Ω characteristic impedance
d	¼ wave low impedance VTL	¼ wave transformer converts low CT impedance (as required for load resilience) to main feed transmission line characteristic impedance	1.765m, 9.5Ω characteristic impedance
e	½ wave transmission line inc Vacuum Window	Air pressurised transmission line (APTL). Window provides mechanical support & vacuum boundary	3.53m, 30Ω characteristic impedance
f	Fixed service stub	¼ wave low impedance stub. Used for services access and to improve frequency response of the fixed transformer (elements d – f)	1.765m, 12Ω characteristic impedance
g	2nd stage matching circuit	Phase shifter & stub. Not part of the real time RDL control system. Pre set to cancel reflections from the fixed transformer as a function of frequency. Located on platform immediately to rear of the antenna	STUB: 0.13-3m, 30Ω Trombone: Δ1.5m stroke
h	Main transmission line	Connects antenna to generator hall	30Ω characteristic impedance

i	Main phase shifter	Used to vary toroidal phasing of the antenna and to compensate for the induced π rad phase delay of the hybrid splitter. Infinitely variable but typically only discrete settings are used. Variable poloidal phasing is not employed [not really true : we do (will) use it to compensate poloidal cross coupling]	0 – π rad toroidal phase difference π rad fixed poloidal phase difference: P: 0 rad , Q: $-\pi$ rad, R: $-\pi$ rad, S: 0 rad
j	3dB Hybrid Splitter	Splits the power between two RDL's and enables passive load resilience by introducing a dummy load for reflected power	4MW in - 2MW per RDL
k	3dB Hybrid combiner	Combines two generators in to one RF source in order to feed (j)	2MW – 4MW
l	Dummy Load	Reflected power is diverted from generator to a dummy load to prevent generator trip	
m	RF source		2 MW Max VSWR of 3 transient, OR max reflected power of 130kW Max VSWR of 1.5 steady state 30 – 55 MHz

3. Conjugate T (CT) circuit model

3.1. Lumped element CT circuit

3.1.1. Circuit description

For JET EP the basic CT circuit is achieved by mounting variable capacitors as matching elements immediately behind poloidally adjacent straps. The T point is directly to the rear of the capacitors.

Therefore, an initial approximation can assume:

1. The straps have different geometries, and so coupling asymmetries exist.
Therefore $R_1 \neq R_2$
2. The geometry of the CT circuit is small in comparison to the wavelength.
Therefore no phase delay due to transmission lines is considered between the T point and strap.
3. Straps & capacitors can be absorbed in to one lumped parameter model where resistance is fixed and impedance varied (by altering the capacitor).
4. The T point can be considered ideal, with no reflections or cross coupling.
5. The currents on the two straps are mutually coupled.

The resulting simplified equivalent circuit is shown in Figure 9. Typical parameters are shown in Table 2.

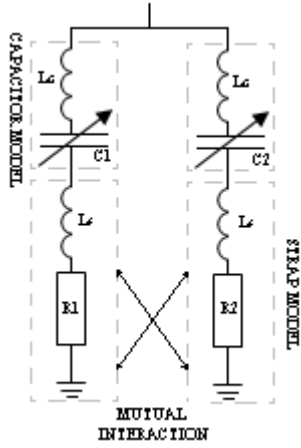


Figure 13: Simplified equivalent circuit

Parameter	Description	Value
Lc	Parasitic capacitor inductance	20 nH
C	Variable Capacitor	80 – 300 pF (0-55mm stroke)
Ls	Strap Inductance	100 nH (50cm of 200 nH/m)
R	Coupling Resistance	0.6 – 0.9 Ω (2-3 Ω/m)
f	Frequency	30 – 55 MHz

Table 2: Typical circuit parameters

For modelling purposes, the strap inductance includes 20cm of transmission line connected to the capacitor. This explains the discrepancy between lengths used for the calculation of strap resistance and inductance. For modelling purposes, strap inductance and capacitor parasitic inductance were combined to form one inductor.

The capacitor construction is summarised in section 2.3.2, where the stroke is linearly proportional to the capacitance. Therefore, the capacitor was modelled as the following simple linear relationship between stroke range & capacitance range, where ‘s’ is the stroke in millimeters, and ‘C’ is in Farads:

$$C = (4.074s + 80) \times 10^{-12} \quad [9]$$

The modelling of the mutual coupling is summarised in section 3.1.3

3.1.2. Definition of resistive asymmetry

Resistive asymmetry affects the antenna performance, and so a mathematical definition of this was required for modelling purposes. This study defines resistive asymmetry as a symmetrical skewing of resistance about a predefined average coupling. Therefore, the strap resistance of section 3.1.1 can be described as:

$$R_1 = a \cdot \bar{R} \quad [10]$$

$$R_2 = b \cdot \bar{R}$$

where \bar{R} is the average strap resistance, and 'a' and 'b' are skewing coefficients.

Therefore, the percentage asymmetry, 'p', is defined as:

$$\frac{a-b}{a} = p \quad [11]$$

where 0 indicates a symmetrical circuit, and 1 an infinitely asymmetric circuit. The requirement for resistance to be symmetrical about a defined average coupling, \bar{R} , implies:

$$\frac{R_1 + R_2}{2} = \bar{R} \Rightarrow \frac{a+b}{2} = 1 \quad [12]$$

Combining equations 11 & 12 provides the definition of the skewing coefficients with respect to the asymmetry circuit parameter:

$$a = \frac{2}{(2-p)} \quad [13]$$

$$b = \frac{2(1-p)}{(2-p)} \quad [14]$$

3.1.3. Equivalent circuit model including mutual coupling

The antenna straps are not perfectly shielded one from another, and so electrically interact. The presence of these mutual impedances can drastically affect the electrical characteristics of the RDL. Mathematically, the action of mutuals is defined as follows:

$$\begin{bmatrix} V_T \\ V_T \end{bmatrix} = \begin{bmatrix} Z_1 & Z_{12} \\ Z_{12} & Z_2 \end{bmatrix} \cdot \begin{bmatrix} I_1 \\ I_2 \end{bmatrix} \quad [15]$$

where ‘ V_T ’ is the voltage at the T point, ‘ Z_n ’ the impedance of arm ‘ n ’, and ‘ Z_{12} ’ the mutual impedance between the two straps. It should be noted that the Z matrix includes the action of the matching capacitors. The mutual impedance contains both real and imaginary parts, and the circuit assumes coupling symmetry, i.e. plasma gyrotropic effects are negligible for poloidal neighbors. Applying Kirchoff’s current law to the T point junction yields:

$$V_T = Z_T(I_1 + I_2) \quad [16]$$

where ‘ Z_T ’ is the Thevinin impedance of the RDL as a lumped element. Combining equations 15 & 16 yields two simultaneous equations:

$$\frac{I_1}{I_2} = \frac{(Z_T - Z_{12})}{(Z_1 - Z_T)} \quad [17]$$

$$\frac{I_1}{I_2} = \frac{(Z_T - Z_2)}{(Z_{21} - Z_T)} \quad [18]$$

Therefore, the equivalent Thevinin impedance of the antenna can be derived, and all analysis of the circuit replaces the antenna as a lumped impedance at the end of a given matching network.

$$Z_T = \frac{Z_{12}^2 - Z_1 Z_2}{2Z_{12} - (Z_1 + Z_2)} \quad [19]$$

As can be seen, the above expression decomposes to the conventional $Z_1 Z_2 / (Z_1 + Z_2)$ of a parallel circuit when mutuals tend to zero. It should be noted that for this study, only one RDL was considered, and therefore the approach does not include inter RDL mutual coupling.

Values of ‘ Z_{12} ’ were provided by the JET ILA team from physical calibrations performed on the antenna. For this study, the mutual coupling impedance was represented by a percentage of the strap base load impedance for the purposes of parameter scans. The impedance matrix supplied for the whole antenna is shown in Appendix B. Representative values of Z_{12} were extracted from this.

3.2. 2nd Stage Matching Circuits

Two methodologies were adopted for modelling the action of the 2nd stage matching circuit.

The first is valid only with purely resistive changes to the straps. Mathematically, if the second stage transforms a given impedance to the line characteristic impedance when viewed from the generator, then it must also transform the line characteristic impedance to a matched T point impedance when viewed from the antenna.

Thus, a simple approach to modelling the action of the 2nd stage match is to replace the second stage with a transmission line of characteristic impedance equal to the Thevinin impedance of the antenna in the matched state. Thus:

$$Z_0 = Z_{T_MS} = \frac{Z_{12}^2 - Z_{1_MS}Z_{2_MS}}{2Z_{12} - (Z_{1_MS} + Z_{2_MS})} \quad [20]$$

where the subscript ‘MS’ denotes the match set-point values required for the correctly configured CT circuit (where $\text{Im}(Z_{T_MS})=0$), which are derived for the ideal circuit in section 4.

However, for reactive changes to the load (where $\text{Im}(Z_{T_MS}) \neq 0$) the above method proved problematic, as it creates a negative resistance, and so for such circuits a more accurate model was required. The JET ILA has a more sophisticated

2nd stage match involving fixed sections of a $1/4\lambda$ transformer and stub, and a classic stub-transformer match. This confers superior bandwidth and reduced strokes for the dynamic sections, however for the purposes of this study the solution was simplified to a basic transformer & shunt stub match of unlimited stroke with characteristic impedance ‘ Z_0 ’ of 30Ω .

The required transformer length ‘ d ’ to match to the real part of the antenna Thevinin impedance ‘ $R_L + jX_L$ ’ was calculated by:

$$\frac{d}{\lambda} = \begin{cases} \frac{1}{2\pi} \tan^{-1} t & \text{for } t \geq 0 \\ \frac{1}{2\pi} (\pi + \tan^{-1} t) & \text{for } t < 0 \end{cases} \quad [21]$$

where ‘ t ’ is defined as the lower of the following two possible values:

$$t = \frac{X_L \pm \sqrt{R_L [(Z_0 - R_L)^2 + X_L^2] / Z_0}}{R_L - Z_0} \quad [22]$$

The required stub length ‘ l ’ to cancel the residual imaginary part of the transformed antenna Thevinin impedance was calculated by:

$$\frac{l}{\lambda} = \frac{-1}{2\pi} \tan^{-1} \left(\frac{1}{Z_0 B_s} \right) \quad [23]$$

where ‘ B_s ’ is defined as:

$$B = \frac{(Z_0 - X_L t)(X_L + Z_0 t) - R_L^2 t}{Z_0 [R_L^2 + (X_L + Z_0 t)^2]} \quad [24]$$

The full derivation is a standard RF solution, and is included for completeness alongside the associated matlab code in Appendix A. The equivalent antenna model was thus:

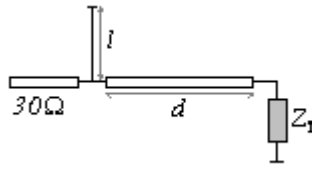


Figure 14: Equivalent circuit for one RDL

3.3. Models of plasma disturbance

Coupling models are based on experimental data, rather than analytical models. Therefore, base load is defined as a constant combination of arm resistance and reactance with complex mutual interaction. The base values can be modified by a coefficient representing transient events, as shown in equations 25 & 26. These transients are assumed to be i) faster than the reaction of the tuning elements, and therefore these remain fixed, and ii) significantly slower than the electrical transient response of the circuit, as discussed in section 2.4. Therefore steady state analysis is used to assess the impact.

Two models were used for evaluating disturbances. The first assumes that the disturbance is purely resistive. This is consistent with early CT circuit assessments (Evrard 2005). Therefore the strap loading may be represented as:

$$Z_{s,n} = \lambda R_n + jX_s \quad [25]$$

where ‘ $Z_{s,n}$ ’ is the strap impedance, ‘ n ’ the arm I.D. (1 or 2), ‘ X_s ’ the strap reactance, and ‘ λ ’ a real scaling coefficient > 1 called the load multiplication factor.

A second more realistic model allows for variation in reactance. In this case

$$Z_{s,n} = \lambda R_n + jkX_s \quad [26]$$

where ‘ k ’ is a real scaling factor coefficient < 1 . It should be noted that in the modeling ‘ X_s ’ was a lumped parameter including feeder & capacitor parasitic inductance for simplicity.

No published data exists for the ILA on the disturbance due to ELMs. In the absence of experimental data, or analytical models of ELM behavior the following assumptions were made:

- This study adopts values for λ & k consistent with ITER studies for a similar short strap design (Lamalle 2005). Therefore, λ is approximately 4-5, and k is approximately 0.75 – 0.9
- Monakhov (2003) reports that for the JET A2 antenna that the dynamic relationship between λ & k is not constant during an ELM and varies from ELM to ELM .
- Monakhov reports no influence on mutual coupling, therefore Z_{12} is assumed ELM invariant
- Monakhov reports mild variable effects on asymmetry. These have been neglected in this study for simplicity

The above assumptions are not ideal, and should be reassessed once experimental data on the ILA is collected.

4. Resilience performance indicator

4.1. Definition of resilience

The CT circuit was conceived to improve resilience of circuits when exposed to a variation in real loading. Therefore, this study began with that assumption and adopted a plasma disturbance as per equation 25. This is consistent with earlier modeling of the ILA for control purposes (Durodie Memo 65 & 68).

The critical reflection limit used by Durodie was a Voltage Standing Wave Ratio (VSWR) of 1.5. This corresponds to the generator steady state reflection rating, which is adopted for this analysis.

Therefore, this study defined resilience as the load multiplication factor (λ as per equation 25) necessary for the VSWR to exceed the critical limit of 1.5.

4.2. Derivation of optimal set-points for ideal circuits

In this analysis ‘optimal’ is defined as maximally resilient for a given perfectly matched system. To derive the set-points required to deliver this state for a generic CT circuit is exceedingly complicated. Therefore, set-points are here derived for an ‘ideal’ circuit, with no mutual impedance, symmetrical resistive loading, & purely resistive load variations.

For such a circuit, the set points for the arm impedances may be derived from the following constraints:

1. The CT circuit Thevinin impedance should be real (this assumption is validated later – see section 4.3.1)

2. The real component of the circuit impedance should equal the system characteristic impedance (no reflections at design load)
3. The characteristic impedance is chosen to maximise resilience.

Consider first the CT circuit in terms of admittance:

$$Y_T = Y_1 + Y_2 = (G + j.B)_1 + (G + j.B)_2 \quad [27]$$

$$\text{where: } G = \frac{R}{R^2 + X^2} \quad [28]$$

$$\text{and: } B = \frac{X}{R^2 + X^2} \quad [29]$$

For a perfect match the CT impedance should be real (as per constraint #1 above). Therefore equating the imaginary part of equation 27 to 0 and substituting in for equations 28 & 29 yields:

$$\left[\frac{X_1}{R^2 + X_1^2} + \frac{X_2}{R^2 + X_2^2} \right] = 0 \Rightarrow X_1 = -X_2 \quad [30]$$

A second solution of $X_2 = -R^2/X_1$ is excluded, as with this solution the admittance of the RDL is invariant of arm reactance X, and hence overly constrained. Therefore, for the ideal CT circuit the net arm reactances should be equal and opposite, and Y_T becomes:

$$Y_T = \frac{2R}{R^2 + X^2} \quad [31]$$

where $X = |X_1| = |X_2|$. Applying the philosophy of the simple 2nd stage match as in section 3.2, the correct value of characteristic impedance can be derived from considering the reflection coefficient, Γ .

$$\Gamma = \frac{Y_T Z_0 - 1}{Y_T Z_0 + 1} \quad [32]$$

Substituting equation 31 into equation 32 yields:

$$\Gamma = \frac{2RZ_0 - R^2 - X^2}{2RZ_0 + R^2 + X^2} \quad [33]$$

The VSWR, ('S' in this nomenclature) is defined as:

$$S = \frac{1+|\Gamma|}{1-|\Gamma|} \quad [34]$$

Plotting VSWR against strap loading 'R' illustrates the relationship between branch impedance 'X' (and hence antenna Thevinin impedance) and resilience. The following figure displays a variety of response plots. The x axis captures the load multiplication factor 'λ' from equation 25. Hence all plots are perfectly matched at '1'.

Resilience is expressed in load multiplication factor, as in section 4.1, and is denoted by an arrow on the diagram. The critical VSWR limit is denoted by the horizontal line.

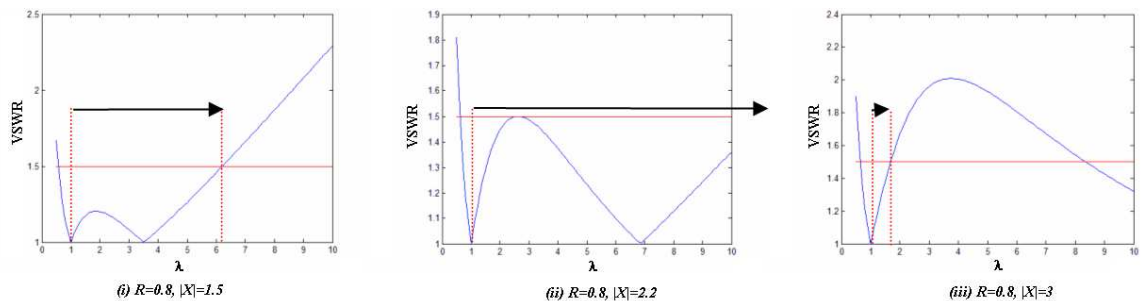


Figure 15: VSWR vs. λ for a selection of arm reactances

As |X| increases (i), resilience initially increases until the local maxima VSWR is equal to the critical maximum VSWR of 1.5 (ii). Further increase in |X| results in a catastrophic collapse of resilience (iii).

Therefore for maximum resilience the characteristic impedance at the T point should be selected such that the local maximum of |Γ| (and hence VSWR) coincides

with the critical cut off reflection coefficient, defined as $|\Gamma_c|$ (and by definition at the critical VSWR, S_c).

Therefore to identify the local maxima of S , the derivative of $|\Gamma|$ (equation 33) with respect to strap resistance shall be zero, thus:

$$\frac{d|\Gamma|}{dR} = \frac{\left[(2RZ_0 + R^2 + X^2) \frac{d}{dR} (2RZ_0 - R^2 - X^2) - (2RZ_0 - R^2 - X^2) \frac{d}{dR} (2RZ_0 + R^2 + X^2) \right]}{(2RZ_0 + R^2 + X^2)^2} = 0 \quad [35]$$

This simplifies to:

$$R = X \quad [36]$$

Therefore, the optimal value of the antenna Thevinin impedance (and desired characteristic impedance) can be derived by setting $|\Gamma|$ to $|\Gamma_c|$ when $R = X$, thus:

$$|\Gamma_c| = \frac{S_c - 1}{S_c + 1} = \frac{2RZ_0 - R^2 - X^2}{2RZ_0 + R^2 + X^2} \quad [37]$$

Substituting equation 36 in to equation 37 yields:

$$Z_0 = X \cdot S_c \quad [38]$$

Finally, the optimal value of X may be deduced by equating the real part of the antenna Thevinin impedance (equation 31, where $Z_T = 1/Y_T$) to the calculated optimal characteristic impedance. Thus, combining equations 31 & 38 yields:

$$X = R \left(S_c \pm \sqrt{S_c^2 - 1} \right) \quad [39]$$

Substituting equation 39 into equation 38 expresses the required characteristic impedance in terms of fixed circuit parameters, as in equation 40 below. Therefore the conditions for an optimal ideal CT circuit are summarised in Table 3.

The derivation was successfully validated by plotting VSWR against load multiplication factor for a range of strap design resistances (an example of which is

shown above, Figure 15(ii)). This validated the approach for solutions along the $X_1=-X_2$ locus.

Requirement	Equation	Equation I.D.
CT impedance is real	$X_1 = -X_2$	[30]
Zero reflection at design load	$ X = R(S_c \pm \sqrt{S_c^2 - 1})$	[39]
Maximum resilience at design load	$Z_0 = RS_c(S_c \pm \sqrt{S_c^2 - 1})$	[40]

Table 3: Optimal set-points for the ideal CT circuit

However, to confirm the algebraic approach detailed above was consistent for all combinations of arm reactance, a full 2D investigation of the solution space was required. Additionally, the derivation of ideal set-points for the antenna including resistive asymmetries and mutual impedances was judged too difficult for an analytical solution. Therefore, a numerical solver was required.

There are two distinct requirements for numerical modelling of resilience with the CT circuit. Firstly, a numerical solution of resilience is required to accommodate the effects of the numerous non ideal parameters on the circuit behavior. Secondly, an optimisation routine is required to derive the optimal set points that maximise resilience of any given CT circuit.

4.3. Derivation of numerical solution algorithms

4.3.1. Resilience solver

The resilience solver accepts as its input a given set of circuit parameters, this being average strap resistance, % asymmetry, real & reactive mutuals and an

arbitrary pair of capacitor values for assessment. Mutuals are expressed as a percentage of the fixed arm impedance (Strap R , strap L , feeder & capacitor L) and thus do not include the matching reactance X_c . λ (as per equation 25) is initially set to 1.

The solver thus models the antenna as its Thevinin impedance, given by equation 19, terminating a transmission line of characteristic impedance derived using equation 20.

The solver then enters a loop where λ is increased iteratively, and the resulting VSWR calculated using equations 32 & 19, where $Y_T = 1/Z_T$. The incremental step in λ is dependant on the proximity to the target VSWR of 1.5, decreasing in step as the target approaches. This feature reduces the solve time. Once a crossing of the VSWR=1.5 locus is detected, the solver converges using Newton Raphson.

Unique features of the problem, which forced the writing of a custom solver, are that i) the solution is only valid for $\lambda > 1$, ii) there may be more than one solution for VSWR=1.5, yet only that with the smallest λ is desired, and iii) the desired solution often lies on a local maximum (as per Figure 15 (ii)). Therefore, solvers regularly miss this solution and overshoot to the next intersection, erroneously returning resilience values significantly greater than would be achieved.

Knowledge of the solution locality enabled the solver to specifically accommodate this effect. The solver would detect the presence of a local maximum within a vicinity of the critical VSWR. If detected, the solver would break off searching for the VSWR=1.5 intersect, and instead solve for the local maxima. If this was greater than 1.5 the program would engage the Newton Raphson routine; whereas if the maxima was < 1.5 the solution would re-engage the variable solver.

Using this approach the solution for critical VSWR could be resolved to a fine accuracy within a short solve time.

The solver code and an associated description are recorded in Appendix C.

Using this code, the resilience could be plotted for a selection of total arm reactances (including X_c), as shown in Figure 16 for an ideal CT circuit (load 0.8Ω , resolution 0.125Ω).

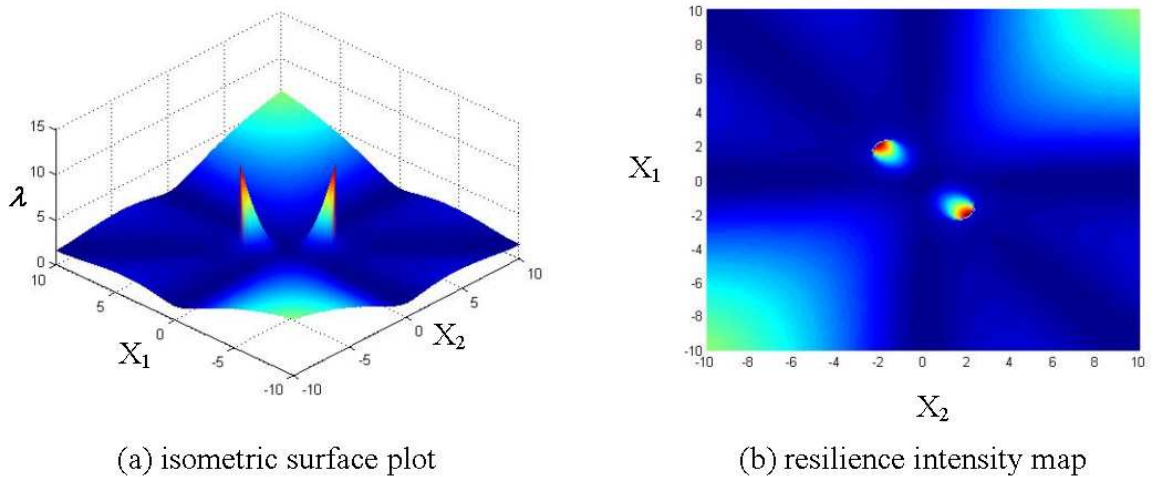


Figure 16: Resilience plotted in arm reactance space

The following conclusions can be drawn from the above plots. Firstly, there are only two equivalent solutions, both lying on the $X_1 = -X_2$ locus, as predicted in section 4.2, and confirming assumption #1 made therein. Secondly, the location of the optimal set-points is highly localised, placing tight accuracy demands on any controller.

4.3.2. Optimal set point derivation

As can be seen from Figure 16, the optimal solution for VSWR lies on a mathematical discontinuity. This effect is caused by the local maximum resilience illustrated in Figure 15 coinciding with the VSWR limit. Increasing $|X|$ further results

in the first VSWR=1.5 intersect jumping from the second positive gradient to the first. This results in a “cliff edge” in solution space.

As the solution is i) highly localised, ii) has multiple local maxima, & iii) lies on a mathematical discontinuity, a custom optimisation routine was required to derive the appropriate set points for configuring the CT circuit.

As traditional gradient ascent methods would be inappropriate given the above constraints, an adaptive mesh solver was developed. The methodology took the design space available to the CT circuit, and meshed it in 2D to form a grid. The resilience at each node was then calculated using the method derived in section 4.3.1, and the maximum value identified.

A window of +/- 2x the initial resolution was then formed around the maximum value, and the design space re-meshed at double the former resolution. At 2x resolution the window was oversized to ensure local maxima did not confuse the solver.

This process was repeated iteratively until a predefined resolution had been achieved. Consequently, a very large solution space could rapidly be assessed and optimal values calculated, without resorting to very fine initial grids. An example of the output of the solver for a non ideal RDL illustrates the adaptive mesh capability. The solver code and an associated description are recorded in Appendix D.

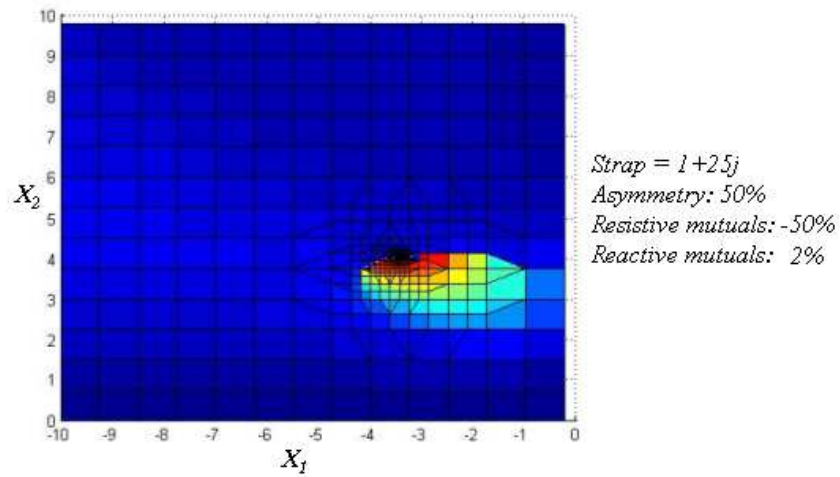


Figure 17: Output of adaptive mesh solver

This code was validated by comparing analytically predicted set-points for a symmetrical ideal RDL, as defined in Table 3, with those numerically derived as above. The results are shown in Figure 18, with spot values compared in Table 4.

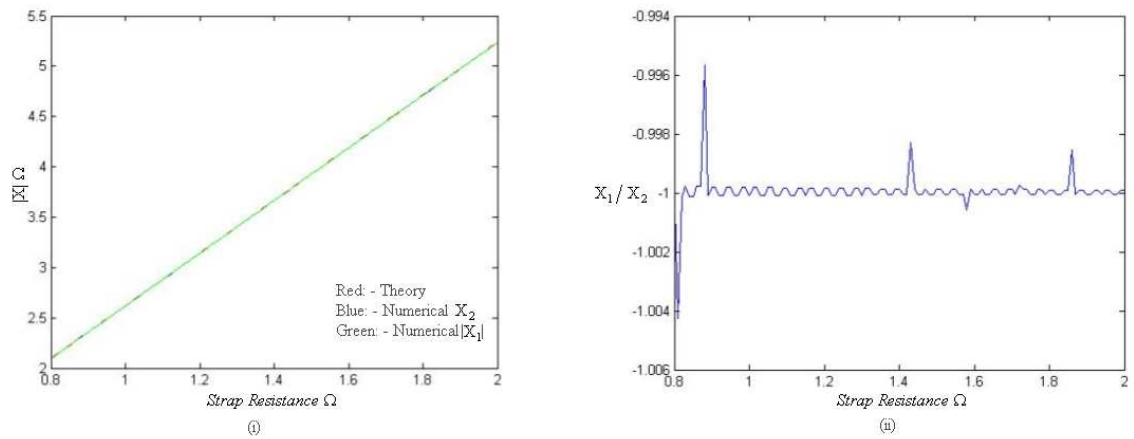


Figure 18: Validation data of adaptive grid solver

Strap Resistance	Algebraic optimal resilience		Numerical optimal resilience	
	X1	X2	X1	X2
0.5	-1.3090	1.3090	-1.3063	1.3062
1	-2.618	2.618	-2.6121	2.6125
1.5	-3.9271	3.9271	-3.9187	3.9192

Table 4: Adaptive grid solver validation data

As can be seen the two results closely parallel one another. Figure 18(ii) illustrates the mild discrepancies between the algebraic & numerical solutions ($X_1/X_2 = -1$ algebraically). Such discrepancies may be attributed to the $\sim 0.001\Omega$ resolution on X & 0.5% error band on VSWR with the numerical resilience solver.

5. Feedback control of optimal resilience

5.1. ILA Control System – Fixed T resilience control

5.1.1. Shortcomings

As discussed in section 2.6.2, the present ILA control methodology has two components, an open loop resilience control system, and a closed loop matching control system.

For resilience control, the second stage circuit is configured pre-pulse to match the optimal antenna Thevinin impedance (equation 40 for an ideal RDL). For matching control the two capacitors of the RDL are varied under closed loop to deliver the pre-calculated T point impedance, where measurements of the real part of the equivalent impedance control the difference in capacitor settings, and the reactive part controls the sum of capacitance settings (Durodie M65).

The algorithm does not necessarily target the matched load, but instead may match to impedances lower than expected. Therefore, this “offset matching” functionality enables greater resilience to increasing loads at the penalty of a fixed VSWR at base load.

However, this open loop approach to controlling resilience suffers from several disadvantages. These are broadly:

1. The average load presented by the plasma changes throughout the pulse, most notably in the L-H transition. An open loop system can only be optimally resilient for one value of load.
2. It is not possible to predict with a high degree of accuracy the actual plasma loading due to the complexity of modelling the plasma. Loading is dependant

on numerous variables as discussed in section 2.4. Therefore the suitability of the pre-calculated T point impedance set point is not guaranteed.

3. Non ideal effects such as RDL resistive asymmetry and strap mutual impedance have a strong influence on the optimal T point impedance set point. These effects complicate the pre-calculation of the optimal set point, as discussed in section 4.3.
4. The non ideal effects are a function of plasma parameters, and as such arguments 1&2 hold when attempting to calculate the optimal T point impedance set point when including the non ideal effects.

If the optimal T point impedance has a low sensitivity to plasma load, asymmetry and mutual impedance, the fixed T approach may be acceptable. The tools discussed in section 4.3 were developed to address this issue.

5.1.2. Fixed – T performance model

A model of the ILA matching algorithm was required to serve as datum for any assessment of performance. This reference model is discussed below.

The selection of offset in the ILA algorithm was at operator discretion and represented another variable for assessment. Therefore, for the purpose of this study the offset was assumed to be 0, enabling a consistent comparison with the automatic matching algorithm.

This study concerned the steady state performance of the control algorithms. Because the dynamics at this stage were not of interest, the ILA control algorithm was not replicated; rather the action of the system in steady state was modelled as follows.

A conventional gradient descent solver was used to derive the values of X_1 & X_2 necessary to give the target T point impedance. This enabled an efficient method so as to minimise computational time and convergence path issues (a source of difficulty with the ILA algorithm development-Durodie M68)

The optimal values of arm reactances \hat{X}_1 & \hat{X}_2 were derived for an arbitrary CT circuit using the adaptive mesh numerical method of section 4.3.2. The target T point impedance for optimal resilience was then calculated using equation 19.

The fixed T solver took an initial combination of target arm reactance $X_{1,i}$ & $X_{2,i}$. About this value a further two “test” reactance combinations were declared, at $(X_{1,i}, 1.01X_{2,i})$, and $(1.01X_{1,i}, X_{2,i})$. This formed a triangular sample area for analysis.

The local T point impedance surface for the three points was then calculated using equation 19. The errors in the solutions were calculated by subtracting them from the target T point impedance. Therefore, this yielded a 3 dimensional error surface which the algorithm sampled at 3 locations.

To determine the correct route to 0 error, partial gradients were taken between the centre reactance combination and the two “test” reactance combinations. The direction of the gradient was extracted only.

Finally, a new arm reactance combination was generated by incrementing $X_{1,i}$ & $X_{2,i}$ by a variable step, using the gradients derived to drive the error toward zero. The step size was dependant on the proximity to 0. This process was iterated until the numerical solution lay within a deadband of the target T point impedance.

As this method can be prone to trapping in local minima, the error space was first plotted to ensure that none were present. The fixed T algorithm is summarised in Appendix E.

5.2. Arm phase control

As the resilient location of the CT circuit is highly localised, it is desirable that, unlike the ILA [at present], the system should bring resilience under closed loop control. As matching is also under closed loop control, this necessitates the inclusion of the 2nd stage match in the real time control system.

Such a system would use the in vessel capacitors to deliver a resilient T point impedance dependant on actual plasma parameters, and the second stage would match the generators to the resulting floating T point impedance.

Matching control of the 2nd stage would be conventional, using a simple PI loop on the stub and trombone. The T point impedance would be measured, and the real part controlled by the trombone to deliver Z_0 , and the imaginary part controlled by the stub to deliver 0 reactance. As this solution is conventional this study will not investigate the matching algorithm. Instead, this study shall investigate the control of the CT circuit to deliver optimal resilience.

Offset matching (deliberately not matching the floating Tpoint impedance to further enhance resilience) will not be investigated at this stage so as to limit the scope of the problem.

The absolute definition of optimal resilience can be derived from analysis of an ideal lumped element conjugate T circuit, of symmetrical resistance, and no mutual coupling. The phasor diagram for the two arms of the circuit is shown in Figure 19:

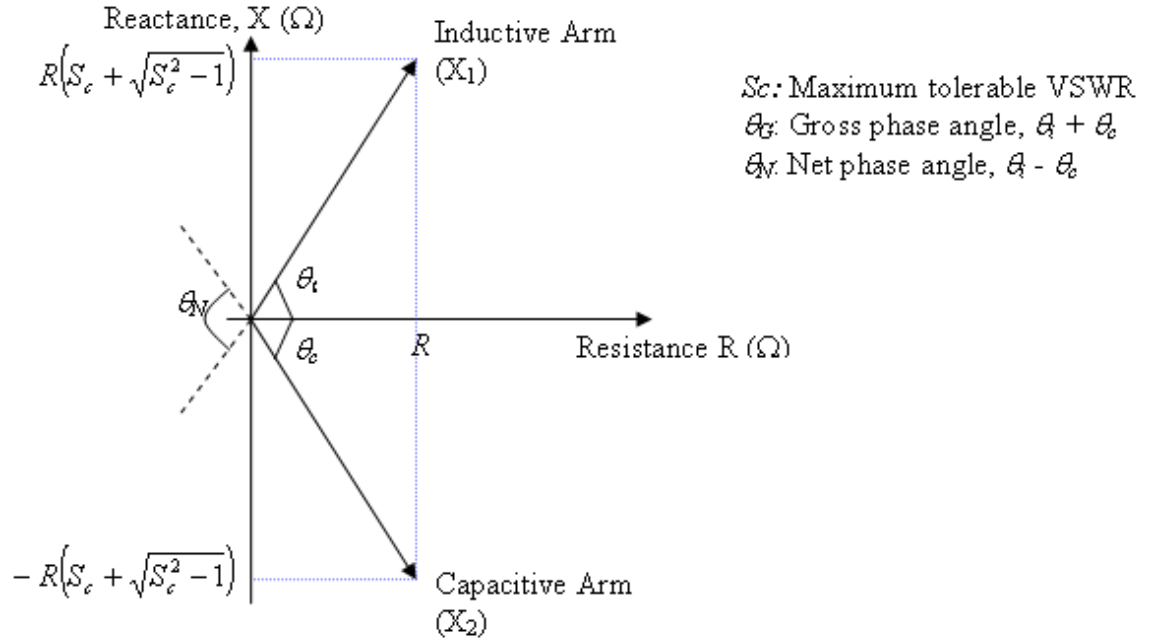


Figure 19: phasor plot for the CT arm impedance

The optimal values of arm reactance are derived as in equation 39, section 4.2. Therefore, the optimal phase of each arm relative to the T point is given by equation 41. As can be seen, this target is independent of plasma parameters, and as such represents the definition of a resilient CT circuit for resistive disturbances.

$$|\theta_i| = |\theta_c| = \tan^{-1} \left[\frac{R(S_c + \sqrt{S_c^2 - 1})}{R} \right] = \tan^{-1} (S_c + \sqrt{S_c^2 - 1}) \quad [41]$$

Therefore, it is proposed that the conjugate T circuit shall be controlled to deliver the correct arm phase targets to deliver optimal resilience, and not a predefined fixed T point.

However, rather than control to the phase across each arm (which would be subject to calibration errors) the algorithm controls to gross and net angle (' θ_G ' & ' θ_N '). As gross angle should be 0 this presents an unambiguous target for the controller. Therefore, the capacitor control set points can be described as the sum

between an average (A) and a difference (D) signal, where the average is the controlled with θ_G as its argument, and the difference with θ_N as its argument.

$$X_1 = A + D = f(\theta_G) + f(\theta_N) \quad [42]$$

$$X_2 = A - D = f(\theta_G) - f(\theta_N) \quad [43]$$

It should be noted that the relationship between arm reactance and the required capacitor set point is not linear. Therefore a formula derived from the calibration model is used to translate the impedance target X_n from the resilience algorithm into a capacitor demand signal. Capacitance as described in equation 9 can be re written as

$$C_n = \frac{\Delta C}{s} x_n + C_{\min} \quad [44]$$

where ' C_n ' is the capacitance of arm ' n ' (1 or 2 from nomenclature of equations 2&3), ' ΔC ' the capacitance range, ' C_{\min} ' the minimum capacitance, ' s ' the actuator stroke and ' x_n ' the capacitor demand signal.

Arm reactance can be expressed as the sum of the variable capacitance and a fixed inductance as in the model in section 3.1.1. Therefore,

$$X_n = \omega(L_S + L_C) - \frac{1}{\omega C_n} \quad [45]$$

Substituting equation 44 into equation 45 and solving for the capacitor demand yields

$$x_n = \frac{s}{\Delta C} \left[\frac{1}{\omega(\omega(L_C + L_S) - X_n)} - C_{\min} \right] \quad [46]$$

As can be seen the position demand is inversely proportional to the reactance set points, with a fixed offset. At present this equation was used to convert the reactance

demand of the algorithm, ' X_n ', into the position demand of the capacitor, ' x_n ', and so linearise the actuator. However, this approach assumes a perfect calibration, and consequent perfect compensation. The physical system cannot guarantee this, and so future studies must assess the algorithm stability with i) no compensation, and ii) sensitivity to imperfect compensation.

It should also be noted that an alternative capacitor configuration where capacitance is varied by adjusting the distance between plates rather than varying the overlapping area requires no linearisation, as reactance demand would be directly proportional to capacitor distance demand, x . However this is applicable only to capacitor matched architectures and presents practical challenges.

Thus, for an ideal stub-transformer matched CT circuit of optimal resilience and zero reflections, the control heuristics are

1. A gross arm impedance phase of 0
2. A net arm impedance phase of 138.2° with reference to the T point (for a maximum VSWR limit of 1.5)
3. A second stage transformer to convert the resulting T point resistance of constraints 1&2 to the transmission line characteristic impedance
4. A second stage stub to cancel the resulting reactance of the T point (if any) to 0.

5.3. Sensitivity studies

5.3.1. Rationale

As observed in section 4.3.1, the set-points for optimal resilience are highly localised. This suggests a tight accuracy requirement for any controller. As discussed

in section 3.1, the ideal circuit is subject to several non ideal parameters. Numerical methods described in section 4.3.2 were developed to quantify this influence of the non ideal parameters. Therefore, a sensitivity study was required to i) ascertain if a fixed T algorithm could capture the uncertainty of plasma loading with one target T point impedance, and, ii) determine if the ideal set-points for arm phase control derived in section 5.2 require modification in the presence of non ideal parameters.

However, as discussed in section 5.2, the least ambiguous definition of resilience is in terms of arm phase angle. Therefore, the solvers of section 4.3 were modified to map reactance space into arm phase space. For this, equation 15 may be re organised to read

$$\begin{bmatrix} I_1 \\ I_2 \end{bmatrix} = V_T \begin{bmatrix} \frac{Z_{12} - Z_2}{Z_{12}^2 - Z_1 Z_2} \\ \frac{Z_{12} - Z_1}{Z_{12}^2 - Z_1 Z_2} \end{bmatrix} \quad [47]$$

Therefore, taking the phase of V_T as reference, the arm phase expressions θ_G and θ_N are given by

$$\theta_G = - \left[\arg \left[\frac{(Z_{12} - Z_2)}{(Z_{12}^2 - Z_1 Z_2)} \right] + \arg \left[\frac{(Z_{12} - Z_1)}{(Z_{12}^2 - Z_1 Z_2)} \right] \right] \quad [48]$$

$$\theta_N = - \left[\arg \left[\frac{(Z_{12} - Z_2)}{(Z_{12}^2 - Z_1 Z_2)} \right] - \arg \left[\frac{(Z_{12} - Z_1)}{(Z_{12}^2 - Z_1 Z_2)} \right] \right] \quad [49]$$

Applying this conversion, the resilience space can be represented as follows:

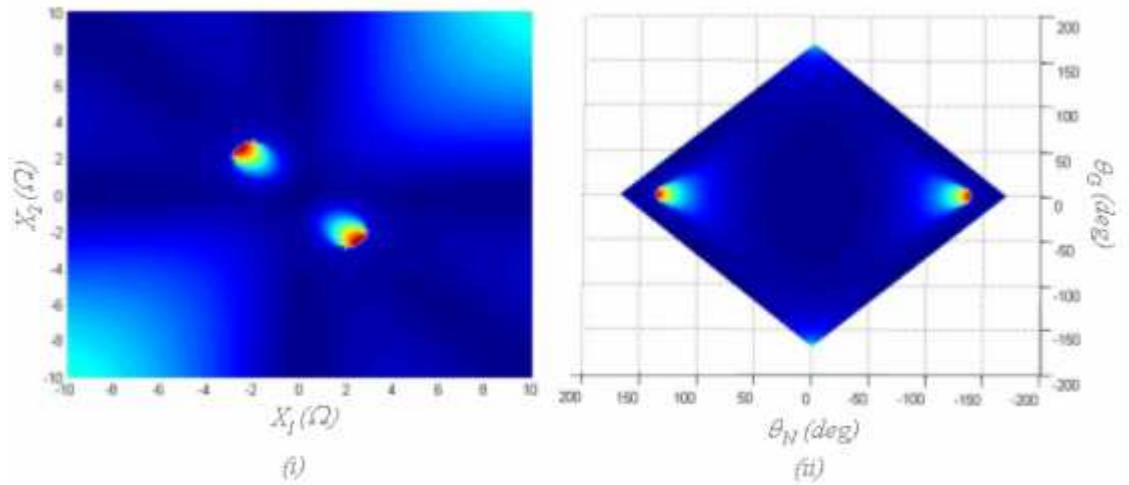


Figure 20: Resilience intensity maps illustrating conversion from reactance (i) to phase space (ii)

As can be seen from Figure 20, the optimal resilience lies at $\theta_G=0^\circ$, and $\theta_N = \pm 138^\circ$ in phase space for an ideal RDL, as predicted in section 5.2.

The sensitivity study has two components. Firstly, the location of the optimal phase targets shall be assessed with respect to a non ideal parameter to ascertain if that parameter must be compensated for in any control regime. In this study, only first order interactions are considered – second order interactions (one non ideal parameter to another) were neglected for simplicity.

Secondly, a critical minimum performance indicator was required to ascertain by what margin the set-points could drift from optimal. This contour was taken as $\lambda = 5$ in equation 25, as in the upper expected ELM disturbance (Lamalle 2005).

The ranges of non ideal parameters were taken from the measured antenna impedance matrix included in Appendix B. Comparing between RDL's at 42.5MHz, the maximum asymmetry was taken to be +/-50%, the maximum resistive mutuals were -50% of strap resistance, and the maximum mutual reactive part 2% of strap reactance. In all cases, frequency was assumed mid band at 42.5MHz, as this simply

varies the phase angle. As long as the capacitor set points remain within the physical range of the actuator this parameter will not affect performance.

5.3.2. Mutual Reactance

The critical contour of $\lambda=5$ for varying mutual reactance is illustrated in Figure 21. As can be seen, the accuracy requirement for net angle is significantly less than that for gross angle, as the solution locus is elongated in θ_N . Additionally, there is no overlap in loci across the range of variation, and therefore the controller will be required to compensate for mutual reactance. It should also be noted that the optimal solution always occurs at the far left edge of the locus (see Figure 22) and therefore on a ‘cliff edge’. This feature is common to all the contour plots in this study.

The trends of the location of the optimal set-points are shown in Figure 22. This quantifies the observations above, indicating a strong sensitivity of θ_G to mutual reactance, and a very weak sensitivity to θ_N .

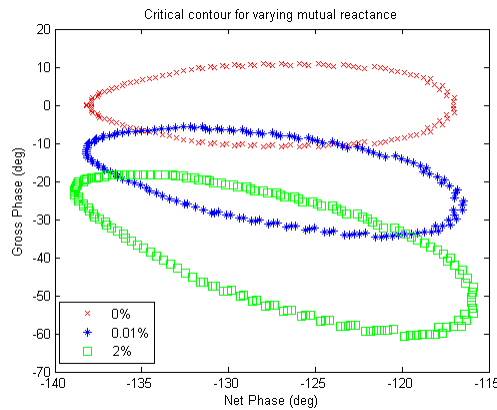


Figure 21: Critical contour evolution with mutual reactance

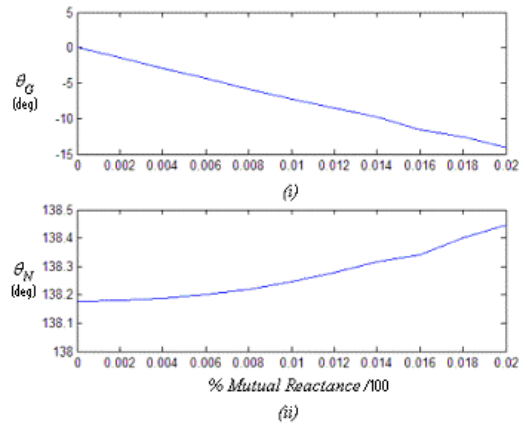


Figure 22: Optimal set-points for varying mutual reactance, (i) gross angle, (ii) net angle

5.3.3. Mutual Resistance

The critical contour of $\lambda=5$ for varying mutual resistance is illustrated in Figure 23. The accuracy requirement for net angle is again significantly less than that for gross angle. Additionally, there is significant overlap in loci across the range of variation, and therefore the controller may be able to neglect compensation for mutual resistance.

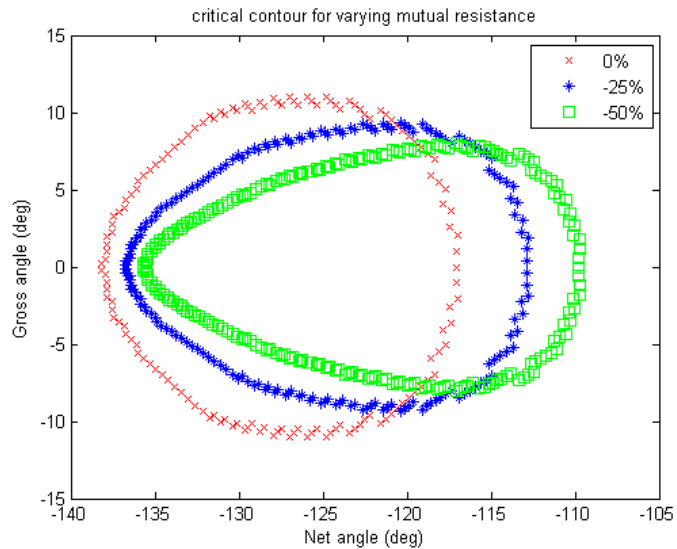


Figure 23: Critical contour evolution with mutual resistance

The trends of the location of the optimal set-points are shown in Figure 24. This indicates an invariance of mutual resistance with θ_G (neglecting the numerical error), and a weak sensitivity to θ_N .

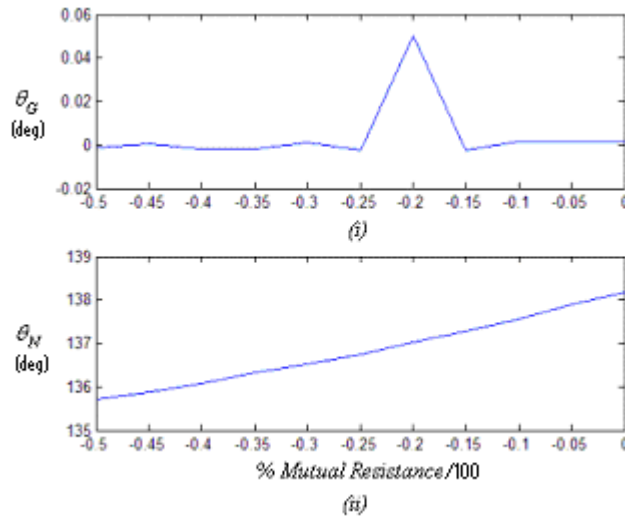


Figure 24: Optimal set-points for varying mutual resistance (i) Gross angle, (ii) net angle

5.3.4. Asymmetry

The critical contour of $\lambda=5$ for varying asymmetry is illustrated in Figure 25. The accuracy requirement for net angle is again significantly less than that for gross angle. Additionally, although there is some overlap in loci across the range of +ve asymmetry variation, if asymmetry is negative the gross phase loci decreases (response is mirrored in $\theta_N = 0$). Therefore, there is no overlap in the range $-50\% < \text{asymmetry} < 50\%$ and thus the controller may need to compensate for asymmetry.

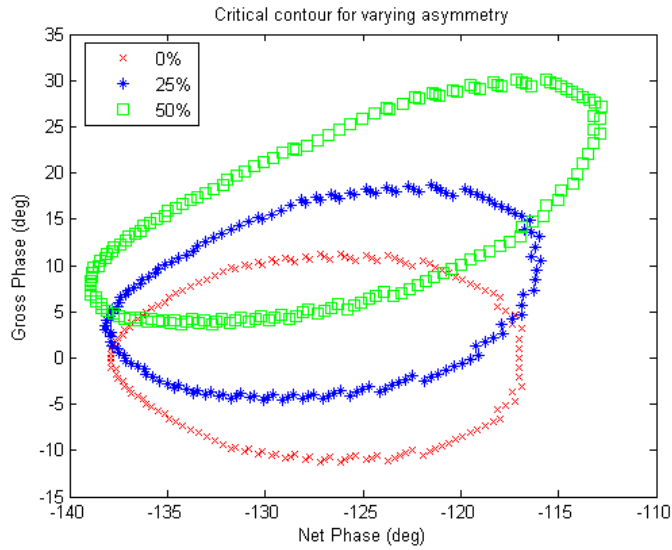
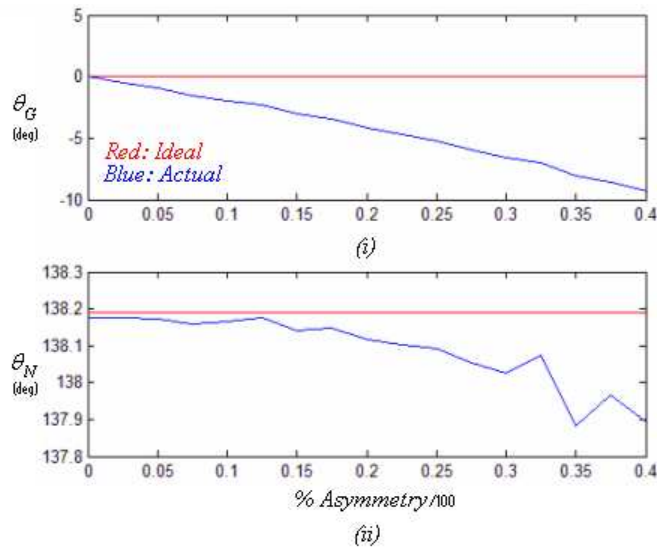


Figure 25: Critical contour evolution with mutual asymmetry

The trends of the location of the optimal set-points are shown in Figure 25. This indicates strong sensitivity of θ_G to asymmetry and a weak sensitivity to θ_N .



5.3.5. Summary of effects & proposals

The following table summarises the influences on the RDL optimal resilience setpoints.

Variable	Gross phase	Net phase	Comments
Strap resistance	Invariant, nominally 0	Invariant, nominally 138.2° for vswr limit of 1.5	
% Strap asymmetry	If $\theta_N > 0$: linear decrease If $\theta_N < 0$: linear increase	Insensitive (within range modelled)	Gradient average resistance dependant Invert relationship if asymmetry -ve
% Resistive mutuals	Insensitive (with no asymmetry)	Decreases linearly with increasing resistance	Always negative. Gradient resistance dependant
% Reactive mutuals	Linear decrease, regardless of quadrant	Insensitive (within range modelled)	Always inductive. Gradient Resistance dependant

Table 5: Summary of observations from sensitivity study

As can be seen, the behaviour of an RDL is complex. It should be stressed that interactions between non ideal parameters, and additionally loading and frequency have not been investigated, due to the multidimensionality of the problem. However, this study is sufficient to identify the following:

- Optimal resilience occurs on a cliff edge in resilience space. Operation near this value will not be robust
- The accuracy requirements of net angle are relatively benign in comparison to gross angle
- No overlap exists in the range of loci for mutual reactance and asymmetry. Therefore a control algorithm with fixed T impedance or fixed arm phase targets will be very challenging
- As θ_N is i) near invariant for mutual reactance and asymmetry, ii) displays low sensitivity to mutual resistance, yet with large overlap in loci, and, iii)

requires a low accuracy for all non ideal parameters; it is proposed that the θ_N set-point can be fixed with no compensation

- As θ_G is i) very sensitive to mutual reactance and asymmetry, and, ii) displays no overlap in loci; it is proposed that any controller must compensate for these effects
- As θ_G for mutual resistance is invariant, no compensation is necessary

5.4. Non Ideal parameter compensation

By definition, resilience cannot be measured directly. Therefore, in order to control for optimal resilience, an indicator for resilience must be found. As discussed in section 5.2, this indicator can be expressed in two parts:

Net phase angle:	$\theta_L - \theta_C$	138.2°
Gross phase angle:	$\theta_L + \theta_C$	0°

Where θ_L is the phase angle of the current across the inductive arm, and θ_C is the phase angle of the current across the capacitive arm. Phases are expressed relative to the voltage at the T point.

Sensitivity studies of section 5.3 demonstrate that the gross arm phase target is strongly dependant on resistive asymmetry and reactive mutuals, and can lead to drifts of up to $10^\circ - 15^\circ$ from the ideal CT circuit settings.

The net arm phase target displays sufficiently low sensitivity that this can be captured by a fixed target, not compensated for by the control system. However, to avoid the “cliff edge” in resilience performance it is proposed that the target of 138.2° is reduced to 135.5° . This has a moderate reduction in baseline resilience, but ensures that the system should remain resilient across the range of mutual resistance.

However, due to the strong variation in the gross arm target of 0° , an alternative measurable indicator for θ_N must be derived that is a function of asymmetry and mutual reactance.

The $\theta_G = 0$ constraint is equivalent to the locus $X_1 = -X_2$. The conjugate T circuit has the property that the T point impedance, ' $|Z_T|$ ', when viewed as a function of frequency has a local maxima on a locus that can be approximated by $X_1 = -X_2$ for the given functional range of the lumped elements representing the RDL.

Moreover, it can be shown that this locus is a function of asymmetry and reactive mutuals. Consequently, an algorithm can compensate for non ideal variables by replacing the $\theta_G = 0$ locus with the locus of $d/df(Z_T) = 0$.

The resulting locus for $d/df(Z_T) = 0$ is shown for the solution space of the ILA at midband frequency of 42.5MHz in Figure 26.

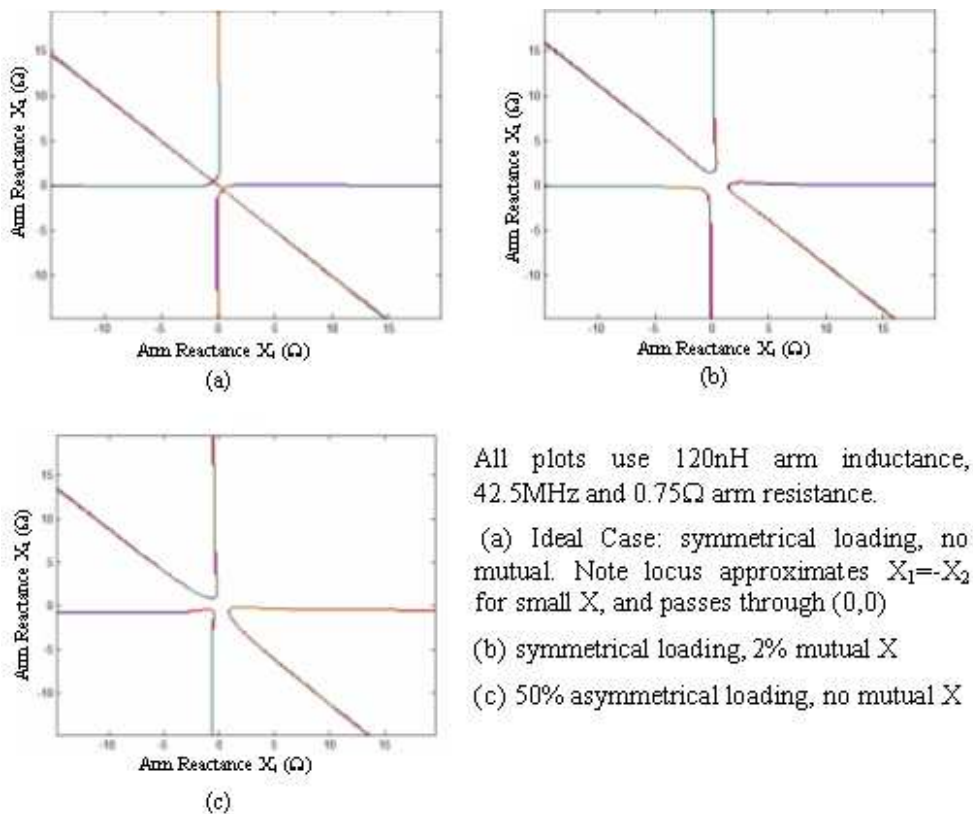


Figure 26: Plots of the locus $dZ_T/df=0$ for a variety of CT circuits

Superimposing the locus of the net arm phase target on the gross phase target yields a singular intersection, demonstrating unambiguous convergence. This is shown in Figure 27.

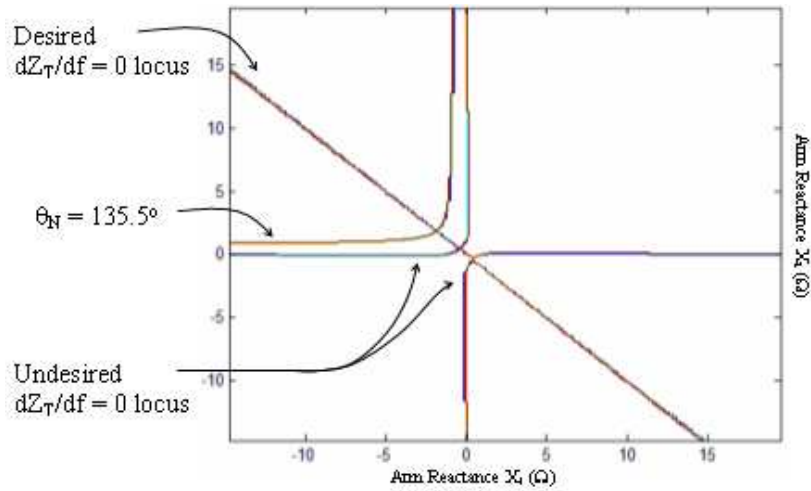


Figure 27: Intersection of gross and net angle target loci

However, there remains spurious contours of $d/df (Z_T) = 0$ that do not correlate to the desired gross angle locus (lying approximately along the locus $X_1=0$ & $X_2 = 0$). These pose traps for any convergence trajectory that must cross them.

This issue is resolved by disabling the gross phase target aspect of the algorithm when the net phase is less than 90° . This excludes all undesirable contours from the search area, and ensures clear convergence, as shown in Figure 28.

$d/df (Z_T) = 0$ can be measured by amplitude modulation. A diagnostic signal of frequency f_d is mixed with the main heating carrier frequency f_c , to produce sidebands at $f_c \pm f_d$. The amplitude of f_d is minimised to maximise power to the carrier, and minimise resultant increase in electric field.

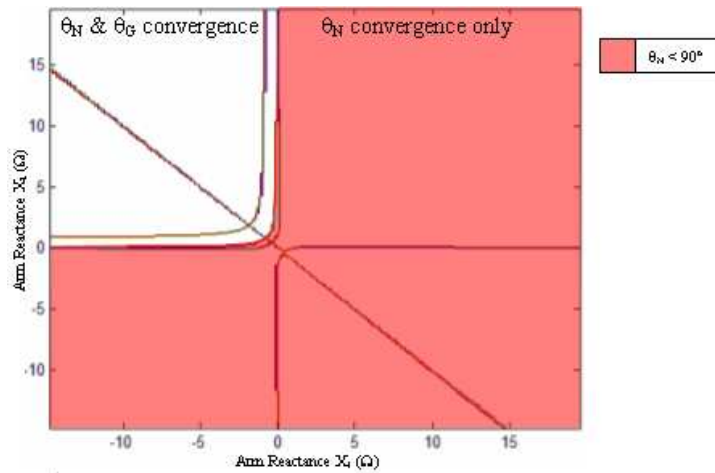


Figure 28: Intersection of loci, showing $\theta_n < 90^\circ$ exclusion zone

A filter is used to discriminate one sideband reflection from the other, and the T point impedance is calculated for each frequency. The algorithm varies θ_G such that the amplitude of both sideband impedances are equal. This is shown in Figure 29.

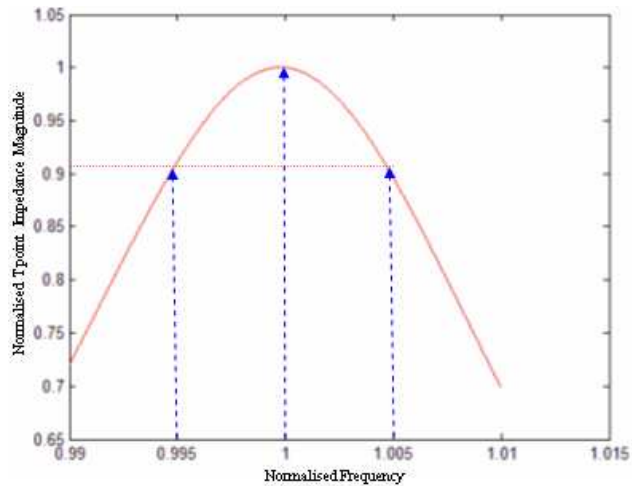


Figure 29: Tpoint Impedance as a function of frequency, showing location of possible sidebands

The algorithm used a 0.5% modulation index, so that the discrete approximation of $d/df (Z_T)$ was not affected by any possible asymmetry about the maximum, and so ensure the accurate resolution of the Z_T peak. However, in reality this would require high performance filters with consequentially large phase delay. This could lead to instability in the controller. Consequently, future studies are required to calculate the

sensitivity of the modulation index to Z_T peak resolution, so that the modulation index can be relaxed.

An alternative method of scanning the carrier frequency sinusoidally could be used, however, this approach has an inferior time resolution (one period of the scan is necessary to resolve $dZ/df = 0$) and the consequential phase delay will reduce the controller phase margin. Additionally, as the main power carrying frequency is being varied from the match, this may confuse the 2nd stage match, and will also reduce power to plasma. The algorithm code realisation, with comments, is included in Appendix F.

5.5. Algorithm assessment

This chapter has thus far:

- Outlined the fixed T point impedance algorithm of the reference ILA for matching control (section 5.1)
- Proposed an alternative arm phase algorithm for resilience control (section 5.2)
- Conducted a study that demonstrated the high sensitivity of the CT circuit to non ideal parameters & consequential need for compensation (section 5.3)
- Proposed a modification to the arm phase algorithm that compensates for non ideal parameters (section 5.4)

Therefore, the performance of the two algorithms, arm phase/AM and fixed T shall be assessed to establish their steady state performance with respect to varying plasma parameters

5.5.1. Base load variation

Figure 30 shows the performance of the two algorithms against the theoretical maximum performance given by the adaptive grid solver of section 4.3.2. As can be seen the AM algorithm displays broadband high resilience, but reduced from the theoretical maximum.

The near load invariance is a consequence of the second stage match being able to compensate for any T point impedance presented. It should be noted that there is a very mild decrease in performance as resistive load increases. This is due to the fact that $dZ_T/df=0$ approximates $X_1=-X_2$ for low values of loading. However, this effect remains negligible for all values in the range of interest, as can be seen.

The reduction in performance of the AM algorithm with respect to the theoretical maximum is a consequence of the θ_N target being reduced from its optimal to 135.5° . This avoids the cliff edge in performance associated with the theoretical maximum (blue line) but results in a mild reduction in overall performance.

The fixed T algorithm has been designed to have the maximum performance possible at the design load. However, as a consequence all loadings below the design value have crossed the “cliff edge” in the solution space and display very poor resilience.

Loadings above the design load show a pronounced roll off in performance. Consequentially, the design impedance should be chosen with care to avoid the cliff edge. Unfortunately, this will entail accepting significantly reduced performance at the design load (dependant on the uncertainty in expected base load resistance).

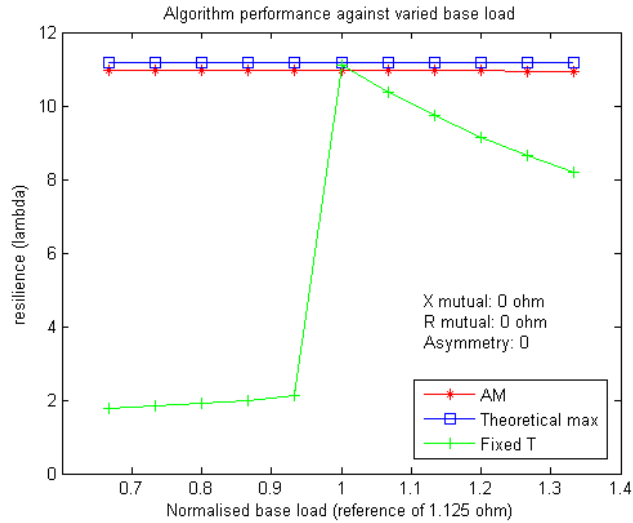


Figure 30: Algorithm performance against varied base load

What is happening in this instance is the CT optimum is tracking along the $X_1 = -X_2$ locus as base load is increased. As the fixed T algorithm does not track this movement, the set points cross the maximum location, showing the cliff edge and the reduced performance “tail” associated with the $X_1 = -X_2$ locus. This effect is illustrated in Figure 31. However, the AM algorithm with a floating T point can successfully follow the optimum location.

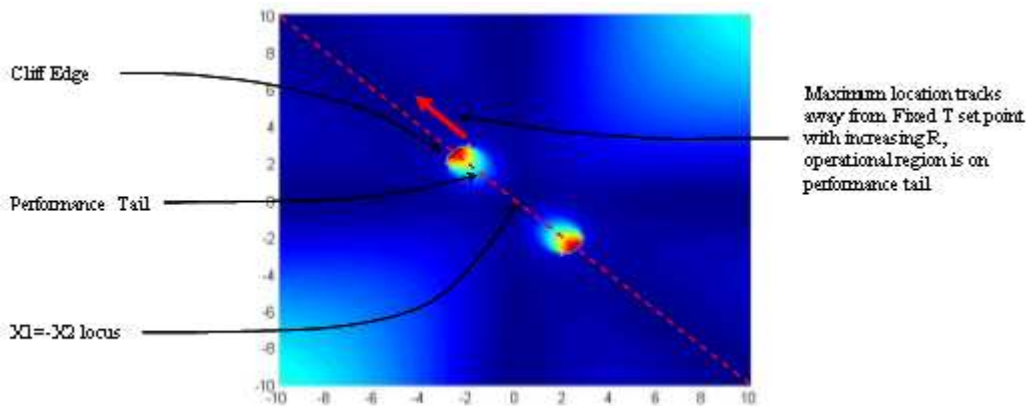


Figure 31: Explanation of resistive load sensitivity behavior

5.5.2. Mutual reactance variation

The results of the mutual reactance comparison are shown in Figure 32 .

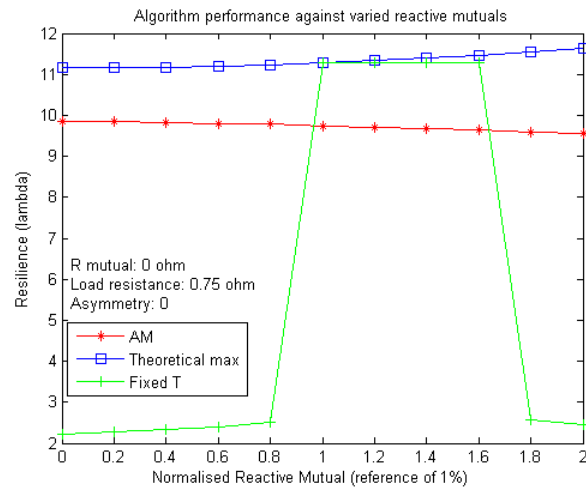


Figure 32: Algorithm performance against varied mutual reactance

As can be seen, the AM algorithm shows only a slight decrease in performance across the operational envelope, demonstrating the accurate and successful tracking of the maximum resilience point by the algorithm.

The fixed T algorithm again shows a pedestal response. In this case less mutual reactance than the design value results in immediate loss of performance. A second cliff edge is present if mutuals are increased above a certain level.

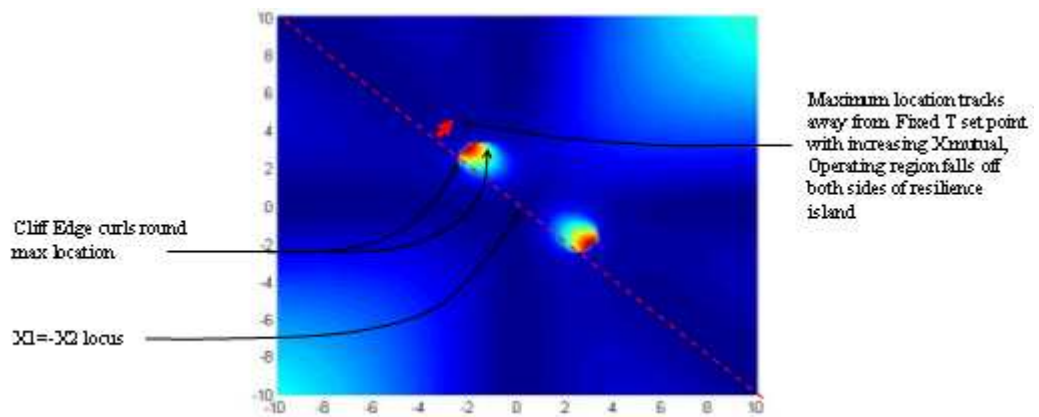


Figure 33: Explanation of reactive mutual pedestal behavior

The pedestal effect is similar to that found in resistive asymmetry, and is due to the cliff edge in the resilience surface extending onto the flanks of the maximum resilience island. The combined movement of the resilient island and T point

impedance adjustments moves the operating set point across the island, encountering two sets of “cliffs” on opposing flanks. This is shown in Figure 33.

5.5.3. Mutual resistance variation

The results of the mutual resistance comparison are shown in Figure 34. Neither the AM or fixed T algorithms compensate for resistive mutuals.

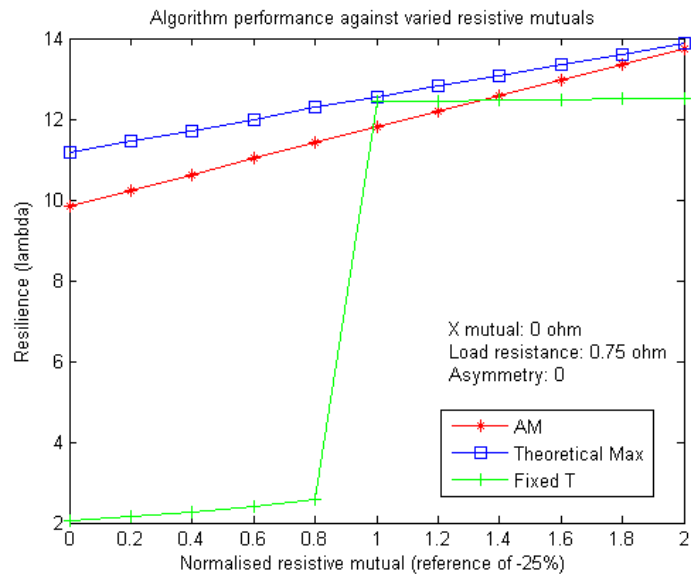


Figure 34: Algorithm performance against varied resistive mutuals

The AM algorithm successfully demonstrates broadband high resilience, showing a pronounced increase in performance with resistive mutuals. However, as this performance converges on the theoretical maximum, it will inevitably intersect at which point performance will collapse as the system encounters a cliff edge in resilience space. However, the study shows that a net angle target of 135.5° is appropriate to avoid this in the range up to -50% mutual resistance.

The fixed T algorithm has been configured to deliver maximum resilience at midband. Consequently, for mutual resistance beneath the design value the system has encountered a cliff edge in the resilience response. Above this the performance is

steady. For this case, broad band compensation for resistive mutuals may be achieved by reducing the generator vswr limit in calculating the optimal set points. This would give broad band resistive mutual tolerance to the system, but entail an associated reduction in performance. (This is the equivalent of reducing the θ_N target in the AM algorithm).

This response can be explained by considering the peak of the resilience island tracks along the $X1=-X2$ locus, increasing $|X|$ with decreasing mutual resistance. This reduces the net phase angle, and so will converge on the AM fixed θ_N target of 135.5° . In so doing, the performance increases as the two θ_N set points converge.

As mutual resistance decreases, maximum resilience increases (mutual resistance being negative). The fixed T algorithm holds a contour on the island's resilient tail, as shown by its flat resilience response. Below the design value, the resilient peak will move across the fixed T operating point and resilience will collapse. This is shown in Figure 35.

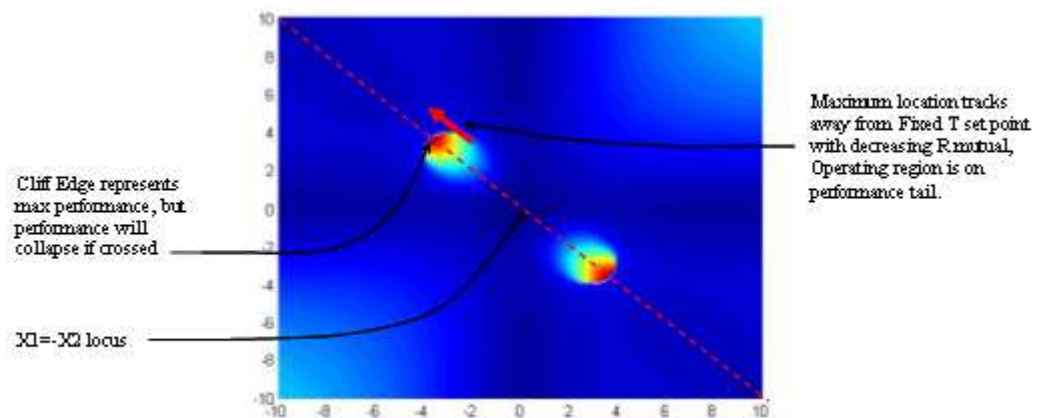


Figure 35: Explanation of resistive mutual performance

5.5.4. Asymmetry variation

The results of the mutual resistance comparison are shown in Figure 36

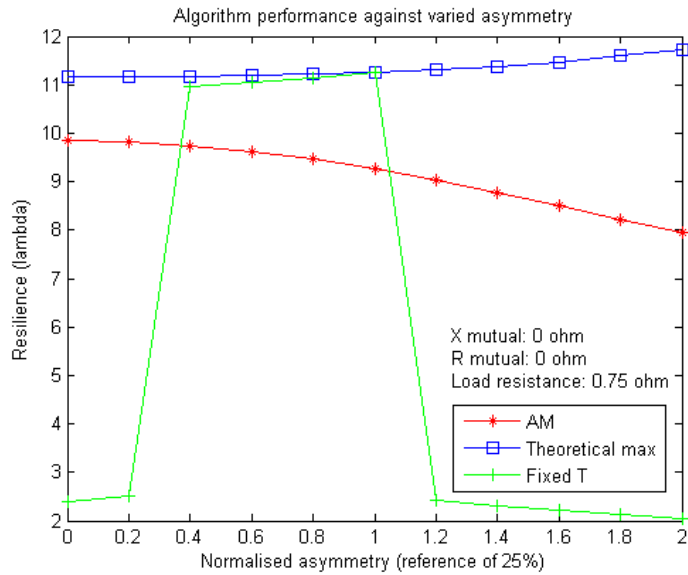


Figure 36: Algorithm performance against resistive asymmetry

As can be seen, the AM algorithm shows a mild drop off in performance as the resistive asymmetry increases, displaying a ~20% decrease in performance across the range of interest. However, the algorithm successfully tracks the location of the maxima, which is clearer when compared with the fixed T algorithm.

The fixed T algorithm is designed to have maximum performance for midband asymmetry. However, for asymmetry greater than the design value the system falls off the cliff edge and displays poor resilience. If the asymmetry is less than designed for, the resilience remains high, yet then collapses as it encounters another cliff edge.

This pedestal performance can be interpreted by noting that the cliff edge in response extends on to the flanks of the CT optimum. Varying asymmetry causes the maximum to move off the $X1=-X2$ locus. As the fixed T algorithm responds to deliver a pre-defined T point impedance, the relative motion results in the operational point traversing the peak in resilience and so encountering two cliff edges, as shown in Figure 37.

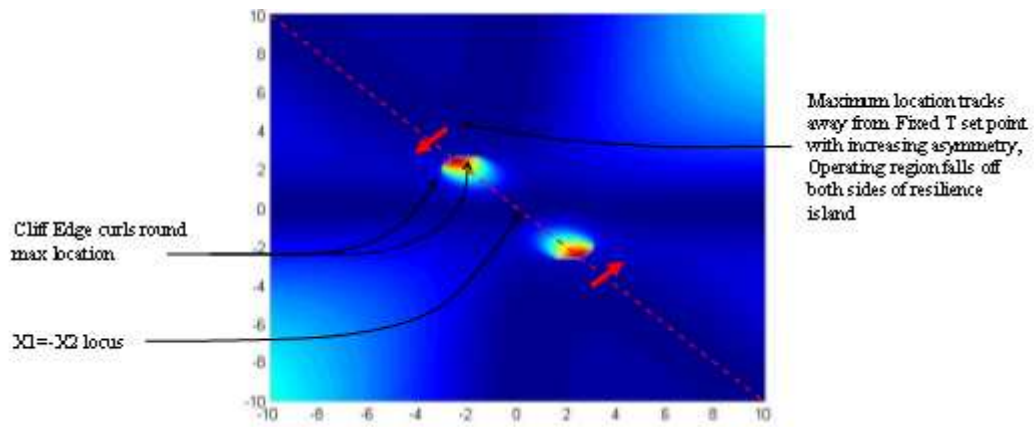


Figure 37: Explanation of asymmetric load pedestal behavior

5.6. Discussion

The following conclusions can be drawn from the algorithm comparative study of this chapter:

- The fixed T algorithm with its dependence on open loop resilience control is shown to display a very narrow band of acceptable resilience about the loading design case. Given this performance, successfully achieving a resilient match is challenging.
- The fixed T algorithm should adopt a lower vswr limit in calculating the optimal T point impedance in order to increase the resilience bandwidth and better centre its passband with respect to non ideal parameters. This, however, will result in a much reduced performance at design load, and will still result in pedestal behaviour as demonstrated by the lack of common set point loci in section 5.3.
- The AM algorithm successfully demonstrated a broadband high resilience with respect to all parameters investigated.

However, there remain outstanding issues to be resolved. These are:

- The conversion from impedance demand to hydraulic actuator demand uses the inverse of the model of the system to linearise. The accuracy of this translation may not be assured, and so the algorithm must be assessed for stability using no linearisation. However, this is relevant for the tuning of the dynamic response.
- A very small modulation index was used for the above study to ensure accurate resolution of the $dZ_T/df = 0$ locus. This ensured that the principle of the AM algorithm was tested, not the realisation of it. It is desirable to have a relaxed modulation for practicality, and therefore further study is required to assess the sensitivity of modulation index to $dZ_T/df = 0$ resolution.
- The above study is underpinned by the assumption that plasma disturbances are resistive in nature, an assumption explained in section 4.1. As discussed in section 3.3, reactive elements to disturbance are present, and the impact of this change to the AM algorithm must be assessed
- The above study assumes that mutual impedance is invariant with disturbance, as discussed in section 3.3. However, it seems plausible that resistive mutuals may be affected by plasma disturbance. Therefore, the impact of this possibility on the AM algorithm should be assessed.
- The $VSWR = 1.5$ critical reflection limit as discussed in section 4.1 results in the cliff edge in resilience space. This hard limit does not exist in reality, with interlock trips, as discussed in section 2.3.2, engaging at a $VSWR$ of 3. Therefore, a modified and more sympathetic measure of circuit performance is required.

6. Average coupled power performance indicator

6.1. *Reactive disturbances*

As discussed in section 5.6, the measure of ELM performance as per section 4.1 is incomplete in that reactive ELM components have been neglected, and circuit interlocks simplified. Moreover, the philosophy does not readily lend itself to incorporating such effects. This chapter sets out an alternative performance measure that is more comprehensive and robust with respect to a multidimensional ELM model.

Present studies which address the issue of a reactive ELM (Lamalle 2005) assume a fixed relationship between the resistive and reactive disturbances. This ‘fixed path’ method is problematic as, i) a multidimensional disturbance’s resilience performance can only be assessed for a predefined trajectory, ii) this becomes very limiting as dimensions increase, and iii) the method is still dependant on the declaration of a simple VSWR limit.

This leads to ambiguity, for as discussed in section 2.4, disturbance trajectories are i) uncertain, ii) vary between disturbances & iii) are multidimensional. Additionally, as discussed in section 2.3.2, VSWR limits are soft, not abrupt, in that power is limited in response to high reflections, up to a limit of VSWR of typically 3. The critical contour approach cannot capture this “soft stop” functionality and is consequently overly pessimistic.

6.2. *Average coupled power model*

An alternative performance measure is required to accommodate the ability of the system to achieve greater resilience, but at reduced power. This is possible by

assessing the coupled power during a disturbance, rather than the vswr. Thus, higher vswr ratings than 1.5 are possible, but with a marked decrease in performance as generator protection interlocks ramp down the driving voltage (see section 2.3.2). The performance measure for a given disturbance trajectory is thus the average coupled power for the period of one disturbance expressed as a percentage of the base load coupled power.

Additionally, the method must be able to account for multiple dimensions in the disturbance, and accommodate the uncertainty in possible disturbance trajectories. This is achieved by defining the multi-dimensional region in which a disturbance trajectory may exist. This is illustrated in Figure 38 for an ELM disturbance.

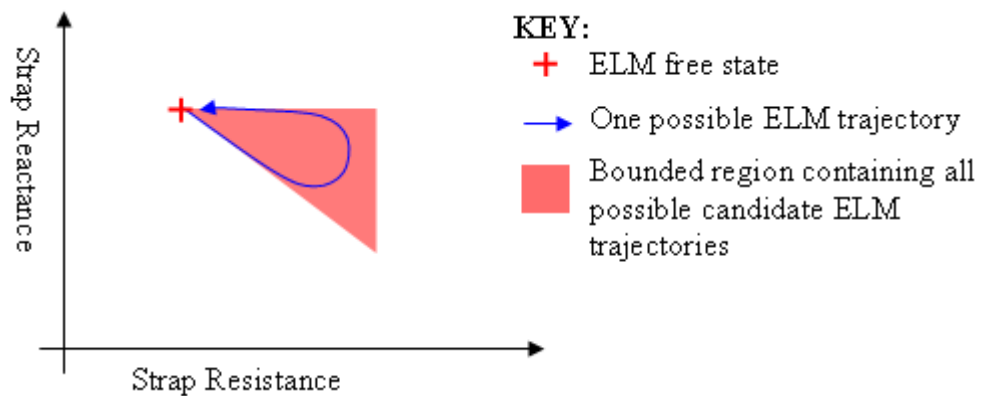


Figure 38: 2D illustration of ELM space

The resulting region (area in 2D ELM, volume in 3D ELM etc) can then be meshed, and the coupled power calculated at each node. The generic performance measure is then the average coupled power across the entire region. This method is particularly robust, as additional dimensions can be added without reappraising the assessment methodology.

An additional feature of the performance is the requirement that the system does not trip protection interlocks, as this results in a large reduction in duty cycle and

hence average delivered power as the system executes safety time outs for each trip. Consequently, if any part of the ELM region causes a trip, the average performance measure is automatically set to zero, i.e. the solution is unacceptable.

As discussed in section 2.4, knowledge of the influence of ELMs is limited. For this study the bounds on reactive and resistive variations shall be assumed to be $\lambda = 5$ and $k = 0.75$ as in equation 26 in section 3.3. Variations in resistive asymmetry were neglected for lack of measured data to set realistic bounds. No variations in mutuals were considered, as discussed in section 3.3. It is assumed that $\Delta R\%$ is always greater than $\Delta X\%$ as per reported by Monakhov (2003).

Thus, with these simplifications it can be assumed that an ELM has 3 dimensions, resistance, reactance, and time. This could be calculated as a series of frames as shown in Figure 39, where when viewed in the X-R plane the resulting overlap of uncertainty ranges approximates to Figure 38.

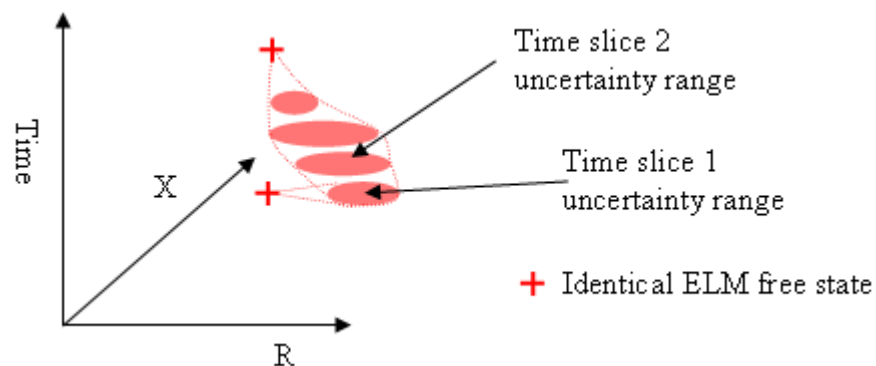


Figure 39: Graphical representation of the solution method for a 3D time dependant ELM

However, for this study time was neglected, and coupled power calculated for one area as per Figure 38.

This was for two key reasons. Firstly, insufficient data was available to assign uncertainty ranges per time slice. Secondly, approximating an ELM by a triangle as

shown in Figure 38 is simpler computationally, and sufficient information is available to put bounds on the region. Additionally, as steady state analysis is used, time is not a variable in the coupled power calculation so considering only the X-R plane is sufficient.

However, the resulting average coupled power calculation is inaccurate, as there is equal weighting applied to all coupled power values, regardless of the overlapping of the R-X uncertainty ranges between time slices. This also affects the location of the true optimal, as including time would bias the average coupled power toward the region of lower disturbance. This is because ELMs classically display a high peak with an exponential roll off. Therefore they spend most time at lower disturbance values. This will move the average coupled power optimal along the $X1=-X2$ locus toward the origin (assuming the ideal CT & ELM models). It is also likely to result in reduced set point sensitivity to disturbance, as the extremes of the ELM have less of an influence on the overall performance.

Therefore, in addition to asymmetry and mutual variations, future ELM experiments should seek to capture time dependency information to enable more accurate CT circuit performance predictions.

6.3. Coupled power modelling

6.3.1. Derivation of coupled power performance measure

The model for coupled power includes both power limitation and interrupt interlock features, as summarised in section 2.3.2. The settings used in this study are those reported by Sibley & Wade (1999). Therefore, coupled power to plasma has three distinct states as follows:

- Below a reflected power of 130kW the coupled power is a function of the load and corresponding reflection.
- Above 130kW, but below a vswr of 3, the driving voltage is reduced such that there is constant reflected power. The response time on this interlock is 0.5ms, which is fast in comparison to the ELM duration of 2.5-4ms. Therefore for simplicity, the steady state coupled power is always used.
- For a reflection of greater than or equal to 3 the power is tripped and coupled power is thus 0.

This behavior was modelled as follows. Consider the definitions for forward and reflected power

$$P_i = \frac{V_i^2}{Z_0} \quad [50]$$

$$P_r = \frac{V_r^2}{Z_0} \quad [51]$$

where P is power, V voltage, Z_0 the characteristic impedance and the subscripts i & r denote incident and reflected respectively.

In the region of no interlock intervention ($P < 130\text{kW}$) the coupled power P_c is thus

$$P_c = \Delta P = \frac{V_i^2 - V_r^2}{Z_0} \quad [52]$$

Substituting in the definition $V_r = \Gamma V_i$ into equation 52, where ‘ Γ ’ is the reflection coefficient, yields:

$$P_c = \frac{V_i^2}{Z_0} (1 - \Gamma^2) = P_i (1 - \Gamma^2) \quad [53]$$

Therefore coupled power may be expressed as a function of VSWR by substituting equation 34 into equation 53

$$P_c = P_i \left[\frac{4S}{(S+1)^2} \right] \quad [54]$$

For interlock intervention the reflected power is maintained at a given critical setpoint, $P_{r_max}=130\text{kW}$. By definition the limiting reflected voltage ' V_{r_max} ' is defined from equation 51 as

$$V_{r_max} = \sqrt{P_{r_max} \cdot Z_c} \quad [55]$$

Therefore the maximum incident power can be determined by combining equations 50 & 55

$$P_{i_max} = \frac{P_{r_max}}{\Gamma^2} \quad [56]$$

Thus, for interlock intervention, the maximum coupled power is obtained by substituting equations 56 & 34 into equation 54. Thus

$$P_c = P_{r_max} \left[\frac{4S}{(S-1)^2} \right] \quad [57]$$

The critical VSWR crossover point, S_{crit} , can be determined from equating equations 54 & 57. Therefore

$$S_{crit} = \frac{\sqrt{P_i} + \sqrt{P_{r_max}}}{\sqrt{P_i} - \sqrt{P_{r_max}}} \quad [58]$$

Therefore, the coupled power can be modelled as a piecewise function summarised in Table 6.

The valid inputs are summarised in Table 7, with the resulting waveform illustrated in Figure 40.

Region of validity	Coupled Power
$VSWR \leq S_{crit}$	$P_i \left[\frac{4S}{(S+1)^2} \right]$
$S_{crit} < VSWR < 3$	$P_{r_max} \left[\frac{4S}{(S-1)^2} \right]$
$VSWR \geq 3$	0

Table 6: Summary of coupled power relationships

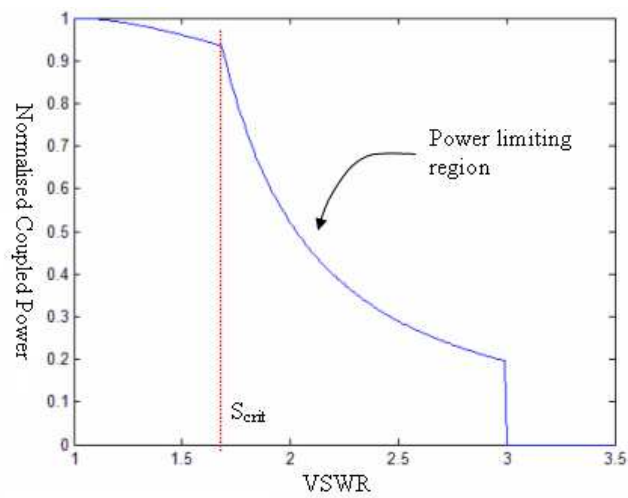


Figure 40: Coupled power vs. VSWR

Nomenclature	Description	Value
P_i	Incident Power	2MW
P_{r_max}	Maximum permissible reflected power	130kW
S_{crit}	The critical value of VSWR for power limitation	$\frac{\sqrt{P_i} + \sqrt{P_{r_max}}}{\sqrt{P_i} - \sqrt{P_{r_max}}}$

Table 7: Parameter description for coupled power analysis

6.3.2. Numerical average X-R performance model

The above performance measure was therefore applied to predicting CT performance for any given arbitrary combination of capacitor set points.

Thus, using the candidate capacitor set point positions, the capacitance was derived using equation 9. The equivalent Thevinin antenna impedance was thus calculated using equation 19. Due to the presence of reactive disturbance, it was found that a more sophisticated 2nd stage model as discussed in section 3.2 was required. Therefore, the 2nd stage transformer and stub settings were calculated using equations 21 & 23 respectively.

Plasma disturbances were considered two dimensional as in section 6.1, and were modelled using equation 26. The instantaneous VSWR was calculated using equation 34, and consequently the resulting coupled power was derived using the relations summarised in Table 6. This was repeated for all nodes in the meshed ELM X-R space and averaged to give the overall performance.

An ELM was considered to exist within a triangular locus when drawn on the X-R plane, with nodes (1,1), (1,5) & (0.75,5) where (1,1) represents the nominal 'ELM free' state. The ELM area was always meshed with 55 nodes. The code for the X-R average coupled power performance is detailed in Appendix G.

As an initial test, the new performance was assessed for an ELM with no reactive component ($k=0$), and $\lambda=5$. The results are shown in Figure 41 for a midband frequency of 42.5MHz, and a coupling resistance of 0.75Ω :

As can be seen, the optimal lies on the $X_1=-X_2$ locus as expected (dotted red line), which is consistent with previous assessment methodologies. Additionally, as

intended the optimum lies away from any discontinuities in the solution, as the cut off now appears on the edge of the cyan coloured region as shown top right.

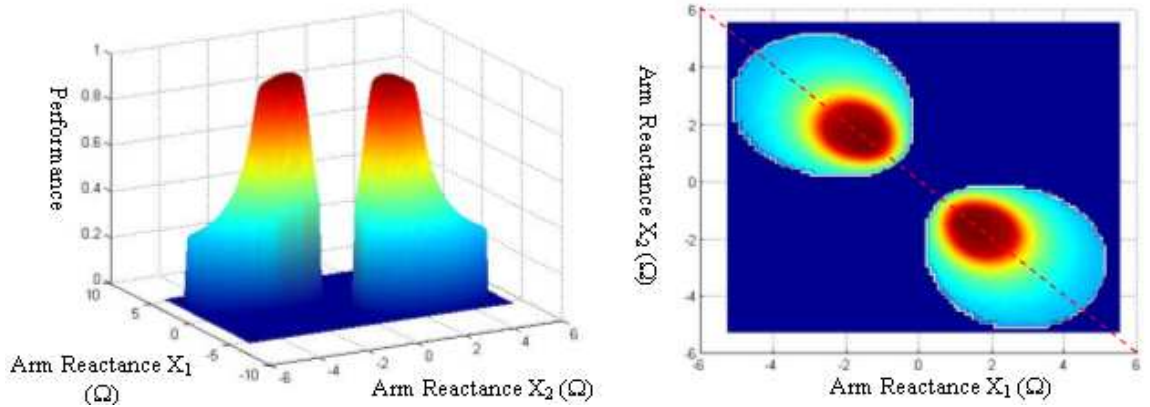


Figure 41: Surface plots of the X-R average coupled power performance measure for an ideal RDL with no reactive disturbance

However, with a reactive component of $k=0.75$ to the ELM enabled, the response is significantly changed, as shown in Figure 42.

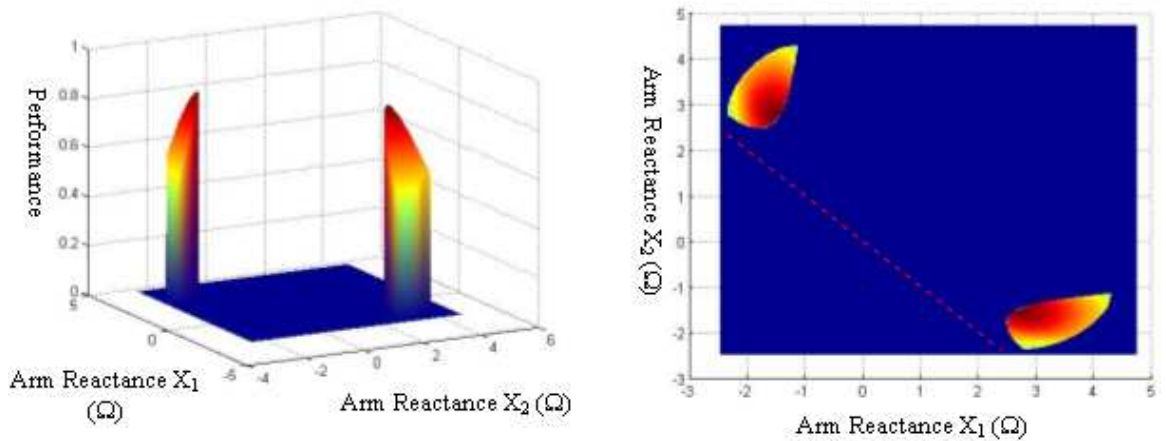


Figure 42: Surface plots of the X-R average coupled power performance measure for an ideal RDL including reactive disturbance

As can be seen, the performance has decreased with reactive ELMs. Additionally, the optimal set points are significantly altered, with the optimum no longer located on the $X_1 = -X_2$ locus. Finally, it appears the optimum again lies on or close to a mathematical discontinuity.

These alterations are more apparent when considering the phase plots of the same two candidate solutions as shown in Figure 43.

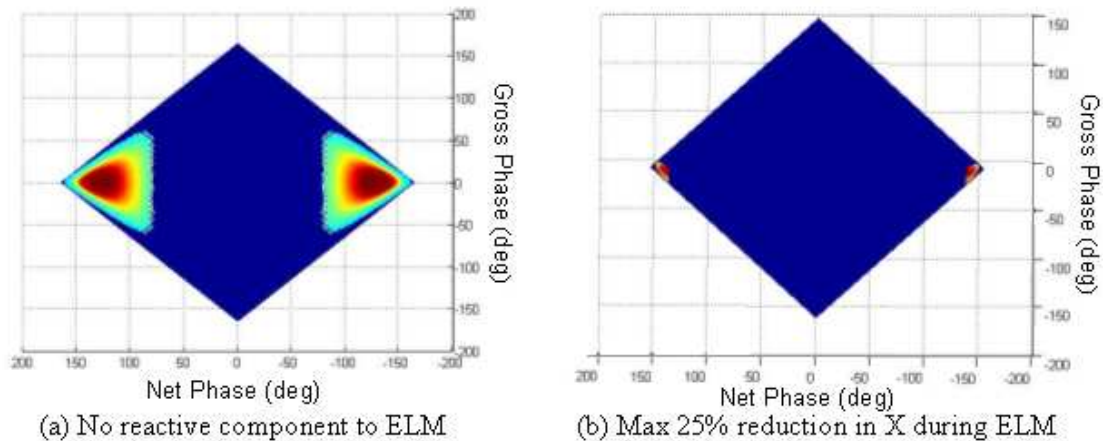


Figure 43: Phase plots for average X-R performance model

As can be seen the valid region is significantly reduced, the gross phase has reduced from 0 to approximately -10° , and the net phase angle has increased from approximately 130° to 140° . Clearly the effects of ELMs are pronounced, and the highly localised nature of the resulting set point presents a distinct control challenge, more demanding than previously encountered. Additionally, a numerical solver is again required to derive set points for optimal RDL performance.

6.3.3. Numerical Set point solver

Section 6.3.2 outlined the requirement for a solver to extract the optimal configuration for an RDL using the average X-R coupled power performance model. It has been observed that the solution again may occur on, or adjacent to, a mathematical discontinuity. Therefore, to prevent solving errors, the numerical solver developed in section 4.3.2 was adapted. This method searched the solution space with a course mesh, identified a local maximum and then re-meshed at twice the resolution in a locality of $\pm 2x$ the previous resolution about the maximum. This

process was repeated iteratively until a predefined resolution had been reached. The following modifications were necessary to the code:

1. The algorithm uses the X-R averaged coupled power performance measure, rather than the former resilience measure. This is described in section 6.3.2.
2. The average X-R performance model uses capacitor stroke rather than arm reactance as its input.
3. Previous code searched only one quadrant of the solution space in the reactance plane as solutions were symmetrical about $X_1=X_2$. This symmetry does not hold for reactive ELMs, and so the code was modified to search a user defined quadrant so that each quadrant can be independently assessed in turn to determine the true global maximum. As stroke is used rather than reactance, arm reactance search “quadrants” have been mapped into the capacitor stroke domain.
4. Previous code would return an error if the search window was too close to the edge of the initial search area (code would try to read a matrix with index 0 or negative). Code now warns that the solution is too close to the edge.
5. The revised X-R performance model yields highly localised solution “islands” Therefore, the code now warns users if the initial search is too course, i.e. all performance values were calculated 0 and the island was missed.

The resulting code is recorded in Appendix H.

7. Implications of reactive ELMs

7.1. Sensitivity studies

It is necessary to repeat the sensitivity study of section 5.3 to establish the extent of influence the reactive component to the ELM has on the arm phase set points. Therefore, an indication of the adjustments required to the AM algorithm may be determined. Specifically, this study will address whether:

1. Optimal gross and net angles remain load invariant
2. Net angle retains a sufficiently low sensitivity to variables that its set point may be fixed
3. Gross phase angle can still be approximated by the indicator $dZ_T/df=0$

Sensitivity studies adopting the resilience approach set out in 5.3 adopted a critical contour of $\lambda=5$ to describe the possible set point loci. This is not transferable to the average coupled power model, and so an alternative critical measure must be applied. Consequently, this analysis applied an arbitrary cut off of 50% average coupled power.

7.1.1. Phase load invariance

The arm phase control algorithm is conceived from the logic that for a resistive disturbance the optimal resilience is a function of arm relative current phasing, and invariant with loading as discussed in section 4.1. For a reactive disturbance it must be assessed if this definition holds.

Using the solver summarised in section 6.3.3, the optimal set points for the arm phases using the average coupled power performance were calculated for i) a purely resistive disturbance, and ii) a resistive and reactive disturbance.

The resulting solution for the purely resistive model is shown in Figure 44. As can be seen, there is a degree of numerical noise in the solution. On inspection of the solution locality in Figure 41, the local gradient is flat, which provides a poor target for the optimisation routine. However, it is clear that the performance and the optimal set points of the circuit are load invariant, as predicted by the former resilience method of section 5.2. Additionally, the gross phase target approximates to 0, as expected. The net angle phase target differs, in that it reduced from 138° to 127° . This is because the modified method is optimising within a bounded range of λ between 1 and 5. The optimal resilience method discussed in section 5.2 is optimised for an unbounded disturbance.

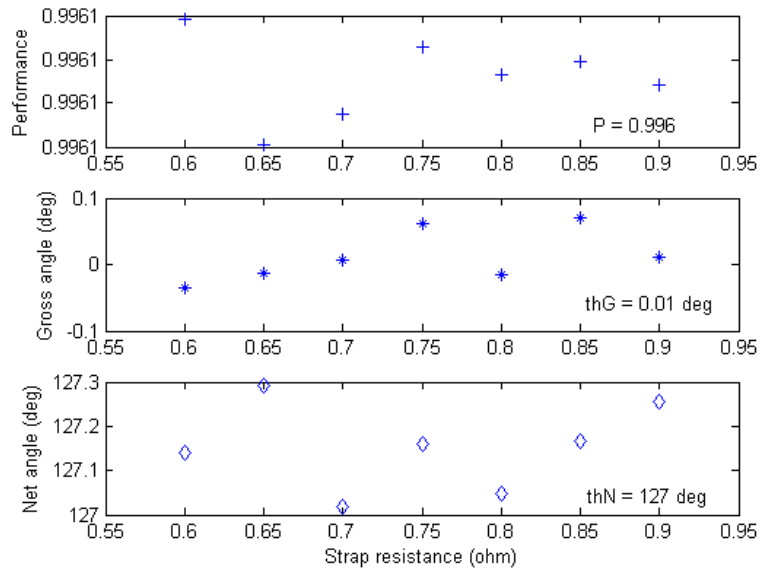


Figure 44: Illustration of loading invariance for real disturbance

The simulation was repeated, including a reactive component on the disturbance of up to $k=0.75$. The results are shown in Figure 45. As can be seen, all parameters show significant sensitivity to loading.

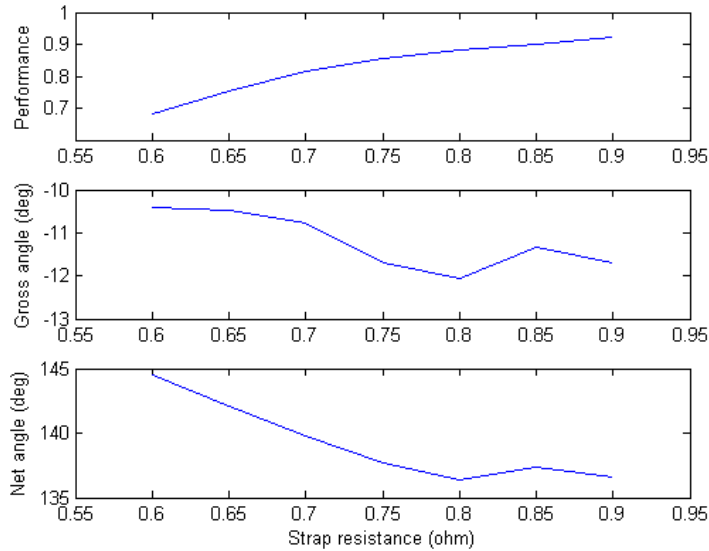


Figure 45: Illustration of load dependency for reactive ELMs

Performance, formerly load invariant, now shows a strong dependence on strap resistance. Performance favours higher coupling which is unfortunate, as disturbance tolerance is mostly required at low coupling (H mode). Additionally, it can be seen that for the majority of the resistance scale, performance is less than the critical VSWR setting for power limitation (0.935 for 2MW). Therefore, operation for reactive ELMs with up to 25% variation from base load is not possible within the $VSWR < 1.5$ limit adopted for the ILA.

The gross angle illustrates a pronounced offset from the ideal 0° , of approximately -10° . This can be rationalised, as if the circuit were pre-configured with +25% additional reactance on each arm, the resulting -25% reactive disturbance would rebalance the circuit. However, the solution also shows a weak sensitivity of offset to loading, of approximately 2° over the range of coupling.

The net angle also shows a pronounced offset from 127° to up to 145° . This can be rationalised as the reactive component is reducing overall performance, and so pushes the system toward maximal resilience (i.e. optimised for an unbounded disturbance). Using equation 41 the set point for an unbounded disturbance may be calculated for and a critical VSWR of 1.5 (free operation) and 3 (cut off). The results are compared with those derived by the average coupled power model. As can be seen, the ratio is similar. Although this does not amount to a proof, it suggests that the drift to 144° from 127° is due to the average power lying mostly in the power limited region for reactive ELMs, and not the free reflection region as for purely resistive ELMs.

Critical VSWR	Optimal Theory (unbounded disturbance, equation 41)	Bounded Disturbance (average coupled power model)	ratio
1.5	138°	127° (purely resistive elm)	0.92
3	160°	144° (reactive elm)	0.9

Table 8: Conceptual justification of net angle set points

The critical contours of 50% power are plotted across the resistance range in Figure 46.

As can be seen, the critical contour for the lowest coupling satisfies the locus for all coupling. Therefore, unless the setpoints become load dependant (an added complexity avoided in algorithms discussed thus far) it is most appropriate to use the lowest intended coupling as target in any control system.

Additionally, the accuracy required for net angle is typically lower than that for gross angle, as encountered before.

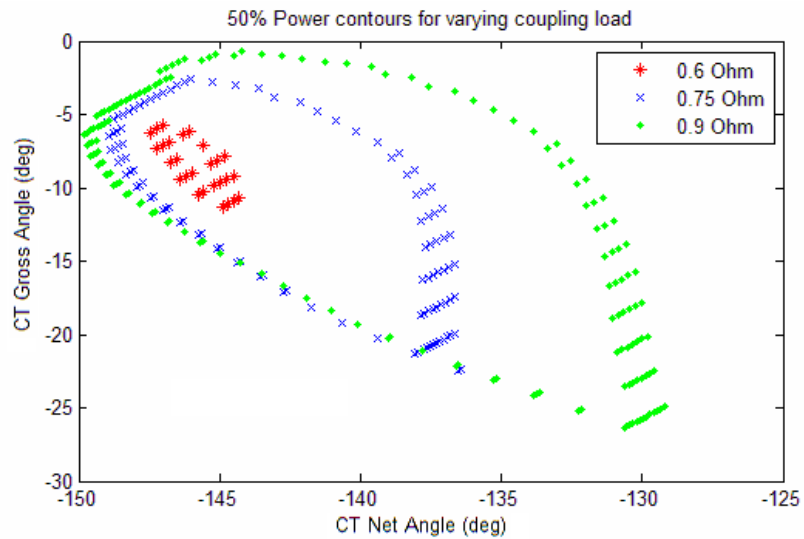


Figure 46: Critical contours for varying resistance

Finally, comparing the drift in gross angle set point shown in Figure 45 with the locus shown in Figure 46, it can be concluded that the $>2^\circ$ drift is within the solution locus, offering the possibility that no compensation is required.

7.1.2. Mutual reactance sensitivity

Mutual Reactance of the CT circuit was varied between 0 and 2% on a circuit with coupling of 0.75 ohm with no resistive mutuals or asymmetry. The trend of performance versus reactive mutuals is shown in Figure 47.

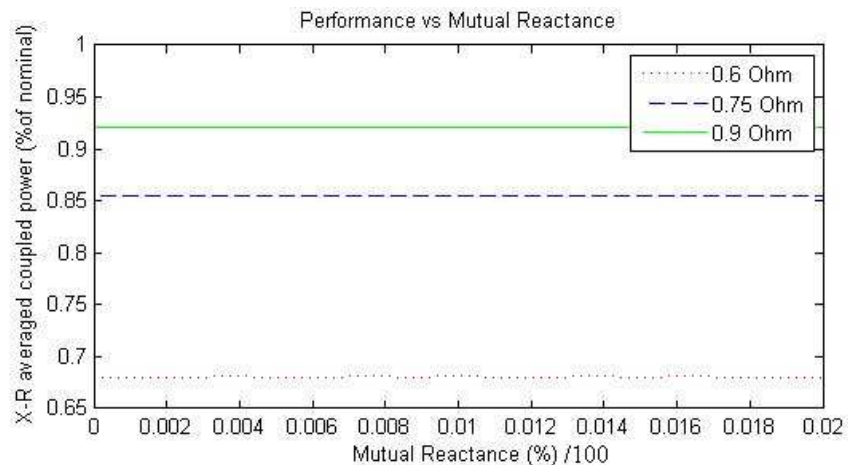


Figure 47: Performance vs. reactive mutuals

The 50% power contour drift is shown in Figure 48. As can be seen, there is no overlap in loci and therefore compensation is required.

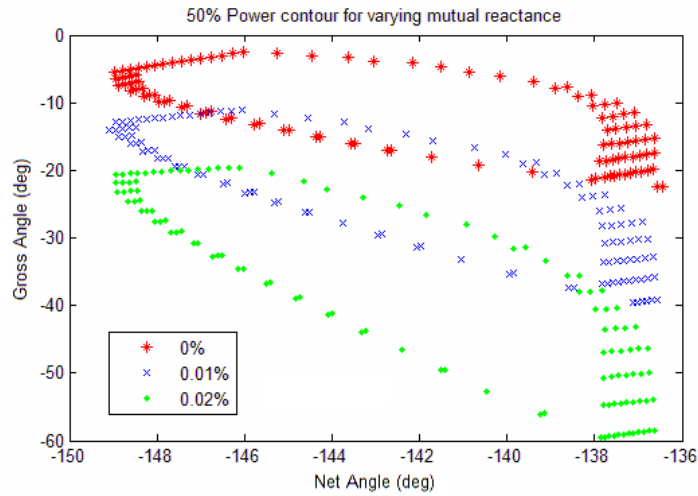


Figure 48: Critical contour for reactive power variations

The optimal set point trends with mutual reactance are illustrated in Figure 49. As can be seen, net angle remains invariant. However, gross angle, as illustrated in Figure 48 and consistent with previous findings shows a pronounced drift. However, it should be noted that i) as discussed in section 7.1.1, there exists an offset in gross angle, and ii) the parameter is almost twice as sensitive as per the sensitivity study of section 5.3.

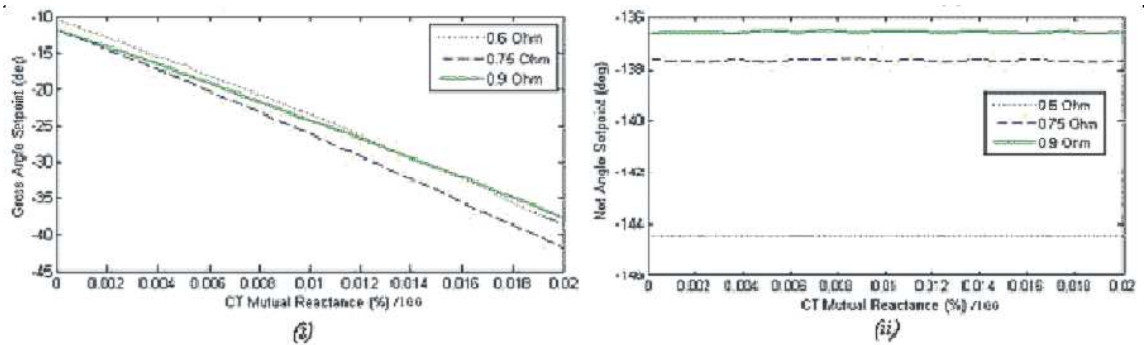


Figure 49: (i) Gross angle (ii) Net angle optimal set point trends with mutual reactance

7.1.3. Mutual resistance sensitivity

Mutual resistance of the CT circuit was varied between 0 and -50% on a circuit with coupling of 0.75 ohm with no resistive mutuals or asymmetry. The trend of performance versus reactive mutuals is shown in Figure 50. As can be seen, performance improves for decreasing mutual resistance.

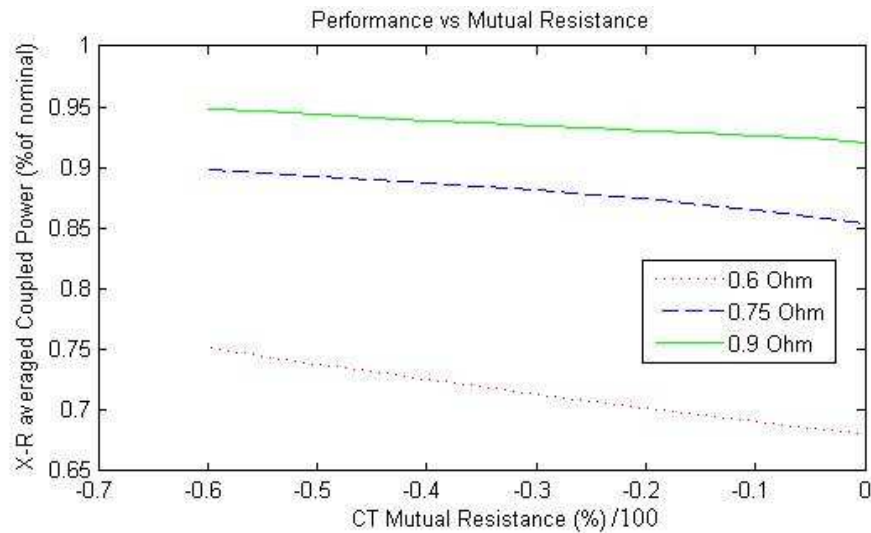


Figure 50: Performance vs. resistive mutuals

The 50% power contour drift is shown in Figure 51. There is very little overlap in loci and therefore, unlike with purely resistive ELMs, compensation is required.

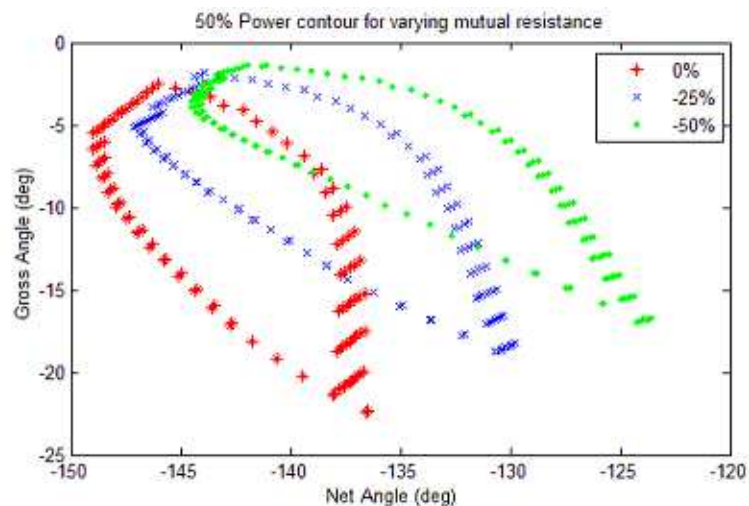


Figure 51: Critical contour for mutual resistance variations

The optimal set point trends with mutual reactance are illustrated in Figure 52. There is pronounced drift for both gross and net angle set points. Unlike in section 7.1.1, gross angle appears to have a strong effect, rebalancing the circuit. Additionally, net angle is approximately twice as sensitive.

Therefore, increasing the magnitude of mutual coupling appears to drive the system toward the ideal reactive ELM free state. However, this should be interpreted with caution, as the model assumed no disturbance to reactive mutuals as discussed in section 6.2.

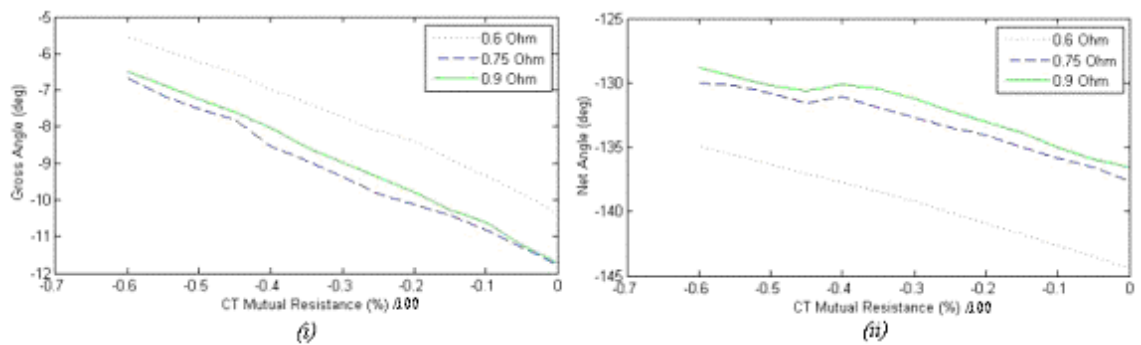


Figure 52: (i) Gross angle (ii) Net angle optimal set point trends with mutual resistance

7.1.4. Resistive asymmetry sensitivity

Resistive asymmetry of the CT circuit was varied between 0 and 50% on a circuit with coupling of 0.75 ohm with no mutual impedance. However, pronounced differences were encountered between the performances of the two possible solutions. For positive asymmetry, solutions with a negative net angle (θ_N) set point improved their performance. However, for the mirror solution with a positive θ_N the performance was degraded, before disappearing altogether. The converse is true for negative asymmetry.

The trend of performance versus asymmetry for the two quadrants is shown in Figure 53. As can be seen, performance improves with increasing asymmetry. Where

the solution disappears (for the sub optimal solution) the graphs show a sharp drop to 0 for all parameters

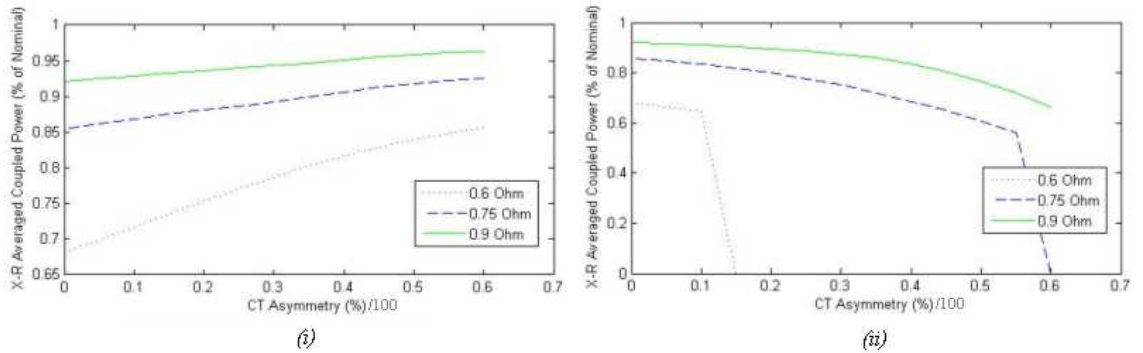


Figure 53: Performance vs asymmetry (i) – θ_G quadrant, (ii) $+\theta_G$ quadrant

The 50% power contour drift is shown in Figure 51 for the dominant solution. As can be seen, there is very little overlap in loci and therefore, as before, compensation is required.

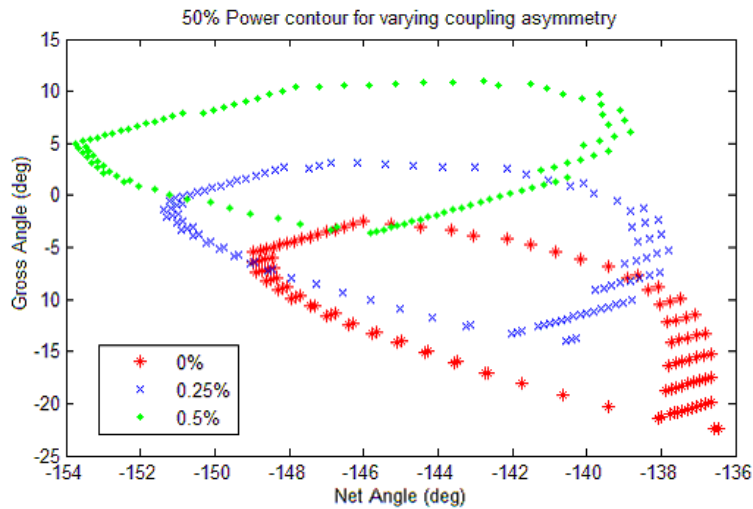


Figure 54: Critical contour for asymmetry variations

The optimal set point trends with asymmetry are illustrated in Figure 55 for the dominant quadrant. There is pronounced drift for both gross and net angle set points. Unlike in section 7.1.1, net angle is now very sensitive to asymmetry. Additionally, gross angle is approximately four times as sensitive as previously.

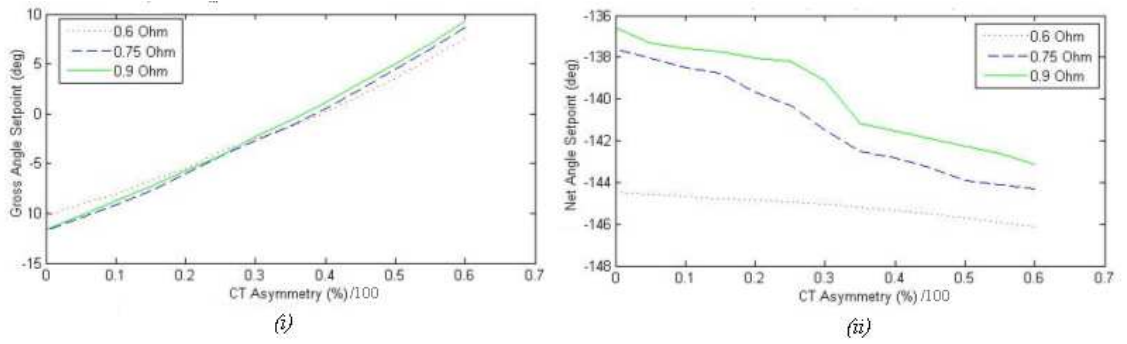


Figure 55: (i) Gross angle (ii) Net angle optimal set point trends with asymmetry

7.1.5. Summary of sensitivity study findings

The following conclusions can be drawn from the sensitivity study of performance with reactive ELMs to non ideal parameters.

Firstly, the optimal gross and net angle targets are no longer load invariant. There is a prominent offset in θ_G from its nominal value of 0, with additional mild sensitivity to load. There is also a pronounced sensitivity of θ_N to load resulting in approximately $\sim 17^\circ$ of drift across the scale of resistance.

Optimal algorithms may seek to design for the lowest level of coupling, as the lowest and highest set point loci entirely overlap.

The net angle cannot be approximated by a fixed target. Mutual resistance and asymmetry both account for drifts of order 6° - 8° across the parameter range, and there is no overlap in set point loci.

The gross angle set point cannot be approximated by the $dZ_T/df=0$ locus, due to the prominent offset from its nominal value of 0.

The gross angle is significantly more sensitive to mutual reactance and asymmetry than for the resistive ELM, and is now sensitive to mutual resistance in addition.

Asymmetry promotes one quadrant solution, while suppressing its mirror. Dominant solutions for positive asymmetry occur for solutions with negative net angle.

The loci for all cases is more localised than for the resilience model, placing an exceptionally tight accuracy requirement on any control algorithm. Additionally, the X-R averaged coupled power is almost always in the power limitation region.

Therefore, the amplitude modulation arm phase control algorithm proposed in section 5.2 requires modification to operate with ELMs of reactive loads up to -25%. Additionally, it can be concluded that fixed set point control is not acceptable, and that resilience must be brought under feedback control.

7.2. Proposals

7.2.1. Gross angle compensation

The sensitivity study of section 7.1.1 illustrated that i) there is a prominent offset in the gross angle from the nominal $\theta_G=0$, and, ii) there is a weak sensitivity of that offset with loading.

Firstly, because the load sensitivity is weak, of order 2° , and small in comparison to the solution locus, it is proposed that load compensation for the θ_G offset is not required.

Secondly, a constant offset from the nominal suggests that a fixed amount of reactance has been added to both arms. As one arm is capacitive and the other inductive, this skews the circuit so that $|X_1| \neq |X_2|$. As the reactance of each arm may be added to by altering the frequency, it is proposed that a modification to the

AM control algorithm may be able to capture the required offset. The principle is illustrated in Figure 56.

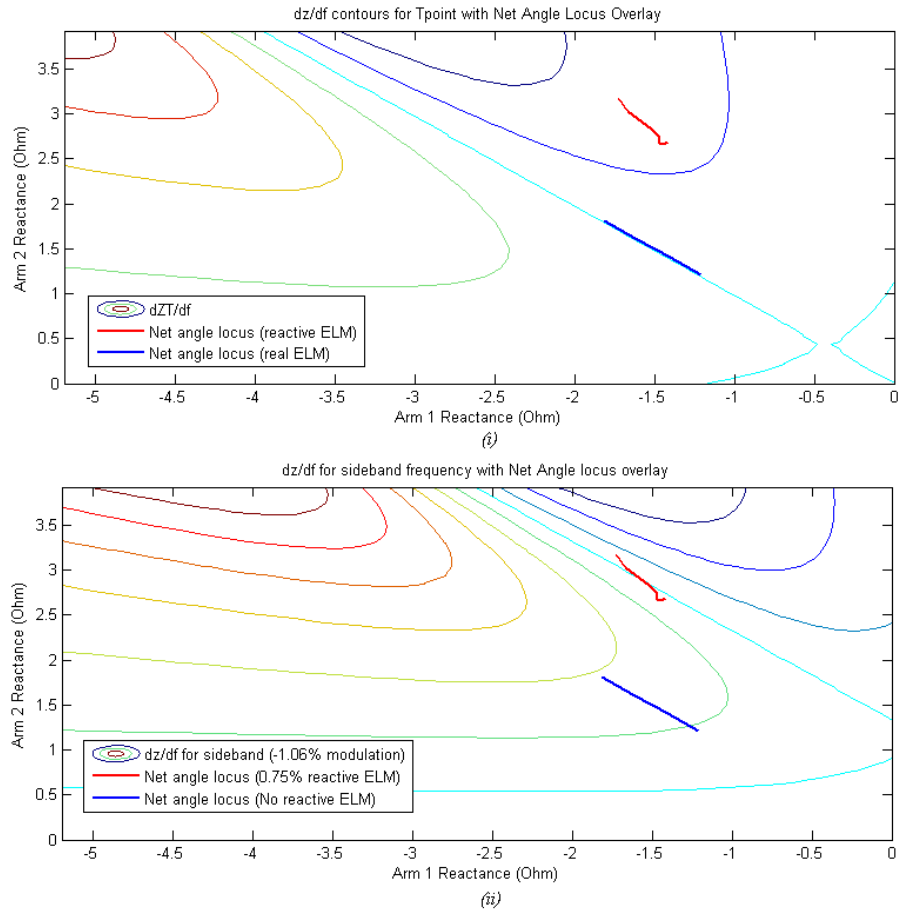


Figure 56: Offsetting frequency to capture gross angle locus (i) controlling to centre frequency; (ii) controlling to sideband

The above figures illustrate a contour plot of dZ_T/df , where ' f ' is the main driving frequency. Overlaid on the contours are the loci of arm reactance set points for varying base load. In Figure 56 (i) the heavy blue trace, representing a resistive ELM, follows the $X_1 = -X_2$ locus as expected. As can be seen, this coincides with $dZ_T/df = 0$. The bold red trace reactive ELM maps out a locus offset and not truly parallel (this is the mild sensitivity of offset to load discussed above)

In Figure 56 (ii), the set point loci remain the same, however, the contour plot is that of dZ_{Tm}/df_m , that is the derivative of the sideband T-point impedance. As can be seen, the modulation index (in this case 1.06%) can be chosen to replicate the

required fixed offset in θ_G . The AM control algorithm can thus control to $dZ_T(f_m)/df_m=0$, thus treating the side band as a “handrail” so that the driving frequency can operate with the required fixed offset in θ_G . This principle is illustrated in Figure 57.

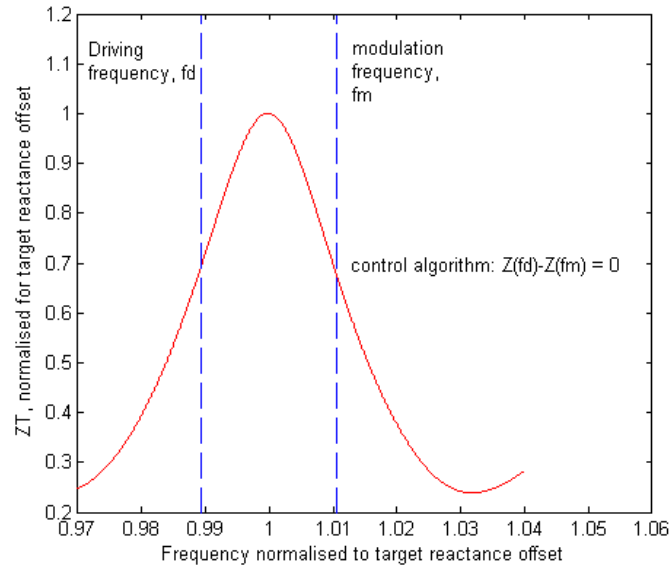


Figure 57: "handrail" principle of proposed modified AM algorithm

In the proposal above, rather than set the sideband on the maximum itself, the modulation index is twice the requirement. Therefore, $dZ_{Tm}(f_m)/df_m=0$ can be approximated by $Z_T(f_d)-Z_T(f_m)=0$, and the filter requirements are reduced. The value of f_m would be a constant, and its magnitude pre-calculated from the required gross angle set point for a symmetric circuit with no mutual impedance (in this case 2.12% modulation index).

Thus, this approach enables the algorithm to compensate for i) the fixed offset in θ_G , and ii) as before the $dZ_{Tm}(f_m)/df_m$ locus is sensitive to mutual reactance and asymmetry, and thus provides automatic compensation.

However, an avenue for compensating for mutual resistance variations still needs to be found.

7.2.2. Net angle compensation

By considering the loci of optimal set-points, it is clear that for all but the lowest coupling, the accuracy target for θ_N is far lesser than that for θ_G as the loci are elongated with θ_N . This again opens the possibility for a fixed target. With regards to asymmetry and mutual reactance, valid solutions exist for all ranges of parameter if the target was simplified to a fixed value of approximately 145° .

However, for the lowest coupling it is unlikely this method would offer sufficient accuracy.

Additionally, to compensate for resistive variations, the overlapping $\theta_N < 145^\circ$, yet for low coupling the target $\theta_N > 0^\circ$. This exclusive nature suggests that some indicator is required to compensate θ_N for mutual coupling.

8. Future work

This study captures initial development of a control methodology, and significant further work is required to realise such a system. The following key issues require further attention:

Excess reactive disturbance: The above study assumed a 25% drop in arm inductance. However, in the model arm inductance is a lumped element comprising strap inductance, strap feeder inductance and capacitor parasitic inductance. The strap itself only accounts for 50% of this lumped element. Therefore, applying an ELM disturbance of 0.75 to the entire arm is overly pessimistic, and if strap inductance alone were influenced this factor should be changed to 0.875. Considering Figure 41 & Figure 42, reducing the reactive component has a very strong beneficial influence on the set point solution loci. Therefore, this will cause the solution for reactive ELMs to converge with that for purely resistive ELMs, and the issues of excessive accuracy requirements and resistive mutual compensation identified in section 7.2 less critical.

“Handrail” AM algorithm testing: The handrailing control method for capturing the fixed offset in θ_G set point requires validation. This is particularly necessary, as the sensitivity of set point to asymmetry and mutual reactance is increased with reactive ELMs. It has not been established that tracking the $dZ_T(f_m)/df_m=0$ provides sufficient compensation for the larger set point drifts involved.

Mutual impedance ELM components: This study has considered that mutual impedance is ELM invariant, based on the observations of Monakhov (2003) on the

JET A2 antennae. However, Lamalle (2003) assumes that strap loading and mutual resistance are both scaled by the same factor during an ELM. Given the difficulties described in section 7.2 with compensating for mutual resistance induced drifts in set point location, it must be established how mutual resistance behaves during an ELM, and the sensitivity studies repeated capturing this effect so that set point trends are known definitively.

Multi-dimensional disturbances: This study considered an ELM affecting arm reactance and resistance only. In reality, ELMs occupy more dimensions, including time, asymmetry, and most likely mutual impedance. Experiments are required to establish by measurement disturbance models for the JET ILA, so that realistic bounds may be placed on them, and the correct dimensions modelled.

L-H transitions: The disturbance modelled in section 6.2 assumed an ELM as the only disturbance. The bounded disturbance area should be increased to include the L-H transition, as the response of the CT circuit to decreasing coupling is significantly different, and less tolerant, than that for increasing coupling.

Dynamic modelling: With an overarching control methodology established (AM phase control) dynamic models of the actuators and the associated control systems are required to demonstrate matching within the target settling time. This is particularly relevant for the 2nd stage match, which on the ILA is not yet available or configured for speed. On an arbitrary antenna design, however, it is proposed that the second stage should use an alternative fast matching network of which there are a variety of candidate architectures (capacitor loaded stubs, fast ferrite tuners etc). As part of the dynamic modelling, it should be noted that the actuators are all strongly non linear.

Amplitude modulation realisation: The study at present assumes that amplitude modulation has perfect accuracy and filtering. In reality, selective filters introduce phase delays that must be captured in the dynamic control algorithm. Additionally, the gain on the sideband must be such that the signal may be extracted from noise. However, larger sidebands are limited by the system maximum voltage, and thus coupled power will be reduced as more power is directed to sidebands.

Inter RDL mutual coupling: The AM control algorithm has been shown to offer promise in compensating for mutual impedance between the two straps of one RDL. However, in any antenna, RDLs shall be mounted adjacent to one another, and so compensation is required for inter RDL mutual coupling. The sensitivity of the system to this additional disturbance must be assessed.

9. Conclusions

This study has investigated control aspects of the conjugate T resilient in-vessel matching architecture for ICRH antennae.

The CT circuit achieves high levels of resilience to loading disturbances by configuring two identical straps in parallel, fed from a common T point. If the phase is appropriately configured between the two arms, a symmetrical disturbance at the load will result in destructive interference at the T point.

This study identified that the definition of resilience was a function of arm relative phasing, and not of the T point impedance as conventionally used. The target angles were derived algebraically for an ideal circuit.

The optimal phase was validated using custom written numerical solvers, necessary due to the presence of mathematical discontinuities in the solution for resilience. Using these tools, sensitivity studies of circuit response revealed a strong dependence of optimal configuration to non ideal parameters.

An alternative algorithm based on controlling the arm phase angle was proposed. An additional diagnostic of antenna state by amplitude modulation was also suggested to provide compensation for non ideal parameters. Matching control required the inclusion of the second stage match in the real time control system. This methodology was compared with the pre existing T point impedance control method and was shown to offer significant performance enhancement in response to resistive disturbances.

However, it is known that reactive disturbances are also present. This report proposed a novel assessment methodology capable of incorporating the real “soft

stop” action of interlocks, and readily scalable with additional disturbance dimensions. This used a disturbance space averaged coupled power measure, and solvers were developed to assess reactive ELM behavior.

Sensitivity studies repeated for the reactive ELM suggest that performance of the CT circuit is strongly degraded, and set point solutions are highly localised. This presents a key accuracy challenge for any controller. They also suggest the additional requirement for compensation of mutual resistance terms, and the imposition of a fixed offset in the gross angle target. However it was noted the levels of reactive disturbance used were pessimistic.

This report proposes that the fixed offset may be compensated for by using an appropriately chosen sideband of the AM diagnostic to guide the gross angle target of the circuit, much like a handrail.

Finally, this study identified various key areas where future work must concentrate. Of these, the most important is to develop a better understanding by measurement on the JET ILA of the bounds and relevant dimensions of plasma disturbances.

10. References

- Becoulet et al, 1996, “*Heating & current drive regimes in the ion cyclotron range of frequency*”, Plasma Physics & Controlled Fusion, 38(1996a)A1-A11.
- Borthwick et al, 2008, “*Mechanical Design Features and Challenges for the ITER ICRH Antenna*”, Proceedings of the Symposium of Fusion Technologies, Rostok, 15-19 Sept 2008
- Bremond et al, 2001, “*A new internal matching impedance concept for ICRF antennas*” Fus Eng & Des 56-57 (2001) 563-567
- Bosia G, 2003, “*High Power Density Ion Cyclotron Antennas for Next Step Applications*” Fusion Engineering & Design, vol. 43, pp 153-160 (2003) ISSN 0920-3796
- Da Silva et al, 2002, *Microwave Engineering*, The Open University, ISBN: 0 7492 4165 9
- Durodie et al, 2005, *Main design features and challenges of the ITER-like ICRF antenna for JET*, Fusion eng. & design 74 (2005)
- Durodie (2), 2002, *FD M65 “Offset Matching Control”*, JET EP ICRH internal Memo 19/07/02
- Durodie (3), 2002, *FD M58 “Actuator Specifications”* JET EP ICRH internal Memo
- Durodie, 2002, *FD M68 “Test of algorithm M65”* Internal Memo 05/08/02
- Evrard et al, 2005, “*RF circuit simulation of the JET-ITER like ICRH Antenna*” AIP Conf. Proc. Sept 26, 2005 Vol 787, pp. 186-189 RADIO FREQUENCY POWER IN PLASMAS: 16th Top. Conf. on RF Power in Plasmas; DOI:10.1063/1.2098220

- Fisch N.J., 1987, “*Theory of current drive in plasmas*” *Reviews of Modern Physics*, 59 (1987) 175-234
- Hoffman et al, “*Experimental measurements of the ion cyclotron antennas’ coupling & RF characteristics*” CONF-850310—98 DE85 011569
<http://www.osti.gov/bridge/servlets/purl/5760508-PqxcEU/5760508.PDF>
- Hoffmeister et al, 1994, *The RF system & matching procedure for ASDEX & ASDEX upgrade*, *Fusion eng. & design* 24 (1994) 83-89
- ITER WBS 5.1, “*Detailed Design Description Ion Cyclotron Heating & Current Drive System*” ITER document, G 51 DDD 4 01-07-19 W 0.2
- Kaye et al, 1994, “*Present & Future JET ICRF Antennae*” *Fusion Eng. & Design* 24 (1994) 1-21
- Koch et al, 1993, “*Enhancement of reactivity by RF*” *Plasma Phys & Contr. Fus.* 35A (1993) A2,11
- Lamalle et al, 2004, “*Recent developments in ICRF antenna modeling*”, 20th IAEA Fusion energy conf., Vilamoura, Portugal, 1-6 Nov 2004 IAEA-CN-116/FT/P7-18
- Lamalle et al, 2003, “*Radio-frequency matching studies for the JET ITER-Like ICRF system*”, 15th Topical Conf. on RF power in plasmas, Moran, Wyoming, USA, May19-21, 2003
- Lamalle et al, 2005, “*Study of mutual coupling effects in the antenna array of the ICRH plug-in for ITER*” *Fus eng & des* 74 (2008)
- Lin et al, 2008, “*Digital real-time control for an ICRF fast ferrite tuning system on Alcator C-Mod*” *Fus eng & des.* 83 (2008) 241-244

- Monakhov et al, 2005, “*Tests of load tolerant external conjugate T matching system for A2 ICRF antenna at JET*”, Fusion eng. & design 74 (2005) 467-471
- Monakhov et al, 2003, “*Studies of JET ICRH Antenna Coupling During ELMs*”, 15th Top. Conf. on RF Power in Plasmas AIP 694 p146-149 (Moran USA 2003)
- Pozar D M, 2005, “*Microwave Engineering*” 3rd Ed ISBN 0-471-44878-8
- Rogers et al, 1996, “*ICRF Heating & current drive experiments on TFTR*” Proc. 16th IAEA Fusion Energy Conference, (1996)F1-CN-64/EP-2
- Saito et al, 2006, “*Real-time impedance matching system using liquid stub tuners in ICRF heating*” Fus. Eng. & Des 81 (2006) 2837-2842
- Sibely, A & Wade, T 1999, “*The JET ICRH System Functional Description*” JET internal document icrh_sfd 6 May 1999
- Stix, T.H., 1992, “*Waves in Plasmas*” American Inst of Physics, 1992
- Wade, 1994, “*Development of the JET ICRH plant*” Fus. Eng. & Des 24 (1994) 23-46
- Wesson, J 1999, “*The Science of JET*”, JET publication JET-R(99)13
- Wesson J 2004, “*Tokamaks*” 3rd edition, Clarendon Press, Oxford, ISBN 0 19 8509227
- Wesner et al, 2nd Europhysics Conf. On Radio Frequency Heating & Current Drive of Fusion Devices, 22A, 13, 1998
- Yoon et al, “*Development of the liquid matching components for the KSTAR ICRF system*” Fus. Eng. & Des. 82 (2007) 771-774

11. Appendix A: Derivation of 2nd Stage Match

Parameters

The required phase shifter length, d , and stub length, l , for the second stage match were calculated as follows¹:

The T point impedance, $R_L + jX_L$, seen through the phase shifter of length d is given by the expression:

$$Z = Z_0 \frac{(R_L + jX_L) + jZ_0 t}{Z_0 + j(R_L + jX_L)t} \quad (1)$$

where $t = \tan \beta d$, and β is the phase shift constant. The admittance at this point is

$$Y = \frac{1}{Z} = G + jB \quad (2)$$

$$G = \frac{R_L(1+t^2)}{R_L^2 + (X_L + Z_0 t)^2} \quad (2a)$$

where:

$$B = \frac{R_L^2 t - (Z_0 - X_L t)(X_L + Z_0 t)}{Z_0 [R_L^2 + (X_L + Z_0 t)^2]} \quad (2b)$$

Now d (which implies t) is chosen such that $G = 1/Z_0$ for a perfect match. From equ

(2a) this results in a quadratic equation for t :

$$\begin{aligned} Z_0(R_L - Z_0) \cdot t^2 - 2X_L Z_0 \cdot t + (R_L Z_0 - R_L^2 - X_L^2) &= 0 \\ \Rightarrow t = \frac{X_L \pm \sqrt{R_L [(Z_0 - R_L)^2 + X_L^2]}/Z_0}{R_L - Z_0} & \quad (3) \end{aligned}$$

These two solutions for t can then be used calculate d as follows and the smaller of the two solutions is then selected (as it displays a higher bandwidth).

¹ Chapter 6.2 Single-Stub Tuning, Pozar

$$\frac{d}{\lambda} = \begin{cases} \frac{1}{2\pi} \tan^{-1} t & \text{for } t \geq 0 \\ \frac{1}{2\pi} (\pi + \tan^{-1} t) & \text{for } t < 0 \end{cases} \quad (14)$$

The stub length l is then calculated by using the value of t obtained above and calculating the stub insertion point susceptance B using equation (12b). The desired stub susceptance B_s is thus $B_s = -B$ for a perfect match. Then, for a short circuited coaxial stub:

$$\frac{l}{\lambda} = \frac{-1}{2\pi} \tan^{-1} \left(\frac{1}{Z_0 B_s} \right) \quad (15)$$

$\lambda/2$ is added to the solution if the calculated length is negative.

The MATLAB code realisation was tested for all combinations of arm reactance in the solution space and successfully demonstrated a VSWR of 1 (i.e successfully matched) for all test cases. It is shown below:

```

%%%%%%%%%%%%%%%%%%%%%%%%%%%%%%%%%%%%%%%%%%%%%%%%%%%%%%%%%%%%%%%%%%%%%%%%
% This function calculates the 2nd stage match parameters d (length
% of transformer TL required, & Zs the impedance of the parallel
% short circuited stub required
%%%%%%%%%%%%%%%%%%%%%%%%%%%%%%%%%%%%%%%%%%%%%%%%%%%%%%%%%%%%%%%%%%%%%%%%

function [d,Zs] = SSM(Z0,RL,XL,B)
% Z0 - characteristic impedance,
% RL - load resistance,
% XL - load reactance
% B - phase shift index Beta

% calculate two versions of parameter 't'
t1=(XL+(RL.*((Z0-RL).^2+XL.^2)./Z0).^0.5)./(RL-Z0);
t2=(XL-(RL.*((Z0-RL).^2+XL.^2)./Z0).^0.5)./(RL-Z0);

%Calc two candidate transformer lengths, adding pi/B if lengths
negative
d1=(atan(t1)+pi*(t1<0))/B;
d2=(atan(t2)+pi*(t2<0))/B;
s1=(d1<d2); % calculate relative length flags
s2=(d2<d1);
d=s1.*d1+s2.*d2; %select lower distance

%calc stub length
t=s1.*t1+s2.*t2; %select correct t value

```

```

% calculate required stub susceptance
Bs = ((Z0-XL.*t).*(XL+Z0.*t)-RL.^2.*t)/Z0./(RL.^2+(XL+Z0.*t).^2);
ls = -atan(1./Bs/Z0)/B; % use the correct for for a short circuited
stub
ls = ls+(ls<0)*pi/B;    %if negagtive length, add half wavelength

%calc stub impedance
Zs = j*Z0*sin(B*ls)./cos(B*ls);

```

12. Appendix B

Impedance Matrix Supplied by the ILA commissioning team:

f=41.976MHz

Dataset JET 2006/Measurements/Tank_ChickenWire_13.09.06/549mm

Measurements on JET-EP antenna, water tank at $(589 - 549) * 0.1 = 4\text{cm}$ from the closest position

Data processed to remove measurement adapters, the following impedance matrix is at the capacitor insertion points.

The straps are numbered as follows:

1 5
2 6
3 7
4 8

Resistance matrix R:

0.3953	-0.1193	0.0885	-0.1134	0.0582	-0.0678	0.0753	-0.1093
-0.1193	0.3494	-0.1652	0.1641	-0.0677	0.0747	-0.0943	0.1486
0.0885	-0.1652	0.3732	-0.2358	0.0743	-0.0920	0.1104	-0.1826
-0.1134	0.1641	-0.2358	0.6013	-0.1085	0.1452	-0.1818	0.2811
0.0582	-0.0677	0.0743	-0.1085	0.3432	-0.1200	0.0927	-0.1185
-0.0678	0.0747	-0.0920	0.1452	-0.1200	0.3076	-0.1680	0.1681
0.0753	-0.0943	0.1104	-0.1818	0.0927	-0.1680	0.3404	-0.2268
-0.1093	0.1486	-0.1826	0.2811	-0.1185	0.1681	-0.2268	0.5691

Reactance matrix X:

25.8622	0.4600	-0.0575	0.0508	0.7876	-0.0575	-0.0144	0.0455
0.4600	23.1897	1.1654	-0.1014	-0.0590	0.5465	-0.1058	-0.0573
-0.0575	1.1654	23.3284	0.4564	-0.0150	-0.1043	0.4965	0.0065
0.0508	-0.1014	0.4564	26.4483	0.0453	-0.0573	0.0101	0.8361
0.7876	-0.0590	-0.0150	0.0453	25.9228	0.4622	-0.0600	0.0537
-0.0575	0.5465	-0.1043	-0.0573	0.4622	22.9934	1.1850	-0.1058
-0.0144	-0.1058	0.4965	0.0101	-0.0600	1.1850	23.3915	0.4754
0.0455	-0.0573	0.0065	0.8361	0.0537	-0.1058	0.4754	26.6804

Impedance matrix = $R + j X$

13. Appendix C

This code calculates the resilience of a given CT circuit, in response to resistive disturbances.

```
%%%%%%%%%%%%%%%%%%%%%%%%%%%%%%%%%%%%%%%%%%%%%%%%%%%%%%%%%%%%%%%%%%%%%%%%
% This function calculates the resilience of an asymmetric RDL with
% no cross coupling. Resilience is defined as the 1st critical vswr
% crossing. It starts from the matched condition, & initially scans
% for sign change to avoid local minima, then converges with Newton
% Raphson
%%%%%%%%%%%%%%%%%%%%%%%%%%%%%%%%%%%%%%%%%%%%%%%%%%%%%%%%%%%%%%%%%%%%%%%%

function [resilience] = Load_tolerance(r,XX1,XX2,ZZm,Scref,acc,Zm)
% This function requires an input of strap resistance (in the form
[r1;r2]), branch1 reactance XX1, branch2 reactance XX2, the
characteristic impedance ZZm, a critical vswr Scref, a solution
tolerance acc, and a mutual impedance Zm. It returns the resilience
of the resulting RDL.

solve = 1;           % set numerical solver flag = 1
VS = 1;             % set solver engine to variable step
initially
P = 0;              % solver will not initially look for peaks
NR = 0;             % solver will not initially use Newton
Raphson
suppress = 0;       % solver will not suppress peak detection

s = 0.5;            % reference step of 0.5 on lambda. This
sets the initial search resolution. Deliberately coarse.
count=1;           % initialise count
lp = (1+s);        % initialise predicted lambda. This is
the first "guess" lambda so that we can initialize the input and
output variables. Lambda is the definition of resilience
rs = [r,lp*r];     % set initial guess to matched
solution. This uses lambda to initialize the resistance register.
The first entry is the former resistance, the 2nd entry the current
solution. Rs is the instantaneous strap resistance, and so is equal
to resilience*strap base load. NOTE THAT THIS DEFINITION IGNORES ANY
SCALING OF INDUCTANCE, AND MUTUALS
lambda = [1,lp];   % initialise load scaling
factor lambda. The first entry is the former lambda, the 2nd the
current

%calculate vswr for the 1st two guesses%
vswr(1) = CT(rs(1:2,1),XX1,XX2,ZZm,Zm); % matched solution
vswr(2) = CT(rs(1:2,2),XX1,XX2,ZZm,Zm); % guess 1 solution

%calculate initial gradient in the solution. Use a local resolution
of +/-0.005% on resistance. This is used in the solver algorithm
l1 = lambda(2)+0.005;
l2 = lambda(2)-0.005;
v1 = CT(l1*r,XX1,XX2,ZZm,Zm);
```

```

v2 = CT(l2*r,XX1,XX2,ZZm,Zm);
gradient = (v2-v1)/(l2-l1)*ones(2,1);    % this is the local
gradient of the vswr solution at the latest guess of lambda

while solve == 1
    % this loop will run until the value of lambda that produces
    a critical vswr is derived.
    % solution possibilities %
    peak_detect = (gradient(2)<0)&&(gradient(1)>=0);
    % this flag shows that the solution has encountered a peak
    (gradient always starts +ve, as the search always starts from
    the matched position)
    close = (vswr(2)<1.5)&&(vswr(2)>1.45);
    % this flag shows that the latest guess is in close proximity
    to the solution
    between = (vswr(1)<Scref)&&(vswr(2)>Scref);
    % this flag shows that the solution lies between the last two
    guesses
    soln = (vswr(2)<Scref*(1+acc/200))&&(vswr(2)>Scref*(1-
acc/200));
    % this flag shows that the solution has been found, within
    acc% margin of error

% the following code selects the correct solver strategy dependant
on the solution flags:

%%%%%%%%%%%%%%%%%%%%%%%%%%%%%%%%%%%%%%%%%%%%%%%%%%%%%%%%%%%%%%%%%%%%%%%%
% if target is between latest two guesses on a positive gradient, %
% OR if already tracking intersection                               %
%%%%%%%%%%%%%%%%%%%%%%%%%%%%%%%%%%%%%%%%%%%%%%%%%%%%%%%%%%%%%%%%%%%%%%%%
    if ((between==1)&&(gradient(2)>=0)) || (NR==1)
        VS = 0; P = 0; NR = 1; %select newton raphson solver -
most robust at tracking a direct intersection

%%%%%%%%%%%%%%%%%%%%%%%%%%%%%%%%%%%%%%%%%%%%%%%%%%%%%%%%%%%%%%%%%%%%%%%%
% if local peak detected in vicinity of target, OR if already    %
% tracking local peak AND peak tracking not suppressed           %
%%%%%%%%%%%%%%%%%%%%%%%%%%%%%%%%%%%%%%%%%%%%%%%%%%%%%%%%%%%%%%%%%%%%%%%%

        elseif ((peak_detect==1)&&(close==1)&&(suppress==0)) || (P==1)
            VS = 0; P = 1; NR = 0; %select peak solver. critical
resilience coincides with a local peak hitting critical
vswr. In this case N-R does not converge well. However,
do not track local peaks if not in vicinity of solution,
as this wastes time

        else
            VS = 1; P = 0; NR = 0; %select the default variable
step solver
        end

%numerical iterations
if (soln == 1)&&(gradient(2)>=0)
    % vswr within solution deadband, and on a positive gradient.
    Therefore solution found, break loop and record result
        solve = 0; % crossing found, break
loop
        resilience = lambda(2); % resilience found
    elseif NR == 1

```

```

% apply Newton raphson numerical iteration
grad = 1/gradient(2); % calc gradient in
solution
lp = grad*(Scref-vswr(2))+lambda(2); % new predicted
critical lambda
elseif P == 1
% investigate local maxima to see if it is the solution

% calculate flag to determine if local gradient of latest
guess is within the solution deadband - (ie local maxima
found)
P = (gradient(2)>-0.001)&&(gradient(2)<0.001);
P=P-1;
if P == 0 % maximum found, we are beneath solution, so
select variable step solver and proceed
VS = 1; P = 0; NR = 0;
suppress = 1; % suppress peak
solve (initially) to enable solution to break out
of peak mode
else
% find local peak by using N_R to converge on local
gradient = 0.
grad = (lambda(2)-lambda(1))/(gradient(2)-
gradient(1)); % calc gradient in the gradient
solution
lp = grad*(0-gradient(1))+lambda(1);
% new predicted crit lambda
end
elseif count>300 % stuck in loop
solve = 0; % break loop
sprintf('failed to converge within 300 cycles')
elseif VS==1
% use variable step to find solution locality INITIALLY.
Resolution increases as solution approaches.
lp = lp+2*(0.1-s)*(vswr(2)-1)+s; % variable step
search, reduces step size from 0.5 to 0.1 when close to
critical vswr to prevent oscillation. overshoot
compensation as steps reverse if overshoot occurs (but this
should trigger NR solve in any case)
suppress = 0; % If solution has
just moved away from a local maxima, this command re-arms
the peak detection algorithm in case another local maxima
is encountered
end
rs = [rs(1:2,2),lp*r]; % update resistance
register. Note that the notation for r is [r1;r2] and for rs
is [rs1(i),rs1(i+1);rs2(i),rs2(i+1)]. This code shifts
register values left, and introduces the latest calculation
in the 2nd entry
lambda = [lambda(2),lp]; % update lambda
register
vswr(1) = vswr(2); % update vswr
solution register
vswr(2) = CT(rs(1:2,2),XX1,XX2,ZZm,Zm); % calculate new
guess vswr
gradient(1) = gradient(2); % update gradient
register
%calc new gradient at latest guess
l1 = lambda(2)+0.005;

```

```

        l2 = lambda(2)-0.005;
        v1 = CT(l1*r,XX1,XX2,ZZm,Zm);
        v2 = CT(l2*r,XX1,XX2,ZZm,Zm);
        gradient(2) = (v2-v1)/(l2-l1);
        count = count+1;                                % increment
iteration count
end

%-----
%%%%%%%%%%%%%%%%%%%%%%%%%%%%%%%%%%%%%%%%%%%%%%%%%%%%%%%%%%%%%%%%%%%%%%%%
% This function calculates the vswr for an Asymmetric RDL with cross
% coupling
%%%%%%%%%%%%%%%%%%%%%%%%%%%%%%%%%%%%%%%%%%%%%%%%%%%%%%%%%%%%%%%%%%%%%%%%

function [vswr] = CT(rs,XX1,XX2,ZZm,Zmutual)

z1 = rs(1,1)+XX1*j;                                     % branch impedance 1
z2 = rs(2,1)+XX2*j;                                     % branch impedance 2
zct = (Zmutual^2-z1*z2)/(2*Zmutual-(z1+z2)); % CT total impedance
including mutuals
G = (ZZm-zct)/(ZZm+zct);                               % calc reflection coefficient
vswr = (1+abs(G))/(1-abs(G));                          % calc vswr

```

14. Appendix D

This code extracts the required net and gross phase angles for optimal resilience performance of any given CT circuit in response to resistive disturbances.

The following code is recorded with added commentary in green

```
%%%%%%%%%%%%%%%%%%%%%%%%%%%%%%%%%%%%%%%%%%%%%%%%%%%%%%%%%%%%%%%%%%%%%%%%
% This program numerically calculates the maximum resilience for a
% asymmetrical CT circuit with cross coupling between straps and a
% perfect 2nd stage matching circuit
%%%%%%%%%%%%%%%%%%%%%%%%%%%%%%%%%%%%%%%%%%%%%%%%%%%%%%%%%%%%%%%%%%%%%%%%

function [max_resilience,x1_max,x2_max,thN,thG] =
resilience_calc(p,e,f,strap)
%This code accepts a strap average loading called "strap", a
percentage asymmetry "p", a percentage resistive mutual "e" and a
percentage reactive mutual "f". it returns the maximum value of
resilience, the corresponding arm reactance setpoints x1max & x2max,
& phase setpoints thN (net phase) and thG (gross phase)

%define degree of mutual coupling - turn variables e&f into ohms
with reference to average strap load
Zm = e*real(strap)+f*imag(strap)*j;
%define load - obtain values of branch resistance to meet asymmetry
criteria.
r1 = 2/(2-p);
r2 = 2*(1-p)/(2-p);
r = real(strap)*[r1;r2];           % nominal strap resistance

%define VSWR limit
Scref = 1.5;                     % max tolerable VSWR

%%%%%%%%%%%%%%%%%%%%%%%%%%%%%%%%%%%%%%%%%%%%%%%%%%%%%%%%%%%%%%%%%%%%%%%%
variable resolution solver - this solver forms an initially course
mesh for the whole solution space in X1 & X2 and calculates the
resulting vswr at each node. The maximum value is then obtained. The
solver then selects an area +/- 2 node around this maximum, and re-
meshes this window at double the resolution. This process is
repeated until the necessary resolution on X has been met, and so
homes in on the maxima. This approach is necessary, as the maxima
exists on a discontinuity. Therefore traditional gradient ascent
methods are not possible.
%%%%%%%%%%%%%%%%%%%%%%%%%%%%%%%%%%%%%%%%%%%%%%%%%%%%%%%%%%%%%%%%%%%%%%%%

optimise = 1;                     % set optimisation flag
count = 1;                       % initialise count
%form initial course grid
grid = 0.75;                     % initialise grid resolution to 0.75
ohms
% 1 solution known to exist in upper left quadrant - limit search to
this area
X1 = -10:grid:0;
X2 = 0:grid:10;
```

```

x1,x2] = meshgrid(X1, X2);      % form grid between orthogonal
vectors X1 and X2
% calculate 2nd stage match parameters. This simplification ignores
the design of the 2nd stage circuit, but rather assumes that whatever
impedance the resulting parallel combination yields, a hypothetical
2nd stage has equalized this with the line characteristic impedance.
Therefore, for all combinations of X the vswr is 0.
z1 = r(1,1)+x1.*j;             % branch impedance 1
z2 = r(2,1)+x2.*j;             % branch impedance 2
zm = (Zm^2-z1.*z2)./(2*Zm-(z1+z2)); % this is the total T point
impedance, and is taken as the characteristic impedance.

a=size(x1);                     % obtain array dimensions of grid
resilience = zeros(a(1),a(2)); % preallocate resilience for speed

while optimise == 1
    % stay within this loop until optimum required resolution found.
    if grid<=0.001              %last resolution sufficient at 0.001
ohm. Therefore finish optimization and break loop
        optimise = 0;
        [re,rr] = max(resilience);
        [Re,column] = max(re);
        row = rr(column);
        max_resilience = Re;      % output global maximum
resilience
        x1_max = x1(row,column); % obtain X1 coordinate of global max
        x2_max = x2(row,column); % obtain X2 coordinate of global max

    elseif count == 1           % establish initial sweep.
        The grid will cover the whole solution space. Solver tolerances
        are relaxed to gain speed.
        for m = 1:1:a(1)        % scan the rows of x1
            for n = 1:1:a(2)    % scan the columns of x1
                % calculate the resilience for course grid, 1% error on result
                [resilience(m,n),record] =
                    Load_tolerance(r,x1(m,n),x2(m,n),zm(m,n),Scref,1,Zm
                    );
                count = count+1;
            end
        end

    else
        % initial grid is complete. obtain maxima from course mesh.
        Re - maximum value, row, & column the matrix address in the
        solution
        [re,rr] = max(resilience);
        [Re,column] = max(re);
        row = rr(column);

        % obtain local grid. Grid space is x coordinate of maximum
        +/- 2*current grid resolution
        X1LL = x1(row,column)-2*grid; %x1 lower limit
        X1UL = x1(row,column)+2*grid; %x1 upper limit
        X2LL = x2(row,column)-2*grid; %x2 lower limit
        X2UL = x2(row,column)+2*grid; %x2 upper limit
        grid = grid/2;              % double resolution for next iteration

        % form new mesh 9x9 window around current maximum

```

```

XX1 = X1LL:grid:X1UL;
XX2 = X2LL:grid:X2UL;
[xx1,xx2] = meshgrid(XX1,XX2);

% insert window into existitng grid, and return the new
% vectors that describe the window location - ro & co
[resilience,ro,co] =
refine_grid(resilience,row,column,zeros(9,9));
[x1,ro,co] = refine_grid(x1,row,column,xx1);
[x2,ro,co] = refine_grid(x2,row,column,xx2);

% enlarge 2nd stage match (insert ones - values outwith
% window are not considered from now on)
a=size(x1);
z1 = ones(a(1),a(2));
z2 = ones(a(1),a(2));
zm = ones(a(1),a(2));
% populate window with updated 2nd stage match parameters
% (assuming an ideal 2nd stage circuit) %
z1(ro,co) = r(1,1)+x1(ro,co).*j; % branch impedance 1
z2(ro,co) = r(2,1)+x2(ro,co).*j; % branch impedance 2
zm(ro,co) = (Zm^2-z1(ro,co).*z2(ro,co))./(2*Zm-
(z1(ro,co)+z2(ro,co))); % 2nd stage match including mutuals
%calculate values of resilience in the window. Reduce error
% to 0.1% for less numerical noise in solution.
final=zeros(a(1),a(2));
for m = ro % scan the rows of window
    for n = co % scan the columns of window
        % calculate the resilience for the window, 0.1% error on result
        [resilience(m,n),record,final(m,n)] =
Load_tolerance(r,x1(m,n),x2(m,n),zm(m,n),Scref,0.1,Zm);
    end
end
count = count+1;
end
end

%calculate phase of max solution%
armz1 = r(1,1)+j*x1_max;
armz2 = r(2,1)+j*x2_max;
q1 = (Zm-armz2)/(Zm^2-armz1*armz2); %a quantity of same phase as
I1 (phase referenced to Tpoint voltage)
q2 = (Zm-armz1)/(Zm^2-armz1*armz2); %a quantity of same phase as
I2 (phase referenced to Tpoint voltage)
qth1 = atan2(imag(q1),real(q1))/pi*180; %extract phase angle of I1
qth2 = atan2(imag(q2),real(q2))/pi*180; %extract phase angles of I2
%remember that angles are of opposite sign - so gross + net angle
definitions have been inverted
thG = qth1-qth2; %output gross phase coord of global max
thN = qth1+qth2; %output net phase coord of global max

%-----

%%%%%%%%%%%%%%%%%%%%%%%%%%%%%%%%%%%%%%%%%%%%%%%%%%%%%%%%%%%%%%%%%%%%%%%%
% This function accepts a nxn matrix & an index and inserts 4 rows &
% columns about the index. values are filled by duplicates of the
% adjoining rows and columns. A refined local grid is then inserted

```

```

% around the maxima location
%%%%%%%%%%%%%%%%%%%%%%%%%%%%%%%%%%%%%%%%%%%%%%%%%%%%%%%%%%%%%%%%%%%%%%%%

function [output,ro,co] = refine_grid(input,row,column,locl_grid)

    % insert new rows in "input"
    upper = input(1:(row-2),:);
    upper_v = input((row-1),:);
    centre_r = input(row,:);
    lower_v = input((row+1),:);
    lower = input((row+2):end,:);
    output =
[upper;upper_v;upper_v;centre_r;centre_r;centre_r;lower_v;lower_v;lo
wer];

    % insert new columns
    left = output(:,1:(column-2));
    left_v = output(:,(column-1));
    centre_c = output(:,column);
    right_v = output(:,(column+1));
    right = output(:,(column+2):end);
    output=
[left,left_v,left_v,centre_c,centre_c,centre_c,right_v,right_v,right
];

    % insert local mesh
    row = row+2;      % convert maxima location indices to new
enlarged matrix
    column = column+2;
    %new search window description vectors
    ro = (row-4):(row+4);
    co = (column-4):(column+4);
    output(ro,co) = locl_grid;

```

15. Appendix E

This code extracts the required gross and net angle set points to deliver a pre declared target T point impedance. It simulates the action of the fixed T control algorithm

The following code is recorded with added commentary in green

```
%%%%%%%%%%%%%%%%%%%%%%%%%%%%%%%%%%%%%%%%%%%%%%%%%%%%%%%%%%%%%%%%%%%%%%%%
% This algorithm calculates the optimal arm reactance set points for
% the fixed T point impedance algorithm. It accepts frequency (w),
% strap resistance (r), resistive mutual (r_mutual), inductive
% mutual (L_mutual)& target T point impedance z_ft
%%%%%%%%%%%%%%%%%%%%%%%%%%%%%%%%%%%%%%%%%%%%%%%%%%%%%%%%%%%%%%%%%%%%%%%%

function [x1_FT,x2_FT] = fixdT(w,r,r_mutual,L_mutual,z_ft)

% calculate mutual impedance %
Z_mutual = r_mutual+L_mutual*w*j;

%define arbitrary starting point for algorithm%
%initial arm reactance
X1=-2;
X2=2;
% initialise data
count = 1;
%start solve
solve = 1;          % solver flag
while solve==1
    %calc error & gradients
    % assign neighboring X values to operating point to make
    triangular sample region. Coordinates are red in columns,
    (X1,X2), (1.001*X1,X2) etc
    xreg = [X1,1.001*X1,X1;X2,X2,1.001*X2];
    %calc arm impedances on triangle nodes
    zreg = [r,r,r]+j*xreg;
    %calc T point impedance on triangle nodes
    zt = (Z_mutual^2-zreg(1,1:end).*zreg(2,1:end))./(2*Z_mutual
    -(zreg(1,1:end)+zreg(2,1:end)));
    %calculate real & imaginary part of the error between actual
    impedance
    and target impedance for all nodes of the triangle %
    E_real = real(z_ft)-real(zt);          % real part
    E_imag = imag(z_ft)-imag(zt);         % imaginary part
    E_T = (E_real.^2+E_imag.^2).^0.5;      % magnitude of error
    % calc partial gradients in error space
    d_e_x1 = (E_T(1)-E_T(2))/(xreg(1,1)-xreg(1,2));
    d_e_x2 = (E_T(1)-E_T(3))/(xreg(2,1)-xreg(2,3));

    % iterate solution
    k = 0.05;          % variable step convergence coefficient
    %%%%%%%%%%%%%%%%%%%%%%%%%%%%%%%%%%%%%%%%%%%%%%%%%%%%%%%%%
    % calc step size. note that sign of gradient used only to give
    % the iteration step the correct polarity. Step size is then a
    % function of absolute error only, and not the gradient
endwhile
```

```

%%%%%%%%%%%%%%%%%%%%%%%%%%%%%%%%%%%%%%%%%%%%%%%%%%%%%%%%%%%%%%%%%%%%%%%%
dx1_t = E_T(1)*d_e_x1/abs(d_e_x1);    % calc step in X1
dx2_t = E_T(1)*d_e_x2/abs(d_e_x2);    %calc step in X2
%calc new X
X1 = X1-k*dx1_t;
X2 = X2-k*dx2_t;

%%%%%%%%%%%%%%%%%%%%%%%%%%%%%%%%%%%%%%%%%%%%%%%%%%%%%%%%%%%%%%%%%%%%%%%%
% declare solution definitions %
%%%%%%%%%%%%%%%%%%%%%%%%%%%%%%%%%%%%%%%%%%%%%%%%%%%%%%%%%%%%%%%%%%%%%%%%
% current T point resistance within +/- 0.013 ohm
real_locus = (E_real(1)>=-0.0065)&&(E_real(1)<=0.0065);
% current T point reactance within +/- 0.013 ohm
imag_locus = (E_imag(1)>=-0.0065)&&(E_imag(1)<=0.0065);
%%%%%%%%%%%%%%%%%%%%%%%%%%%%%%%%%%%%%%%%%%%%%%%%%%%%%%%%%%%%%%%%%%%%%%%%
% if the operating point lies on intersect of real & imaginary %
% T point loci %
%%%%%%%%%%%%%%%%%%%%%%%%%%%%%%%%%%%%%%%%%%%%%%%%%%%%%%%%%%%%%%%%%%%%%%%%
if (real_locus==1)&&(imag_locus==1)
    solve = 0;          % solution found, break loop
    x1_FT = X1;        % declare capacitive arm reactance
    x2_FT = X2;        % declare inductive arm reactance
elseif count == 1000  % if solver stuck in loop
    solve = 0;         % exit solver
    sprintf('fixd T failed to converge') % report error
end
count = count+1;      % increment counter
end

```

16. Appendix F

Amplitude Modulation Algorithm for automatic non ideal parameter compensation

of θ_G .

```
The following code is recorded with added commentary in green
%%%%%%%%%%%%%%%%%%%%%%%%%%%%%%%%%%%%%%%%%%%%%%%%%%%%%%%%%%%%%%%%%%%%%%%%
% This program returns the optimal x set points using the frequency
% stabilised algorithm for a single RDL asymmetrical with mutuals.
% It accepts as arguments frequency (w), Strap fixed inductance
% (strap_L), arm resistance (r), resistive mutual (rm), mutual
% inductance (Lm), & the maximum vswr tolerable (vswr_target)
%%%%%%%%%%%%%%%%%%%%%%%%%%%%%%%%%%%%%%%%%%%%%%%%%%%%%%%%%%%%%%%%%%%%%%%%
function [x1_max,x2_max] = algorithm(w,strap_L,r,rm,Lm,vswr_target)

% calculate mutual impedance %
Z_mutual = rm+Lm*w*j;

% define gross angle target %
ThG_trget = 135.5; % maximum possible of ~138.2°; for ideal
                  circuit & vswr limit of 1.5
%define arbitrary starting point for algorithm%
%initial arm reactance
a=-2;
b=2;
% calculate initial Capacitor values
C1s = 1/w/(w*strap_L-a);
C2s = 1/w/(w*strap_L-b);
% calculate initial stroke values for actuators
s1 = (C1s*1e12-80)/4.0740741;
s2 = (C2s*1e12-80)/4.0740741;
% initial reactance demand signals
average = (a+b)/2; %initial average demand signal
differential = abs((a-b)/2); %initial differential demand signal
% initialise counter
count = 1;

%start solve
solve = 1; %solver flag
while solve==1
    % calc arm impedances at all frequencies. Note the use of 0.5%
    % modulation index %
    z1 = Zarm(s1,strap_L,w,r(1,1)); % branch impedance 1 -
centre
    z2 = Zarm(s2,strap_L,w,r(2,1)); % branch impedance 2 -
centre
    z1f1 = Zarm(s1,strap_L,1.005*w,r(1,1));% branch impedance 1,
upper sideband
    z1f2 = Zarm(s1,strap_L,0.995*w,r(2,1));% branch impedance 1,
lower sideband
    z2f1 = Zarm(s2,strap_L,1.005*w,r(1,1));% branch impedance 2,
upper sideband
    z2f2 = Zarm(s2,strap_L,0.995*w,r(2,1));% branch impedance 2,
lower sideband
```

```

%calc dz/dw of T point
zt_f1 = ZTF(z1f1,z2f1,rm,Lm,1.005*w); % calc upper frequency
% calc upper frequency
% impedance magnitude
zt_f2 = ZTF(z1f2,z2f2,rm,Lm,0.995*w); % calc lower frequency
% calc lower frequency
% impedance magnitude
dz = zt_f1-zt_f2; % calculate the
difference in sideband T point impedances.(should be 0 when properly
configured)
%calculate phase angles%
q1 = (Z_mutual-z2)/(Z_mutual^2-z1*z2); % a quantity of same
phase as I1 (phase referenced to T point voltage)
q2 = (Z_mutual-z1)/(Z_mutual^2-z1*z2); % a quantity of same
phase as I2 (phase referenced to T point voltage)
qth1 = atan2(imag(q1),real(q1))/pi*180; %extract phase angle of
I1
qth2 = atan2(imag(q2),real(q2))/pi*180; %extract phase angles
of I2
gross_angle = qth1-qth2; % Angles are of
opposite sign, hence negative
er = ThG_trget-gross_angle; % Calculate the error in  $\theta_G$ 
solution

%declare solution definitions%
valid_region = (gross_angle>=90); % valid region of
convergence for  $\theta_N$ 
thN_locus1 = (dz>=-0.005)&&(dz<=0.005); % within +/- 0.01
ohm of
dz/df = 0
thN_locus = thN_locus1&&valid_region; % operating point
must lie on net angle solution locus in region of validity
thG_locus = (er>=-0.005)&&(er<=0.005); % operating point
must be within +/- 0.01 deg of gross angle target

%%%%%%%%%%%%%%%%%%%%%%%%%%%%%%%%%%%%%%%%%%%%%%%%%%%%%%%%%%%%%%%%%%%%%%%%
% if the operating point lies on the intersect of gross & net angle
% loci
%%%%%%%%%%%%%%%%%%%%%%%%%%%%%%%%%%%%%%%%%%%%%%%%%%%%%%%%%%%%%%%%%%%%%%%%
if (thN_locus==1)&&(thG_locus==1)
    solve = 0; % solution found, exit iterative
solver
    x1_max = X1d; % capacitive reactance solution
    x2_max = X2d; % inductive reactance solution

elseif count == 500 % if solver stuck in loop
    solve = 0;
    % exit solver
    sprintf('failed to converge'); % report error

%%%%%%%%%%%%%%%%%%%%%%%%%%%%%%%%%%%%%%%%%%%%%%%%%%%%%%%%%%%%%%%%%%%%%%%%
% if solution not found, iterate reactance demand signals %
%%%%%%%%%%%%%%%%%%%%%%%%%%%%%%%%%%%%%%%%%%%%%%%%%%%%%%%%%%%%%%%%%%%%%%%%
else
% update net angle by variable step. Maintain value if outside
thevalid region
    average = average + 0.01*dz*valid_region;
% update gross angle by variable step.
    differential = differential + 0.01*er;
% calculate the resulting reactance demand signal

```

```

        X1d = (average-differential);           % capacitive
        X2d = (average+differential);         % inductive
%%%%%%%%%%%%%%%%%%%%%%%%%%%%%%%%%%%%%%%%%%%%%%%%%%%%%%%%%%%%%%%%%%%%%%%%
% use the inverse of the model to translate reactive demand
% to capacitive demand
%%%%%%%%%%%%%%%%%%%%%%%%%%%%%%%%%%%%%%%%%%%%%%%%%%%%%%%%%%%%%%%%%%%%%%%%
        C1d = 1/w/(w*strap_L-X1d);
        C2d = 1/w/(w*strap_L-X2d);
%%%%%%%%%%%%%%%%%%%%%%%%%%%%%%%%%%%%%%%%%%%%%%%%%%%%%%%%%%%%%%%%%%%%%%%%
% use the inverse of the model to translate capacitive demand
% to position demand
%%%%%%%%%%%%%%%%%%%%%%%%%%%%%%%%%%%%%%%%%%%%%%%%%%%%%%%%%%%%%%%%%%%%%%%%
        s1 = (C1d*1e12-80)/4.0740741;
        s2 = (C2d*1e12-80)/4.0740741;

        count = count+1;           % increment counter
    end
end

%-----%

%%%%%%%%%%%%%%%%%%%%%%%%%%%%%%%%%%%%%%%%%%%%%%%%%%%%%%%%%%%%%%%%%%%%%%%%
% This function calculates a CT arm impedance for a given capacitor
% stroke (s), frequency (w), strap inductance (strap_L) & strap
% resistance,(r)
%%%%%%%%%%%%%%%%%%%%%%%%%%%%%%%%%%%%%%%%%%%%%%%%%%%%%%%%%%%%%%%%%%%%%%%%

function [z] = Zarm(s,strap_L,w,r)
x = reactance(s,w,strap_L);           % branch reactance
z = r+x*j;                             % branch impedance

%-----%

%%%%%%%%%%%%%%%%%%%%%%%%%%%%%%%%%%%%%%%%%%%%%%%%%%%%%%%%%%%%%%%%%%%%%%%%
% This function calculates the magnitude of the CT Tpoint impedance
% for 2 branch impedances, (z1 & z2), mutual inductance (L_mutual) &
% mutual resistance (R_mutual) at a given frequency (w)
%%%%%%%%%%%%%%%%%%%%%%%%%%%%%%%%%%%%%%%%%%%%%%%%%%%%%%%%%%%%%%%%%%%%%%%%

function [z] = ZTF(z1,z2,R_mutual,L_mutual,w)
ZM = R_mutual+j*L_mutual*w;           %define mutual
z = (ZM.^2-z1.*z2)./(2*ZM-(z1+z2));    %calc t point
impedance
z = abs(z);                             % extract magnitude

%-----%

%%%%%%%%%%%%%%%%%%%%%%%%%%%%%%%%%%%%%%%%%%%%%%%%%%%%%%%%%%%%%%%%%%%%%%%%
% This function calculates a CT arm reactance for a given capacitor
% stroke,(s), frequency (w), & strap inductance (strap_L)
%%%%%%%%%%%%%%%%%%%%%%%%%%%%%%%%%%%%%%%%%%%%%%%%%%%%%%%%%%%%%%%%%%%%%%%%

function [x] = reactance(s,w,strap_L)
C = (4.0740741*s+80)*1e-12;           %capacitance
x = (w.^2*strap_L*C-1)./(w*C); % branch reactance

```

17. Appendix G

This code calculates the resilience performance of any given CT circuit using the average coupled power measure.

The following code is recorded with added commentary in green

```
%%%%%%%%%%%%%%%%%%%%%%%%%%%%%%%%%%%%%%%%%%%%%%%%%%%%%%%%%%%%%%%%%%%%%%%%
% This program calculates & plots CT performance with a triangular
% ELM locus. It assumes mutuals are fixed in ELMs. a stub & line
% transformer 2nd stage match are used
%%%%%%%%%%%%%%%%%%%%%%%%%%%%%%%%%%%%%%%%%%%%%%%%%%%%%%%%%%%%%%%%%%%%%%%%
function [] = ELM_model3()

%declare parameters
Sc=3;           %cutoff vswr
Prm=130e3;      %maximum allowable reflected power Watts
Pi=2e6;         %input power Watts
Z0=30;         %characteristic impedance of system Ohms

%calculate power limit vswr
Sl=(Pi^0.5+Prm^0.5)^2/(Pi-Prm);

%define second order effects for both arms%
p = 0;         % resistive asymmetry (0 = symmetrical, 1 =
asymmetric)
e = 0;         % percentage of real mutual impedance between straps
f = 0;         % percentage of imaginary mutual impedance between
straps

% define match frequency
Hz = 42.5e6;   % midband frequency Hz
w = 2*pi*Hz;  % frequency in radians
B = w/3e8;    % phase shift constant in vacuum

%define average strap impedance
strap_L = 120e-9; % 50cm of 200nH/m plus 20nH capacitor parasitic
inductance
strap_R = 0.75;  % midband resistance of 30cm of 2-3 ohm/m

%calculate asymmetry coefficients (average strap resistance held
constant)
r1 = 2./(2-p);
r2 = 2*(1-p)./(2-p);

%define degree of mutual coupling
L_mutual = f*strap_L;
Z_mutual = e*strap_R+w*L_mutual*j;

%define ELM values
Rfactor=5;     %elms increase resistance by up to 5
times
Xfactor=0.75;  %elms decrease reactance by up to 25%
```

```

Rmax = Rfactor*strap_R;           %max assumed resistive ELM disturbance
Lmin = Xfactor*strap_L;           %max assumed reactive ELM disturbance
resolution=10;                     % define resolution for meshing ELM area
ELMR = (strap_R+(Rmax-strap_R)/resolution):(Rmax-
strap_R)/resolution:Rmax; %generate resistance variation vector
excluding matched value, would otherwise give NaN
if Xfactor == 1                     % special case of no reactive components to
ELM
    ELM_L = Lmin*ones(1,resolution); % use strap_L for all coupled
power calcs
Else
%generate reactance variation vector excluding matched value, would
otherwise give NaN
    ELM_L = (strap_L+(Lmin-strap_L)/resolution):(Lmin-
strap_L)/resolution:Lmin;
end
[elmR,elmL] = meshgrid(ELMR,ELM_L); %generate mesh from the X&R
variation vectors

%elm space
elmSpace=zeros(resolution,resolution); %define a region for ELM
variation
i=0;
%form a Boolean operator in the form of a triangle to select the ELM
valid area. Count the node number for future averaging calcs%
for o=1:1:(resolution) %rows
    for q=1:1:(resolution) %columns
        if q>=o
            elmSpace(o,q)=1;
            i=i+1;
        end
    end
end
end

% define the design space %
s = 5:0.05:15; % define capacitor stroke, full design space is
0:54mm
x = reactance(s,w,strap_L); %convert stroke to arm reactance

[SS1,SS2] = meshgrid(s,s); %define capacitor stroke space
[XX1,XX2] = meshgrid(x,x); %define reactance space
[row,col] = size(SS1); %get the size of the solution
space

%2nd stage match
zT = Timpedance(r1,r2,strap_R,XX1,XX2,Z_mutual); %calc Tpoint
impedance
[d,Zs] = SSM(Z0,real(zT),imag(zT),B); %calc matching
parameters d (length of transformer, and Zs stub impedance

%%%%%%%%%%%%%%%%%%%%%%%%%%%%%%%%%%%%%%%%%%%%%%%%%%%%%%%%%%%%%%%%%%%%%%%%
%check success of 2nd stage match - this code demonstrated the 2nd
% stage match successfully matched for all the solution space
%ZL = load(d,Zs,zT,B,Z0);
%swr = VSWR(Z0,ZL);
%surf(XX1,XX2,swr);
%shading interp

```

```

%%%%%%%%%%%%%%%%%%%%%%%%%%%%%%%%%%%%%%%%%%%%%%%%%%%%%%%%%%%%%%%%%%%%%%%%
%%%%%%%%%%%%%%%%%%%%%%%%%%%%%%%%%%%%%%%%%%%%%%%%%%%%%%%%%%%%%%%%%%%%%%%%
%calculate performance%
%%%%%%%%%%%%%%%%%%%%%%%%%%%%%%%%%%%%%%%%%%%%%%%%%%%%%%%%%%%%%%%%%%%%%%%%

%preallocate for speed
Cav=zeros(row,col);           %declare matrix to hold average
coupling
performance=zeros(row,col);   %declare matrix to hold performance

for m = 1:1:row                % scan the rows
    for n = 1:1:col            % scan the columns
        %calc vswr for each position in ELM space
        X1_N = reactance(SS1(m,n),w,elmL);%calc arm reactance during
ELM
        X2_N = reactance(SS2(m,n),w,elmL);%calc arm reactance during
ELM
        %calc the Tpoint impedance during ELM
        ZT = Timpedance(r1,r2,elmR,X1_N,X2_N,Z_mutual);
        %calc the load seen through 2nd stage match during ELM
        ZL = load(d(m,n),Zs(m,n),ZT,B,Z0);
        swr = VSWR(Z0,ZL);           %calc the vswr due to elm
        %calc the coupling for each node in rectangular grid containing
        ELMspace
        C = coupling(swr,Pi,S1,Sc,Prm);
        C=C.*elmpace; %select triangular ELMspace from rectangular
grid
        %establish if cut off occurs in elmspace (matrix variable)
        Ctest = ((C>0)==elmpace);
        minCtest = min(min(Ctest)); %1 - cut off, 0 - no cut off
        Cav(m,n) = sum(sum(C))/i;    %calc average coupling for ELM
area

        performance(m,n)=Cav(m,n)*minCtest; %calc elm performance
measure
    end
end

% display results
plot_flag = 1;                %1 = phase plot, 0 = reactance plot
if plot_flag == 0            %plot results in X space
    surf(XX1,XX2,performance);
elseif plot_flag == 1        %plot results in phase space
    %calculate phase%
    zarm1 = r1*strap_R+XX1.*j;           % branch impedance 1 over
grid
    zarm2 = r2*strap_R+XX2.*j;           % branch impedance 2 over
grid
    %a quantity of same phase as I1 (phase referenced to Tpoint voltage)
    q1 = (Z_mutual-zarm2)./(Z_mutual^2-zarm1.*zarm2);
    %a quantity of same phase as I2 (phase referenced to Tpoint voltage)
    q2 = (Z_mutual-zarm1)./(Z_mutual^2-zarm1.*zarm2);
    %extract phase angle of I1
    qth1 = atan2(imag(q1),real(q1))/pi*180;
    %extract phase angles of I2
    qth2 = atan2(imag(q2),real(q2))/pi*180;

```

```

%remember that angles are of opposite sign - so gross + net angle
definitions have been inverted
    gross_angle = qth1-qth2;
    net_angle = qth1+qth2;

    surf(net_angle,gross_angle,performance);
end
shading interp

%-----%
% This function calculates a CT arm reactance for a give capacitor
% stroke frequency & strap inductance
%-----%

function [x] = reactance(s,w,strap_L)
C = (4.0740741*s+80)*1e-12; % calculate the capacitance using a
linear model
x = (w^2*strap_L.*C-1)./(w*C); % calc branch reactance as series sum
of capacitor & strap

%-----%
% This function calculates the vswr
%-----%

function [vswr] = VSWR(Z0,ZL)

G = (ZL-Z0)./(ZL+Z0); % calc reflection
coefficient
vswr = (1+abs(G))./(1-abs(G)); % calc vswr

%-----%
% This function calculates the coupling ratio as a function of vswr
%-----%

function [coupling] = coupling(vswr,Pi,Sl,Sc,Prm)
a=vswr<Sl; %flag for reflections less than power limit (full power
mode)
b=vswr>=Sl; %flag for reflections greater than or equal to power
limit
c=vswr<Sc; %flag for reflections less than power cut off limit (cut
off mode)
d=b.*c; %flag for reflections in power limit mode
%calculate the coupled power
Pc=a.*(Pi*4*vswr./(1+vswr).^2)+d.*(Prm*4*vswr./(vswr-1).^2);
coupling=Pc/Pi; %normalise coupled power

%-----%
% This function calculates the 2nd stage match parameters d (length
% of transformer TL required, & Zs the impedance of the parallel
% short circuited stub required
%-----%

function [d,Zs] = SSM(Z0,RL,XL,B)

```

See Appendix A

```
%-----%
%%%%%%%%%%%%%%%%%%%%%%%%%%%%%%%%%%%%%%%%%%%%%%%%%%%%%%%%%%%%%%%%%%%%%%%%
% This function calculates the T point impedance inc mutuals
%%%%%%%%%%%%%%%%%%%%%%%%%%%%%%%%%%%%%%%%%%%%%%%%%%%%%%%%%%%%%%%%%%%%%%%%

function [ZT] = Timpedance(a1,a2,R,X1,X2,Zmutual)

z1 = a1*R+X1*j;           % branch impedance 1
z2 = a2*R+X2*j;           % branch impedance 2
% calc Tpoint impedance including effect of mutuals
ZT = (Zmutual^2-z1.*z2)./(2*Zmutual-(z1+z2));

%-----%
%%%%%%%%%%%%%%%%%%%%%%%%%%%%%%%%%%%%%%%%%%%%%%%%%%%%%%%%%%%%%%%%%%%%%%%%
% This function calculates the impedance seen through the 2nd stage
% match assumes a line transformer and short circuit shunt stub
%%%%%%%%%%%%%%%%%%%%%%%%%%%%%%%%%%%%%%%%%%%%%%%%%%%%%%%%%%%%%%%%%%%%%%%%

function [ZL] = load(d,Zs,ZT,B,Z0)

%calc load seen through transformer
Zin = Z0*(ZT.*cos(B*d)+j*Z0*sin(B*d))./(Z0*cos(B*d)+j*ZT.*sin(B*d));
%calc effective load as parallel combination of transformed load and
stub
ZL = Zin.*Zs./(Zin+Zs);
```

18. Appendix H

This code extracts the required gross and net angle set points for optimal resilience performance using the average coupled power measure. It is configured to do this to either a vector of input parameters (used for sensitivity studies), or a single value.

```
%%%%%%%%%%%%%%%%%%%%%%%%%%%%%%%%%%%%%%%%%%%%%%%%%%%%%%%%%%%%%%%%%%%%%%%%
% This program calculates the sensitivity of the average coupled
% power ELM model to resistive asymmetry. It detects & prompts if
% initial search not correctly bounded. individual quadrants are
% searched. The full domain of 0-54mm is included (not so in v4)
%%%%%%%%%%%%%%%%%%%%%%%%%%%%%%%%%%%%%%%%%%%%%%%%%%%%%%%%%%%%%%%%%%%%%%%%

function [thG_register,thN_register,performance_register] =
asymetry_trends5()

%declare parameters
Sc=3;           %cutoff vswr (due to interlock interrupt)
Prm=130e3;      %maximum allowable reflected power
Pi=2e6;        %input power
Z0=30;         %characteristic impedance of system

%calculate power limitation interlock vswr cut in point
Sl=(Pi^0.5+Prm^0.5)^2/(Pi-Prm);

%define average strap impedance
strap_L = 120e-9;           % 50cm of 200nH/m plus 20nH capacitor
parasitic inductance
strap_R = 0.75;            % midband resistance of 30cm of 2-3 ohm/m

%define varied parameter
para = 4; %1 - asymmetry, 2 - real mutual, 3 - imaginary mutual, 4
- single circuit to be assessed.

%define parameter range
if para==1 %asymmetry range 0 - 60%
    range = 0:0.05:0.6;
elseif para==2 %real mutuals range 0 - -60%
    range = 0:-0.05:-0.6;
elseif para==3 %imaginary mutuals range 0 - 0.02%
    range= 0:0.00125:0.02;
else %calculate on one value only
    range = 1;
end
%get size of range
[range_ro,range_co]=size(range);

%define variable parameters for both arms%
% use Boolean selectors to define a vector if variable has range
p = (para==1)*range+(para~=1)*0*ones(range_ro,range_co); %
resistive asymmetry (0 = symmetrical, 1 = asymmetric)
```

```

e = (para==2)*range+(para~=2)*0*ones(range_ro,range_co);    %
percentage of real mutual impedance between straps
f = (para==3)*range+(para~=3)*0*ones(range_ro,range_co);    %
percentage of imaginary mutual impedance between straps

% define match frequency
Hz = 42.5e6;          % midband frequency
w = 2*pi*Hz;         % frequency in radians
B = w/3e8;           % phase shift constant in vacuum

%calculate asymmetry coefficients
r1 = 2./(2-p);
r2 = 2*(1-p)./(2-p);

%define degree of mutual coupling
L_mutual = f*strap_L;
Z_mutual = e*strap_R+w*L_mutual*j;

%define ELM values
Rfactor=5;           %elms increase resistance by upto 5
times
Xfactor=0.75;       %elms decrease reactance by upto 25%
Rmax = Rfactor*strap_R; %max assumed resistive ELM
disturbance
Lmin = Xfactor*strap_L; %max assumed reactive ELM disturbance
resolution=10;      %mesh ELMspace with 55 nodes
ELMR = (strap_R+(Rmax-strap_R)/resolution):(Rmax-
strap_R)/resolution:Rmax; %define a range of R for elms, excluding
matched value, would otherwise give NaN
if Xfactor == 1     %if no reactive ELM compoinent
    ELML = Lmin*ones(1,resolution); %use strap_L for all range or
disturbance
else                %define a range of strap_L for elms
    ELML = (strap_L+(Lmin-strap_L)/resolution):(Lmin-
strap_L)/resolution:Lmin;
end
[elmR,elmL] = meshgrid(ELMR,ELML);

%elm space - form a boolean selection matrix to select a triangular
half of the matrix (as ΔR is always larger than ΔX)
elmspace=zeros(resolution,resolution); %pre allocate size for speed
i=0; % initialise count
for o=1:1:(resolution) % scan rows
    for q=1:1:(resolution) %scan columns
        if q>=o
            elmspace(o,q)=1; % select triangle
            i=i+1;
        end
    end
end

%preallocate for speed
s1_register = zeros(range_ro,range_co); %optiaml stroke 1 record
s2_register = s1_register; %optimal stroke 2 record
x1_register = s1_register; %optimal arm reactance 1
record

```

```

x2_register = s1_register; %optimal arm reactance 2
record
performance_register = s1_register; %maximum performance
register

%calc optimal locations
for m = 1:1:range_ro % scan the rows
    for n = 1:1:range_co % scan the columns
        %calc optimal setpoints & performance for the variable range

[s1_register(m,n),s2_register(m,n),x1_register(m,n),x2_register(m,n)
,performance_register(m,n),XX1,XX2,performance] =
set_points(w,B,strap_R,strap_L,r1(m,n),r2(m,n),Z_mutual(m,n),elmR,el
mL,Z0,Pi,S1,Sc,Prm,elmspace,i);

    end
end

%now map reactance set points into phase space
[thG_register,thN_register] =
XtoP(x1_register,x2_register,r1,r2,strap_R,Z_mutual);

%-----%
%%%%%%%%%%%%%%%%%%%%%%%%%%%%%%%%%%%%%%%%%%%%%%%%%%%%%%%%%%%%%%%%%%%%%%%%
% This function calculates a CT arm reactance for a give capacitor
% stroke frequency & strap inductance
%%%%%%%%%%%%%%%%%%%%%%%%%%%%%%%%%%%%%%%%%%%%%%%%%%%%%%%%%%%%%%%%%%%%%%%%

function [x] = reactance(s,w,strap_L)
C = (4.0740741*s+80)*1e-12; %capacitance
x = (w^2*strap_L.*C-1)./(w*C); % branch reactance

%-----%

%%%%%%%%%%%%%%%%%%%%%%%%%%%%%%%%%%%%%%%%%%%%%%%%%%%%%%%%%%%%%%%%%%%%%%%%
% This function calculates the vswr
%%%%%%%%%%%%%%%%%%%%%%%%%%%%%%%%%%%%%%%%%%%%%%%%%%%%%%%%%%%%%%%%%%%%%%%%

function [vswr] = VSWR(Z0,ZL)

G = (ZL-Z0)./(ZL+Z0); % calc reflection coef
vswr = (1+abs(G))./(1-abs(G)); % calc vswr

%-----%
%%%%%%%%%%%%%%%%%%%%%%%%%%%%%%%%%%%%%%%%%%%%%%%%%%%%%%%%%%%%%%%%%%%%%%%%
% This function calculates the coupling ratio as a function of vswr
%%%%%%%%%%%%%%%%%%%%%%%%%%%%%%%%%%%%%%%%%%%%%%%%%%%%%%%%%%%%%%%%%%%%%%%%

function [coupling] = coupling(vswr,Pi,S1,Sc,Prm)
a=vswr<S1; %flag for reflections less than power
limit (full power mode)
b=vswr>=S1; %flag for reflections greater than or
equal to power limit
c=vswr<Sc; %flag for reflections less than power
cut off limit (cut off mode)
d=b.*c; %flag for reflections in power limit
mode

```

```
Pc=a.*(Pi*4*vswr./(1+vswr).^2)+d.*(Prm*4*vswr./(vswr-1).^2);
coupling=Pc/Pi; %normalise coupled power
```

```
%-----%
%%%%%%%%%%%%%%%%%%%%%%%%%%%%%%%%%%%%%%%%%%%%%%%%%%%%%%%%%%%%%%%%%%%%%%%%
% This function calculates the 2nd stage match parameters d (length
% of transformer TL required, & Zs the impedance of the parallel
% short circuited stub required
%%%%%%%%%%%%%%%%%%%%%%%%%%%%%%%%%%%%%%%%%%%%%%%%%%%%%%%%%%%%%%%%%%%%%%%%
```

```
function [d,Zs] = SSM(Z0,RL,XL,B)
```

See Appendix A

```
%-----%
%%%%%%%%%%%%%%%%%%%%%%%%%%%%%%%%%%%%%%%%%%%%%%%%%%%%%%%%%%%%%%%%%%%%%%%%
% This function calculates the T point impedance inc mutuals
%%%%%%%%%%%%%%%%%%%%%%%%%%%%%%%%%%%%%%%%%%%%%%%%%%%%%%%%%%%%%%%%%%%%%%%%
```

```
function [ZT] = Timpedance(a1,a2,R,X1,X2,Zmutual)
```

```
z1 = a1*R+X1*j; % branch impedance 1
z2 = a2*R+X2*j; % branch impedance 2
ZT = (Zmutual^2-z1.*z2)./(2*Zmutual-(z1+z2)); % CT total impedance
including mutuals
```

```
%-----%
%%%%%%%%%%%%%%%%%%%%%%%%%%%%%%%%%%%%%%%%%%%%%%%%%%%%%%%%%%%%%%%%%%%%%%%%
% This function calculates the impedance seen through the 2nd stage
% match assumes a line transformer and short circuit shunt stub
%%%%%%%%%%%%%%%%%%%%%%%%%%%%%%%%%%%%%%%%%%%%%%%%%%%%%%%%%%%%%%%%%%%%%%%%
```

```
function [ZL] = load(d,Zs,ZT,B,Z0)
```

```
%calc load seen through transformer
Zin = Z0*(ZT.*cos(B*d)+j*Z0*sin(B*d))./(Z0*cos(B*d)+j*ZT.*sin(B*d));
%calc effective load as paralel combination of transformed load and
stub
ZL = Zin.*Zs./(Zin+Zs);
```

```
%-----%
%%%%%%%%%%%%%%%%%%%%%%%%%%%%%%%%%%%%%%%%%%%%%%%%%%%%%%%%%%%%%%%%%%%%%%%%
% This function calculates the performance of a CT circuit in
% response to ELMS for a given capacitor stroke location
%%%%%%%%%%%%%%%%%%%%%%%%%%%%%%%%%%%%%%%%%%%%%%%%%%%%%%%%%%%%%%%%%%%%%%%%
```

```
function [performance] =
```

```
performance_calc(w,B,s1,s2,r1,r2,Z_mutual,elmR,elmL,d,Zs,Z0,Pi,S1,Sc
,Prm,elmspace,i)
```

```
%%%%%%%%%%%%%%%%%%%%%%%%%%%%%%%%%%%%%%%%%%%%%%%%%%%%%%%%%%%%%%%%%%%%%%%%
% w- frequency (rad), B- phase shift constant, s - capacitor stroke,
% r - asyetry coefficient, Z_mutual - strap mutual impedance
% elmR - range of resistance in ELM, elmL - range of inductance in
% ELM, d - 2nd stage transformer length, Zs - 2nd stage shunt stub
% impedance, Z0 - line characteristic impedance, Pi - input power,
% S1 - vswr crossover value, Sc - cutoff vswr, Prm - max reflected
```

```

% power, elmspace - boolean matrix to select elm values, i - number
% of nodes in elmspace
%%%%%%%%%%%%%%%%%%%%%%%%%%%%%%%%%%%%%%%%%%%%%%%%%%%%%%%%%%%%%%%%%%%%%%%%

%calc vswr for each position in ELM space
X1_N = reactance(s1,w,elmL); %reactance with
ELM
X2_N = reactance(s2,w,elmL);
ZT = Timpedance(r1,r2,elmR,X1_N,X2_N,Z_mutual); %Tpoint
impedance with ELM
ZL = load(d,Zs,ZT,B,Z0); %load seen through 2nd stage match with ELM
swr = VSWR(Z0,ZL); %VSWR due to elm
C = coupling(swr,Pi,S1,Sc,Prm); %instantaneous coupling in elm

%at this point we have a square matrix of coupled power, We need to
select from this matrix the bounded region relevant to ELM
disturbances

C=C.*elmspace; %select valid region for ELMs
Ctest = ((C>0)==elmspace); %establish if cut out interlock
occurs in selected matrix
minCtest = min(min(Ctest)); %Cut out flag: 1 - cut off did
not occur, 0 - cut off occurred
Cav = sum(sum(C))/i; %calc average coupling for ELM
area
performance=Cav*minCtest; %calc elm performance measure

%-----%

%%%%%%%%%%%%%%%%%%%%%%%%%%%%%%%%%%%%%%%%%%%%%%%%%%%%%%%%%%%%%%%%%%%%%%%%
% This function accepts a nxn matrix & an index and inserts 4 rows &
% columns about the index. values are filled by duplicates of the
% adjoining rows and columns. A refined local grid is inserted
around
% the maxima location. This padding out of the matrix enables former
values to be retained, and plotted to illustrate the adaptive
meshing
%%%%%%%%%%%%%%%%%%%%%%%%%%%%%%%%%%%%%%%%%%%%%%%%%%%%%%%%%%%%%%%%%%%%%%%%

function [output,ro,co] = refine_grid(input,row,column,locl_grid)

% insert new rows
upper = input(1:(row-2),:);
upper_v = input((row-1),:);
centre_r = input(row,:);
lower_v = input((row+1),:);
lower = input((row+2):end,:);
output =
[upper;upper_v;upper_v;centre_r;centre_r;centre_r;lower_v;lower_v;lo
wer];

% insert new columns
left = output(:,1:(column-2));
left_v = output(:,(column-1));
centre_c = output(:,column);
right_v = output(:,(column+1));
right = output(:,(column+2):end);

```

```

output =
[left,left_v,left_v,centre_c,centre_c,centre_c,right_v,right_v,right
];

% insert local mesh around former maxima
row = row+2; % calc new maxima indices after padding operation
column = column+2;
%new search window
ro = (row-4):(row+4);
co = (column-4):(column+4);
output(ro,co) = locl_grid;

%-----%

%%%%%%%%%%%%%%%%%%%%%%%%%%%%%%%%%%%%%%%%%%%%%%%%%%%%%%%%%%%%%%%%%%%%%%%%
% variable resolution solver - iterate mesh resolution in locality
% of latest global maxima to find optimal resilience
%%%%%%%%%%%%%%%%%%%%%%%%%%%%%%%%%%%%%%%%%%%%%%%%%%%%%%%%%%%%%%%%%%%%%%%%

function
[s1_opt,s2_opt,x1_opt,x2_opt,max_performance,XX1,XX2,performance] =
set_points(w,B,strap_R,strap_L,r1,r2,Z_mutual,elmR,elmL,Z0,Pi,S1,Sc,
Prm,elmspace,i)

% design space - define initial search area %
grid_res = 200; %define an initial course search resolution
quadrant_flag=1; %toggle to switch between quadrants for
search

%map capacitor stroke space to reactance space and select the
correct search quadrant, as asymmetry creates one dominant
solution.

%calc stroke required for resonant arm (X = 0 locus)
s_crit = (1-(w^2*strap_L*80e-12))/4.0740741e-12/w^2/strap_L;
% ensure that quadrants are possible - eg at high frequency
if (s_crit<0)|| (s_crit>54)
    sprintf('warning, critical stroke outwith total search
area')
end

%calc the resulting search domains for 0mm to s_crit, & s_crit
to 54mm. use different resolutions to have same size of vectors
incl = s_crit/grid_res; % define increment 1
inc2 = (54-s_crit)/grid_res; % define increment 2
grid = (incl+inc2)/2; % extract average resolution

% define a vector of stroke values equivalent to available +ve
reactance design space:
SA = 0:incl:s_crit;
% define a vector of stroke values equivalent to available -ve
reactance design space:
SB = 54:-inc2:s_crit;

%select quadrant - i.e. mapping from desired reactance design
space space to stroke space complete

```

```

stroke1=SA*(quadrant_flag==1)+SB*(quadrant_flag==0);
stroke2=SB*(quadrant_flag==1)+SA*(quadrant_flag==0);

%calc arm reactances for selected stroke vectors
x1 = reactance(stroke1,w,strap_L);
x2 = reactance(stroke2,w,strap_L);
% define assessed stroke space
[SS1,SS2] = meshgrid(stroke1,stroke2);
% define assessed reactance space
[XX1,XX2] = meshgrid(x1,x2);
[row,col] = size(SS1); %get the size of the assessed space

%calculate the required 2nd stage match for assessed space
%calc Tpoint impedance
zT = Timpedance(r1,r2,strap_R,XX1,XX2,Z_mutual);
%calc matching parameters
[d,Zs] = SSM(Z0,real(zT),imag(zT),B);

%%%%%%%%%%%%%%
%calculate performance%
%%%%%%%%%%%%%%

%preallocate for speed
performance=zeros(row,col);

%initial sweep of total design quadrant - course resolution
for m = 1:1:row % scan the rows
    for n = 1:1:col % scan the columns
        %calc performance for each position in design space
        performance(m,n) =
performance_calc(w,B,SS1(m,n),SS2(m,n),r1,r2,Z_mutual,elmR,elmL,d(m,
n),Zs(m,n),Z0,Pi,S1,Sc,Prm,elmspace,i);
    end
end
% obtain maxima & address from course sweep
[re,rr] = max(performance);
[Re,COLUMN] = max(re);
ROW = rr(COLUMN);

% detect if max is on edge of search & prompt action
EF1 = (ROW==1) || (ROW==row) || (COLUMN==1) || (COLUMN==col);
EF2 = (ROW==2) || (ROW==(row-1)) || (COLUMN==2) || (COLUMN==(col-1));
EF = EF1 || EF2;
if (EF == 1)&&(Re>0)
    grid = 0.01; % break loop
    sprintf('solution too close to edge, enlarge search area')
elseif Re==0
    grid = 0.01; % break loop
    sprintf('grid too course, OR, not in search area')
end

% systematically refine grid about location of maximum
performance, until last resolution sufficient at 0.01 mm,
10xaccuracy of actuators.

while grid>0.01
    % obtain local grid round maximum location

```

```

S1LL = SS1(ROW,COLUMN)-2*grid;    %stroke1 lower limit
S1UL = SS1(ROW,COLUMN)+2*grid;    %stroke1 upper limit
S2LL = SS2(ROW,COLUMN)-2*grid;    %stroke2 lower limit
S2UL = SS2(ROW,COLUMN)+2*grid;    %stroke2 upper limit
grid = grid/2;                    % double resolution
LGs1 = S1LL:grid:S1UL;            % define stroke vector +/-
2x former grid about maxima
    LGs2 = S2LL:grid:S2UL;
    LGx1 = reactance(LGs1,w,strap_L);% calc reactance vector +/-
2x former grid about maxima
    LGx2 = reactance(LGs2,w,strap_L);
    [ss1,ss2] = meshgrid(LGs1,LGs2); % form Local Grid (LG) 9x9
round maximum
    [xx1,xx2] = meshgrid(LGx1,LGx2);

% calculate new grids, where ro,co is the new address of the
inserted grid
    %insert blank grid into results
    [performance,ro,co] =
refine_grid(performance,ROW,COLUMN,zeros(9,9));
    %insert local grid into previous capacitor stroke mesh
    [SS1,ro,co] = refine_grid(SS1,ROW,COLUMN,ss1);
    [SS2,ro,co] = refine_grid(SS2,ROW,COLUMN,ss2);
    %insert local grid into previous arm reactance mesh

    [XX1,ro,co] = refine_grid(XX1,ROW,COLUMN,xx1);
    [XX2,ro,co] = refine_grid(XX2,ROW,COLUMN,xx2);

% calculate 2nd stage match for window only
%form dummy matrices of same dimension as design space to
hold
    %2nd stage match parameter local grids
    zT = ones(size(SS1));    %Tpoint impedance matrix
    d = zT;                  %transformer length matrix
    Zs = zT;                 %stub impedance matrix
    %calc Tpoint impedance for window only
    zT(ro,co) =
Timpedance(r1,r2,strap_R,XX1(ro,co),XX2(ro,co),Z_mutual);
    %calc matching parameters for window only
    [d(ro,co),Zs(ro,co)] =
SSM(Z0,real(zT(ro,co)),imag(zT(ro,co)),B);

    %calculate performance in the window
    for m = ro                % scan the rows of window
        for n = co            % scan the columns of window
            performance(m,n) =
performance_calc(w,B,SS1(m,n),SS2(m,n),r1,r2,Z_mutual,elmR,elmL,d(m,
n),Zs(m,n),Z0,Pi,S1,Sc,Prm,elmspace,i);
        end
    end
    % obtain maxima & address from course mesh
    [re,rr] = max(performance);
    [Re,COLUMN] = max(re);
    ROW = rr(COLUMN);
end

%obtain global maximum & setpoints
[re,rr] = max(performance);

```

```

[Re,column] = max(re);
row = rr(column);
max_performance = Re;
s1_opt = SS1(row,column);
s2_opt = SS2(row,column);
x1_opt = reactance(s1_opt,w,strap_L);
x2_opt = reactance(s2_opt,w,strap_L);

%-----%

%%%%%%%%%%%%%%%%%%%%%%%%%%%%%%%%%%%%%%%%%%%%%%%%%%%%%%%%%%%%%%%%%%%%%%%%%%%%%%
% reactance to phase space calculator
%%%%%%%%%%%%%%%%%%%%%%%%%%%%%%%%%%%%%%%%%%%%%%%%%%%%%%%%%%%%%%%%%%%%%%%%%%%%%%

function [thG,thN] = XtoP(x1,x2,r1,r2,strap_R,Z_mutual)

%calculate phase%
zarm1 = r1*strap_R+x1.*j;           % branch impedance 1
zarm2 = r2*strap_R+x2.*j;           % branch impedance 2
%a quantity of same phase as I1 (phase referenced to Tpoint voltage)
q1 = (Z_mutual-zarm2)./(Z_mutual.^2-zarm1.*zarm2);
%a quantity of same phase as I2 (phase referenced to Tpoint voltage)
q2 = (Z_mutual-zarm1)./(Z_mutual.^2-zarm1.*zarm2);

qth1 = atan2(imag(q1),real(q1))/pi*180; %extract phase angle of
I1
qth2 = atan2(imag(q2),real(q2))/pi*180; %extract phase angles
of I2
thG = qth1-qth2;           %remember that angles are of opposite sign
- so gross + net angle definitions have been inverted
thN = qth1+qth2;

```